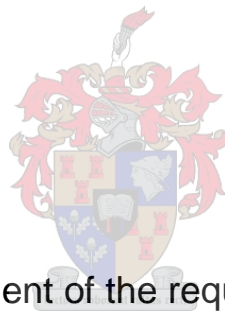


Factors that Affect the Adipocytic Differentiation of Adipose-Derived Mesenchymal Stem Cells

By

Caitlin McCaffrey



Thesis presented in fulfilment of the requirements for the degree of
Master of Medical Physiology in the Faculty of Medicine and Health Sciences
at Stellenbosch University

Supervisor: Professor William F. Ferris

Co-Supervisor: Dr Derick van Vuuren

April 2022

Declaration

By submitting this thesis electronically, I declare that the entirety of the work contained therein is my own, original work, that I am the sole author thereof (save to the extent explicitly otherwise stated), that reproduction and publication thereof by Stellenbosch University will not infringe any third-party rights and that I have not previously in its entirety or in part submitted it for obtaining any qualification.

April 2022

Dedication

I would like to dedicate this thesis to my lost loved ones as well as to the women who have raised me.

To my grandfather, **Barrie Clifford Wardill**, over the years I was fortunate enough to have learnt countless lessons from you. “Do your best and leave the rest” is an adage that I will always live by, thanks to you. I hope to make you proud.

To my cousin, **Toni-lee Kirkbride**, taken from us too soon. Your terrible singing, endless selfie-taking, and ‘organised chaos’ will always be fondly remembered, but it is your kind, loving, selflessness that has left the world worse off without you in it.

To my dad, **John McCaffrey**. I will always miss our Sunday lunches and piano lessons. Though our relationship had its flaws, I always loved you and I hope you knew that.

To my nana, **Norma Elizabeth Wardill**, my rock. Your love and encouragement through every phase of my life have been appreciated more than you will ever know.

To my aunt, **Samantha Jane Kirkbride**, my “other mother”. In these last three years, you have shown me so much love and support despite the pain you have had to endure. I don’t think I could ever thank you enough for all that you have done for me. You are the strongest woman I know.

To my mom, **Sarah McCaffrey**, my best friend and pillar of strength. To paraphrase the Gilmore Girls; “My mother never gave me any idea that I couldn’t do whatever I wanted to do or be whomever I wanted to be... As she guided me through these incredible 26 years, I don’t know if she ever realized that the person I most wanted to be was her.” I love you.

Abstract

Background –

Increased adiposity, particularly the accumulation of visceral adipose tissue is linked to the onset and progression of the metabolic syndrome. Despite the known pathogenicity of excessive visceral fat accrual, a paucity of knowledge on the mechanism behind its expansion exists. We hypothesise that hypertrophy and cellular dysfunction of subcutaneous adipocytes leads to the secretion of endocrine factors which stimulate adipogenesis in visceral adipose-derived mesenchymal stem cells (AD-MSCs) and that this communication might be affected by diet. We also postulate that the endocrine-induced adipogenesis of visceral AD-MSCs is amplified in individuals prescribed the PPAR γ agonist, rosiglitazone for treatment of type II diabetes mellitus.

Methods –

Male Wistar rats at 3-weeks of age were fed either control lab chow, a high-fat diet (HFD), or an elevated sugar diet (ESD) ($n = 7/\text{group}$) *ad libitum* for 16 weeks and euthanised. The rat weights and endpoint fasting blood glucose were recorded and bilateral inguinal subcutaneous and retroperitoneal visceral adipose tissue depots excised. Histological studies of the tissue allowed adipocyte structure to be observed and measured. AD-MSCs from each depot were also isolated and expanded *in vitro*. The *in vitro* morphology of AD-MSCs was characterised, proliferation monitored, and the expression of the MSC markers (CD90+ and CD45-) measured. Adipogenesis was induced in the AD-MSCs, and conditioned media (CM) – containing the secretome of the mature adipocytes – was collected. Naïve AD-MSCs isolated from both adipose depots of age-matched control rats ($n = 3$) were then treated with the subcutaneous- and visceral conditioned media alone or in combination with either standard growth media (SGM) or adipocyte differentiation media (AM). This was repeated with and without the addition of 1 μM rosiglitazone (Rosi). The effects of these treatments were qualitatively assessed by microscopy of oil red O-stained lipids and quantitatively assessed by *in-silico* micrograph- and spectrophotometric analyses.

Results –

The findings of this study indicate that feeding male Wistar rats a HFD or an ESD increases the mass of the inguinal and retroperitoneal adipose depots and cause hypertrophy in the constituent adipocytes. The diets also affected the MSC marker expression of the AD-MSCs from both adipose depots, having elevated the expression of CD90 in the HFD AD-MSCs but decreased the CD90 expression in the ESD AD-MSCs. The CM samples collected from the chow-fed control, HFD, and ESD adipocytes stimulated lipid accrual in the visceral AD-MSCs when added alone or in combination with SGM or AM, but the most significant adipogenic effects were induced by the ESD

visceral CM in all three formulations. Only the control subcutaneous- and ESD visceral CM, when supplemented with AM, were able to elicit significant lipid accrual in the subcutaneous AD-MSCs. Following Rosi supplementation, the visceral AD-MSCs treated with HFD- and control CM treatments accumulated significant quantities of intracellular lipids. None of the CM+Rosi treatments stimulated significant lipid accrual in the naïve subcutaneous AD-MSCs. The CM and Rosi experiments revealed that subcutaneous AD-MSCs are less susceptible to CM-induced adipogenesis than visceral AD-MSCs.

Conclusion –

This study provides evidence for a possible endocrine communication between the subcutaneous and visceral adipose depots which appears to be amplified by the chronic consumption of an elevated sugar diet as well as by supplementation with rosiglitazone. These novel findings may contribute towards elucidating the underlying mechanisms behind the pathogenic expansion of visceral adipose tissue.

Opsomming

Agtergrond –

'n Toename in adipositeit, spesifiek die ophoping van visserale adipose weefsel is verwant aan die intrede en verloop van die metaboliese sindroom. Ten spyte van die bekende patogeniteit betrokke by die akkumulering van oortollige visserale vet, is daar gebrekkige kennis aangaande die meganisme van uitsetting van hierdie tipe vet. Ons hipotese is dat hipertrofie en sellulêre disfunksie van subkutane adiposiete die afskeiding van endokriene faktore tot gevolg het, wat adipogenese in visserale adipose-afgeleide mesenchimale stamselle (AD-MSCs) stimuleer en dat hierdie kommunikasie deur dieet beïnvloed kan word. Ons postuleer ook dat die endokriene-geïnduseerde adipogenese van visserale AD-MSCs versterk word in individue wat die PPAR γ agonis rosiglitason, vir die behandeling van tipe II-diabetes mellitus, voorgeskryf is.

Metodes -

Drie week oud manlike Wistar rotte is óf kontrole laboratorium rotte, óf 'n hoë-vet dieet (HFD), óf 'n verhoogde suiker dieet (ESD) (n = 7 / groep) *ad libitum* gevoed vir 16 weke waarna hulle uitgesit is. Die liggaamsgewigte en eindpunt vastende bloedglukose vlakke van die rotte is aangeteken. Bilaterale subkutane inguinale en viscerale retroperitoneale adipose weefsel depots is chirurgies verwyder. Histologiese studies van die weefsel is onderneem om adiposiet-struktuur waar te neem

en te meet. AD-MSCs is ook vanuit elke depot geïsoleer en *in vitro* uitgebrei. Hierdie AD-MSCs is gekarakteriseer in terme van *in vitro* morfologie, proliferasie en die uitdrukking van MSC merkers (CD90 + en CD45-). Adipogenese is geïnduseer in die AD-MSCs en gekondisioneerde media (KM) – wat die sekreetoom van volwasse adiposiete bevat – versamel. Naïewe AD-MSCs wat geïsoleer is vanuit beide adipose depots van ouderdom-ooreenstemmende kontrole rotte (n = 3) is vervolgens behandel met die gekondisioneerde media afkomstig vanaf die subkutane- en visserale selle alleen of in kombinasie met óf standaard groei media (SGM) of adiposiet differensiasie media (AM). Dit is herhaal met en sonder die toevoeging van 1µM rosiglitasoon (Rosi). Die gevolge van hierdie behandelings is kwalitatief geassesseer deur mikroskopie van olie rooi o-gekleurde lipiede en gekwantifiseer met behulp van *in-silico* mikrograaf- en spektrofotometriese ontledings.

Resultate -

Die bevindings van hierdie studie dui daarop dat die voeding van manlike Wistar rotte met 'n HFD of 'n ESD die massa van die inguinale en retroperitoneale adipose depots verhoog en ook hipertrofie veroorsaak in die adiposiete waaruit hierdie weefsels saamgestel is. Hierdie diëte het ook die MSC-merkeruitdrukking in die AD-MSCs van beide adipose depots beïnvloed. Die uitdrukking van CD90 is in die HFD AD-MSCs verhoog, terwyl CD90-uitdrukking in die ESD AD-MSCs verminder is. Alle KM monsters wat versamel is vanaf rotkos-gevoerde kontrole, HFD, en ESD adiposiete het lipied akkumulاسie in die visserale AD-MSCs gestimuleer, maar die mees uitgesproke adipogeniese effekte is veroorsaak deur die ESD visserale KM. Die CM monsters versamel uit die chow-gevoed beheer, HFD, en ESD adipocytes gestimuleer lipied aanwas in die viscerale AD-MSCs wanneer alleen of in kombinasie met SGM of AM bygevoeg, maar die belangrikste adipogene effekte is veroorsaak deur die ESD viscerale CM in al drie formulerings. Slegs die beheer subkutane- en ESD viscerale CM, wanneer dit met AM aangevul is, kon beduidende lipied-aanwas in die subkutane AD-MSC's ontlok. Na aanleiding van Rosi-aanvulling het die viscerale AD-MSC's wat met HFD- en beheer CM-behandelings behandel is, beduidende hoeveelhede intrasellulêre lipiede opgehoop. Nie een van die CM + Rosi behandelings gestimuleer beduidende lipied aanwas in die naïewe subkutane AD-MSCs. Die CM- en Rosi-eksperimente het aan die lig gebring dat subkutane AD-MSC's minder vatbaar is vir CM-geïnduseerde adipogenese as viscerale AD-MSC's.

Gevolgtrekking –

Hierdie studie bied bewyse vir moontlike endokriene kommunikasie tussen die subkutane en viscerale adipose depots wat blyk te wees versterk deur die chroniese verbruik van 'n verhoogde suiker dieet sowel as deur aanvulling met rosiglitazone. Hierdie nuwe bevindings kan bydra tot die verduideliking van die onderliggende meganismes agter die patogene uitbreiding van viscerale vetweefsel.

Acknowledgements

Research and personal funding for this project were awarded by:

National Research Foundation

I would like to express my gratitude to the following people, without whom the completion of this degree would not have been possible.

My supervisor, **Prof William Ferris**, thank you for your terrible jokes and guidance throughout the study.

My co-supervisor, **Dr Derrick van Vuuren**, thank you for your constructive suggestions and assistance with the translation of my Abstract.

My unofficial co-co-supervisor, **Ms Kayla Howard**, I honestly do not know what I would have done without your guidance, friendship, and support. Thank you.

Prof Barbara Huisamen, thank you for providing us with information on the high-fat and elevated sugar diets and allowing us to collect tissue from the rats from your study.

Dr Mari van de Vyver, thank you for answering all of my questions and providing me with advice when I needed it most.

Mr Noel Markgraaf, Dr Sven Parsons, and the staff at the FMHS animal research facility thank you for caring for our rats.

Mr Reggie Williams, thank you for your assistance with the histology staining.

Dr Michael McCaul, thank you for your assistance with the statistical analyses and data interpretation.

Dr Dalene de Swardt, thank you for all your assistance with the flow cytometry and data analysis and for providing some much-needed emotional support.

Finally, a special thank you to my friends and family, specifically to **Ms Sarah McCaffrey, Mr Kevin Turner, Mrs Norma Wardill, Mrs Samantha Kirkbride, Mr Steven Kirkbride, Ms Justine Kirkbride**, and **Mr John-Ross Holliday**. Thank you for always believing in me.

Table of Contents

Declaration	i
Dedication	ii
Abstract	iii
Opsomming	iv
Acknowledgements	vi
Table of Contents	vii
Table of Figures	x
Table of Tables	xiii
Abbreviations	xiv
Chapter 1	1
Introduction and Literature Review	1
1.1 Obesity.....	1
1.2 Adipose Tissue Cellularity	2
1.2.1 Thiazolidinediones	5
1.3 Adipose Tissue Types.....	5
1.3.1 Brown and Beige Adipose Tissue	5
1.3.2 White Adipose Tissue.....	7
1.4 Subcutaneous and Visceral White Adipose Tissue.....	7
1.4.1 Subcutaneous White Adipose Tissue.....	8
1.4.2 Visceral White Adipose Tissue	9
1.5 Dynamics of Subcutaneous and Visceral Adipose Tissue Expansion	9
1.5.1 The Role of Intracellular Signalling in Adipose Tissue Accrual	10
1.6 The Present Study.....	11
1.6.1 Rationale for Research	11
1.6.2 Aims and Objectives of the Present Study.....	12
Chapter 2	14
Methods and Materials	14
2.1 Materials and Reagents.....	14
2.2 Ethical Approval	15
2.3 General Overview of Study Methods	15
2.4 Experimental Animals	18
2.5 Adipose tissue isolation	19
2.6 Histological Staining of Subcutaneous and Visceral Adipose Tissue.....	20
2.6.1 Tissue Processing for Histological Staining.....	20

2.6.2	Haematoxylin and Eosin staining of Adipose Tissue	21
2.6.3	<i>In silico</i> Analyses of H&E-Stained Adipose Tissue.....	22
2.7	Isolation and Culture of Adipose-derived Mesenchymal Stem Cells (AD-MSCs).....	23
2.7.1	Isolation of Subcutaneous and Visceral AD-MSCs from White Adipose Tissue.....	23
2.7.2	Standard Cell Culture Conditions	23
2.8	Subculturing Cells	24
2.9	Cell Counting	24
2.10	Growth Curves	24
2.11	Flow Cytometry	25
2.12	Adipocytic Differentiation	27
2.13	Harvesting Conditioned Media from <i>in vitro</i> Differentiated Subcutaneous and Visceral Adipocytes.....	28
2.14	Preparation of Rosiglitazone for <i>in vitro</i> cell treatment	28
2.15	Quantification of Lipid Accumulation by Oil Red O and Crystal Violet Staining, Spectrophotometry, and <i>in-silico</i> Photomicrograph Analyses	28
2.16	Statistical Analyses.....	30
Chapter 3	31
Results	31
3.1	Diets	33
3.2	Histological Staining of Subcutaneous and Visceral White Adipose Tissue	34
3.3	Characterisation of Inguinal and Retroperitoneal AD-MSCs from Control, HFD and ESD fed rats.....	40
3.3.1	Growth Kinetics of Subcutaneous and Visceral AD-MSCs	41
3.3.2	Flow Cytometric Analyses	43
3.3.3	Adipogenic Potential of Control, HFD and ESD Subcutaneous and Visceral AD-MSCs	48
3.4	Impacts of Varying Concentrations of Adipogenic Media – A Preliminary Study	49
3.5	Effects of Control, HFD and ESD Conditioned Media on the Adipocytic Differentiation of Subcutaneous and Visceral AD-MSCs.....	53
3.6	Effects of Control, HFD, and ESD Conditioned Media Supplemented with Rosiglitazone on the Adipocytic Differentiation of Subcutaneous and Visceral AD-MSCs	60
Chapter 4	68
Discussion	68
4.1	Diets	69
4.2	Histological Staining of Subcutaneous and Visceral Adipose Tissue.....	72
4.3	Characterisation of Inguinal and Retroperitoneal AD-MSCs from Control, HFD, and ESD fed rats.....	74
4.4	Effects of Varying Concentrations of Adipogenic Media – A Preliminary Study	80

4.5	Effects of Control, HFD, and ESD Conditioned Media on the Adipocytic Differentiation of Inguinal and Retroperitoneal AD-MSCs	81
4.6	Effects of Control, HFD, and ESD Conditioned Media Supplemented with Rosiglitazone on the Adipocytic Differentiation of Inguinal and Retroperitoneal AD-MSCs	83
4.7	Study Limitations and Recommendations for Future Studies	85
Chapter 5	87
Conclusion	87
References	89
Appendices	107
	Appendix A – Ethical approval.....	107
	Appendix B – Consumables.....	110
	Appendix C – Composition of Media and Reagents.....	112
	Appendix D – Supplementary Tables and Figures for Preliminary and Conditioned Media Experiments.....	114

Table of Figures

Figure 1.1: Simplified adipose tissue cellularity.....	2
Figure 1.2: Basic overview of adipogenic differentiation.....	4
Figure 1.3: Intercalation of brown and white adipocytes within the inguinal adipose tissue of a male Wistar rat.....	7
Figure 1.4: Distribution of brown and white adipose tissue within the subcutaneous and visceral depots of a male Wistar rat.....	8
Figure 1.5: Paracrine and autocrine signalling.....	10
Figure 2.1: Isolation and purification of subcutaneous and visceral adipose-derived mesenchymal stem cells.....	16
Figure 2.2: Collection of conditioned media from mature subcutaneous and visceral adipocytes and treatment of cells.....	17
Figure 2.3: The process of analyzing haematoxylin and eosin-stained adipose tissue using AdipoGauge software (© Moussa Lab, Texas Tech University, November 25, 2020).....	22
Figure 2.4: Quantification of oil red O (ORO) staining by thresholding based on hue, saturation, and brightness in ImageJ Fiji.....	30
Figure 3.1: Bodyweight growth curve of the control (n = 7), high-fat diet (n = 7), and elevated-sugar diet (n = 7) fed male Wistar rats over the 16-week diet feeding period.....	33
Figure 3.2: Haematoxylin and eosin-stained inguinal subcutaneous and retroperitoneal visceral adipose tissue harvested from 12-week-old control, 19-week-old control, high-fat diet- and elevated-sugar diet-fed male Wistar rats.....	35
Figure 3.3: Morphometric indices of haematoxylin and eosin-stained inguinal and retroperitoneal white adipocytes within adipose tissue samples isolated from 12-week-old- and 19-week-old control male Wistar rats.....	36
Figure 3.4: Morphometric indices of haematoxylin and eosin-stained inguinal and retroperitoneal adipocytes within adipose tissue samples isolated from age-matched 19-week-old control, high-fat diet-, and elevated sugar diet-fed male Wistar rats.....	37
Figure 3.5: Frequency of adipocytes present in various size classes within haematoxylin and eosin-stained (A) inguinal and (B) retroperitoneal adipose tissue samples isolated from 12-week-old control, 19-week-old control, high-fat diet-, and elevated sugar diet-fed male Wistar rats.....	39

Figure 3.6: Representative micrographs showing the in vitro adherent morphology and the non-adherent size of inguinal and retroperitoneal AD-MSCs isolated from male Wistar rats.....	40
Figure 3.7: Aggregation of inguinal and retroperitoneal AD-MSCs at P0 and P3 following purification by serial subculture.....	41
Figure 3.8: 7-day growth curves of subcutaneous and visceral AD-MSC of inguinal and retroperitoneal AD-MSCs isolated from (A) 12-week-old control, (B) 19-week-old control, (C) high-fat- and (D) elevated sugar diet-fed male Wistar rats.....	42
Figure 3.9: Population doubling times (hours) of inguinal and retroperitoneal AD-MSCs isolated from 12-week-old control, 19-week-old control, high-fat- and elevated-sugar diet-fed male Wistar rats.....	43
Figure 3.10: Titration of CD90 in rat inguinal and retroperitoneal adipose-derived mesenchymal stem cells (AD-MSCs).....	44
Figure 3.11: Representative forward-scatter vs. side-scatter and single-cell plots showing the gating strategies used for the control, high-fat diet, and elevated sugar diet AD-MSCs.....	45
Figure 3.12: Mesenchymal cell surface marker expression profile of inguinal subcutaneous and retroperitoneal visceral AD-MSCs isolated from control, high-fat diet-, and elevated sugar diet-fed male Wistar rats.....	46
Figure 3.13: Percentage of control, high-fat diet, and elevated sugar diet subcutaneous and visceral AD-MSCs demonstrating positive expression of mesenchymal stem cell marker CD90 and haematopoietic marker CD45.....	47
Figure 3.14: Representative images of oil red O-stained lipid droplets accumulated in vitro by inguinal subcutaneous and retroperitoneal visceral AD-MSCs following 14 days of adipogenesis.....	48
Figure 3.15: Micrographs, in-silico lipid quantification and spectrophotometric analysis of inguinal AD-MSCs subjected to 14-day treatment with varying concentrations of adipogenic media (AM).....	51
Figure 3.16: Micrographs, in-silico lipid quantification and spectrophotometric analysis of retroperitoneal AD-MSCs subjected to 14-day treatment with varying concentrations of adipogenic media.....	52
Figure 3.17: Representative micrographs, in-silico, and spectrophotometric quantification of oil red O-stained inguinal subcutaneous and retroperitoneal visceral AD-MSCs treated with conditioned media harvested from control, high-fat diet, and elevated sugar diet-fed rats.....	55

Figure 3.18: Representative micrographs, in-silico, and spectrophotometric of oil red O-stained inguinal subcutaneous and retroperitoneal visceral AD-MSCs treated with a combination of conditioned media and standard growth media.....	57
Figure 3.19: Representative micrographs, in-silico, and spectrophotometric quantification of oil red O-stained inguinal subcutaneous and retroperitoneal visceral AD-MSCs treated with a combination of conditioned media and adipogenic media.....	59
Figure 3.20: Representative micrographs, in-silico, and spectrophotometric quantification of oil red O-stained inguinal subcutaneous and retroperitoneal visceral AD-MSCs treated with conditioned media harvested from control, high-fat diet and elevated sugar diet-fed rats supplemented with 1 μ M Rosiglitazone.....	62
Figure 3.21: Representative micrographs, in-silico, and spectrophotometric of oil red O-stained inguinal subcutaneous and retroperitoneal visceral AD-MSCs treated with a combination of conditioned media, standard growth media, and 1 μ M Rosiglitazone.....	64
Figure 3.22: Representative micrographs, in-silico, and spectrophotometric quantification of oil red O-stained inguinal subcutaneous and retroperitoneal visceral AD-MSCs treated with a combination of conditioned media and adipogenic media supplemented with 1 μ M Rosiglitazone	66
Figure 4.1: Typical 7-day growth kinetic curve of adipose-derived mesenchymal stem cells.....	75
Figure 4.2: Representative phase-contrast micrographs of adipose-derived mesenchymal stem cells on days 1, 3, 10, and 14 of adipogenesis.....	78
Figure 4.3: Schematic of an indirect co-culture system.....	86
Figure D.1: Haematoxylin and Eosin-stained inguinal adipose tissue samples.....	115
Figure D.2: Forward-scatter vs. side scatter and singlet plots of subcutaneous and visceral adipose-derived stem cells from control, high-fat diet, and elevated sugar diet-fed male Wistar rats.....	116
Figure D.3: 24-well plate set-up for preliminary adipocyte differentiation media experiments.....	117
Figure D.4: 12-well plate set-up for conditioned media and rosiglitazone experiments conducted in duplicate wells.....	117
Figure D.5: Simplified timelines of the first (2020) and second (2021) years of this MSc project.....	120

Table of Tables

Table 2.1: Reagents used throughout the present study.....	14
Table 2.3: Nutritional composition of the control, high-fat diet, and elevated sugar diet	19
Table 2.4: Dehydration and xylene infiltration of adipose tissues for histological staining.....	20
Table 2.5: Haematoxylin and Eosin staining protocol conducted within the Leica Auto Stainer XL.....	21
Table 2.6: Fluorescently conjugated antibodies for use in the flow cytometric analysis of inguinal and retroperitoneal AD-MSCs.....	26
Table 3.1: Biometric data generated during and after the feeding of a control, high-fat, and elevated sugar diet to male Wistar rats (n = 21).....	34
Table 3.2: Composition of the conditioned media treatments for addition to control subcutaneous and visceral recipient AD-MSCs.....	54
Table B.1: Consumables utilised throughout this study.....	110
Table C.1: Preparation of 10% Phosphate Buffered Formalin fixative solution from stock solutions.....	112
Table C.2: Composition of Adipocyte Differentiation Media.....	112
Table D.1: Composition of conditioned media and rosiglitazone treatments for 12-well plates.....	119

Abbreviations

ADIPOQ	Adiponectin
AD-MSCs	Adipose-derived mesenchymal stem cells
AM	Adipogenic media
ANOVA	Analysis of Variance
ARBP	Acidic ribosomal phosphoprotein P0
ATP	Adenosine triphosphate
BAT	Brown Adipose Tissue
BeAT	Beige Adipose Tissue
BMI	Body Mass Index
BM-MSCs	Bone-marrow Mesenchymal Stem Cells
BSA	Bovine Serum Albumin
BSL1	Biosafety Level 1
C/EBPα	CCAAT/enhancer-binding protein α
C/EBPβ	CCAAT/enhancer-binding protein β
C/EBPδ	CCAAT/enhancer-binding protein δ
CM	Conditioned media
CV	Crystal Violet
DEXA	Dual-energy X-ray Absorptiometry
DMEM	Dulbecco's Modified Eagle's medium
DMSO	Dimethyl sulfoxide
dNTPs	Deoxynucleotide triphosphates
ESD	Elevated Sugar Diet
FFA	Free Fatty Acids
GBD	Global Burden of Disease
GPDH	Glycerol-3-phosphate Dehydrogenase

HBSS	Hank's Balanced Saline Solution
HFD	High-fat Diet
HGF	Hepatocyte Growth Factor
HSL	Hormone-sensitive lipase
IBMX	3-isobutyl-1-methylxanthine
IGM	Initial growth medium
LPL	Lipoprotein lipase
MRI	Magnetic Resonance Imaging
MSC	Mesenchymal stem cell
ORO	Oil Red-O
PBS	Phosphate buffered saline
PenStrep	Penicillin-streptomycin
PPARγ	Peroxisome proliferator-activated receptor- γ
qRT-PCR	Quantitative Real-time Polymerase Chain Reaction
SEM	Standard Error of the Mean
sWAT	Subcutaneous White Adipose Tissue
SVF	Stromal Vascular Fraction
TZDs	Thiazolidinediones
VC	Vehicle control
vWAT	Visceral White Adipose Tissue
WAT	White Adipose Tissue
WHO	World Health Organisation

Introduction and Literature Review

To provide an overview of the current knowledge, this chapter will begin with a short description of the link between adiposity and obesity and will then elaborate on the cellular composition of adipose tissue. Thereafter, thiazolidinediones, a class of insulin-sensitising drugs that have been associated with adipose tissue redistribution, will be introduced. The adipose tissue types and depots will then be discussed, along with the dynamics involved in determining the anatomical location of fat accrual. Lastly, the rationale, aims, and objectives of the present study will be detailed to indicate what this investigation hoped to achieve.

1.1 Obesity

The term “obesity” is derived from the Latin word “*obesus*” meaning fat, plump or swollen ¹. Though this term was introduced in 1651, the origins of obesity can be traced back thousands of years to an age where the capacity to store excess energy contributed greatly to survival through periods where resources were scarce ^{2,3}. This led to excess adiposity being perceived as a sign of good health and affluence in later years ⁴. Today, however, the strong association between obesity and the development of metabolic comorbidities such as insulin resistance, type II diabetes mellitus, cardiac disease, stroke, and hypertension has been recognised ^{5,6}. This led to it being classified as a chronic non-communicable disease by the American Medical Association in 2013 ^{7,8}. The widespread consumption of the calorie intensive, Western diet comprising of highly processed palatable foods with excess saturated fats and refined sugars is thought to be mostly responsible for the escalating prevalence of obesity ⁹.

Obesity is a phenotypically variable disorder, thus, in an effort to provide a measurable metric that would enable health professionals to determine whether an individual was of a healthy weight, the body-mass index (BMI) was developed in the 1930s ^{5,10,11}. Calculated by dividing a person's weight in kilograms by their height in metres squared, this much-disputed measurement is widely used today by various prominent medical research institutions, including the World Health Organisation (WHO) ^{12–14}. According to this categorization index, having a BMI of 25 or more suggests overweight and a BMI of 30 or more is indicative of obesity ¹². Recently, cross-sectional analyses have shown that waist circumference presents a more accurate predictor of morbidity than BMI due to the correlation between central, visceral fat mass and metabolic dysregulation ¹⁵.

As a result of the widespread use of these measures, obesity's predominance worldwide became evident, culminating in the WHO declaring it as a global epidemic and international public health crisis in 1997 ¹⁶. The most recent statistics published by the *Global Burden of Diseases, Injuries, and*

Risk Factors Study (GBD) 2017 reported that approximately 39% of adults (over the age of 18) have a BMI high enough to classify them as overweight or obese. Obesity was also linked to 4.72 million deaths worldwide in 2017, making it one of the top five global risk factors for premature death ¹⁷. Though obesity can be subcategorised into varying levels of severity based on the individual's BMI and metabolic health, the accumulation of adipose tissue which surpasses physical necessity is recognised as the characteristic feature of this disease ¹⁸.

1.2 Adipose Tissue Cellularity

Adipose- or fat tissue exists in varying quantities and locations in all individuals. Having been understudied for decades as a result of the misconception that it was simply a passive storage depot for cellular energy and served only to provide insulation and protection to vital organs, a paucity of information on this tissue remains ¹⁹. The ever-increasing burden of obesity and its associated co-morbidities on health systems worldwide, as well as the increased mortality rates of individuals with co-morbidities such as obesity during the ongoing SARS-CoV-2 pandemic, has recently brought adipose tissue to the forefront of scientific research ^{12,20,21}. The complex structure and organisation of this multi-depot organ are, therefore, slowly being revealed through extensive study.

For many years as a result of their considerable size, mature adipocytes were believed to be the only cellular constituent of adipose tissue, but it has since been determined that they only occupy between 60-80% of the tissue's mass ²²⁻²⁴. The remaining tissue is composed of an assortment of cell types, some of which include preadipocytes, adipose-derived mesenchymal stem cells (AD-MSCs), endothelial cells, macrophages, neutrophils, and lymphocytes ²². This collection of cells is referred to as the stromal vascular fraction (SVF) ²². Comprising of various immune and fibroblast-like cell types, the SVF performs immunomodulatory and anti-inflammatory roles and maintains the structural integrity of the tissue together with the extra-cellular matrix (Figure 1.1) ²⁵⁻²⁷.

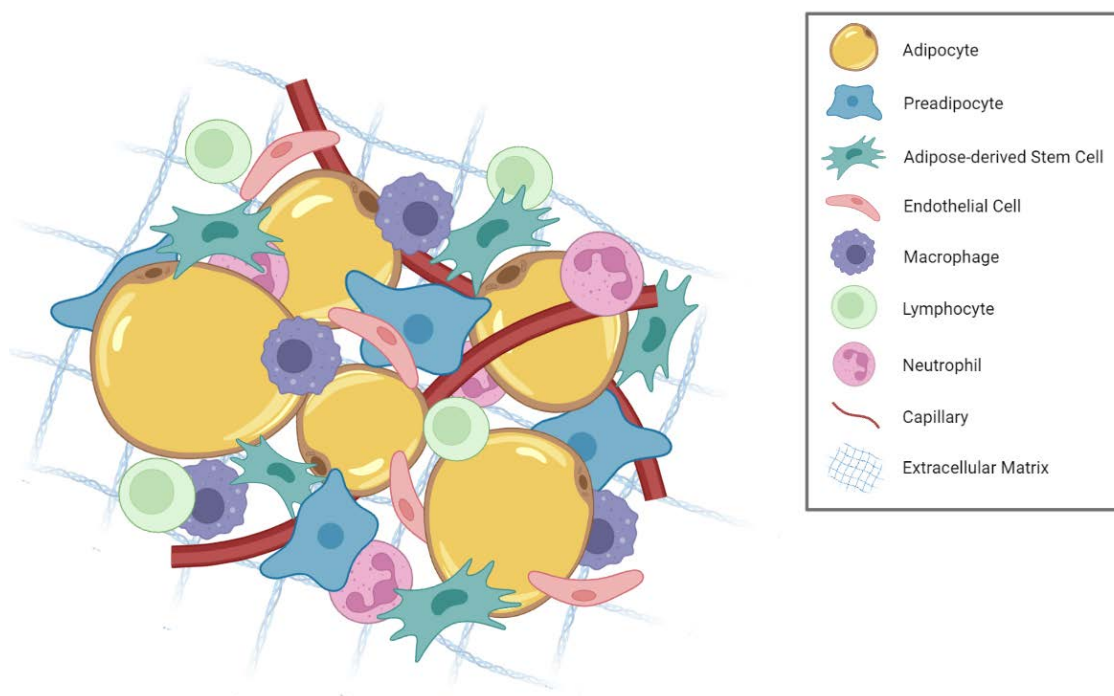


Figure 1.1: Simplified adipose tissue cellularity. Mature, unilocular adipocytes intercalated with the preadipocytes, adipose-derived stem cells, endothelial cells, macrophages, lymphocytes, and neutrophils of the stromal vascular fraction all surrounded by the extracellular matrix (Adapted from Bourgeois et al. 2019, created with BioRender.com).

Through the metabolism of dietary carbohydrates and fats, adipose tissue is able to store glucose and free fatty acids (FFAs) in the form of triglycerides²⁸. Whilst some of the SVF cells have the ability to sequester and store circulating FFAs and glucose as intracellular triglyceride (lipid) droplets, adipocytes function as the primary lipid storage sites within the adipose tissue^{29,30}. Generally, the process of fat accumulation is determined by a balance between lipogenesis – fatty acid synthesis and conversion of fatty acids into triglycerides – and lipolysis – the catabolism of triglycerides for the provision of energy – which occur within the liver and adipose tissue³¹. Lipogenesis is heavily influenced by dietary carbohydrate and glucose levels and is mediated by several hormones including leptin, angiotensin, insulin, glucagon, growth hormone, and catecholamines³². Through lipolysis and subsequent β -oxidation (the breakdown of lipids), stored triglycerides can be used, when required, to generate adenosine triphosphate (ATP) – the primary carrier of cellular energy^{30,33}.

To facilitate the storage of excess triglycerides when an imbalance in energy uptake and expenditure occurs, adipose tissue may increase its storage capacity by enlarging the constituent adipocytes (hypertrophy)^{34,35}. Whilst adipocyte hypertrophy is an energy-efficient lipid storage solution, studies have shown that the adipocytes have a threshold of expansion beyond which the cells become stressed and dysfunctional^{36–38}. Hypertrophy-induced adipocytic dysfunction causes the secretion of FFAs and pro-inflammatory cytokines, the mobilisation of immune cells within the adipose tissue, and hypoxia due to inadequate vascularisation of the expanding adipose tissue^{36–38}. To compensate for the reduced lipid storage capacity of the hypertrophic adipocytes, new adipocytes develop from the AD-MSCs within the SVF through a process referred to as hyperplasia^{39,40}. Adipocyte hyperplasia entails the recruitment and commitment of AD-MSCs to the adipocyte lineage, followed by the induction of adipogenesis^{35,41}.

Briefly, the process of adipogenic differentiation can be divided into two phases, phase I being the adipocyte lineage commitment phase and phase II being the terminal adipocytic differentiation phase (Figure 1.2)^{42–44}. Whilst the precise molecular events of the adipocytic commitment process in phase I have yet to be fully delineated, researchers have hypothesised that it likely occurs as a result of a combination of signalling from neighbouring hypertrophic adipocytes or from other cells within the SVF^{42–44}. During this process, the AD-MSCs undergo asymmetrical cell division which results in one daughter cell taking on the lineage-restricted preadipocyte phenotype, whilst the other daughter cell remains a pluripotent AD-MSC to perpetuate the SVF stem cell population⁴⁵. The committed preadipocytes continue to proliferate until growth is arrested through the stimulation of adipogenic genes such as peroxisome-proliferator activated receptor- γ (PPAR γ) and CAAT/enhancer-binding

protein α (C/EBP α)^{44,46,47}. The upregulation of PPAR γ and C/EBP α subsequently induce a signalling cascade which activates further adipogenic genes as the second phase of adipogenesis begins.

At the start of phase II, structural changes in the extracellular matrix and cytoskeleton of the preadipocytes prompt the cells to condense and become spherical which distinguishes the differentiating cells from the fibroblastic, naïve precursors^{44,48}. As the cells progress through the various stages of adipogenesis the characteristic features of adipocytes are acquired. Thus, once terminally differentiated, the newly differentiated adipocytes are able to facilitate the storage, synthesis, and transport of lipids, can secrete adipocyte-specific bioactive peptides (discussed further in section 1.3) and have become insulin sensitive^{42–44}. Each stage of adipogenesis can be identified by the changes in gene expression of the cell, with markers such as C/EBP β and C/EBP δ being highly expressed mid-way through differentiation, and genes such as leptin, lipoprotein lipase (LPL), and adiponectin (ADIPOQ) being markers of terminal differentiation (Figure 1.2).

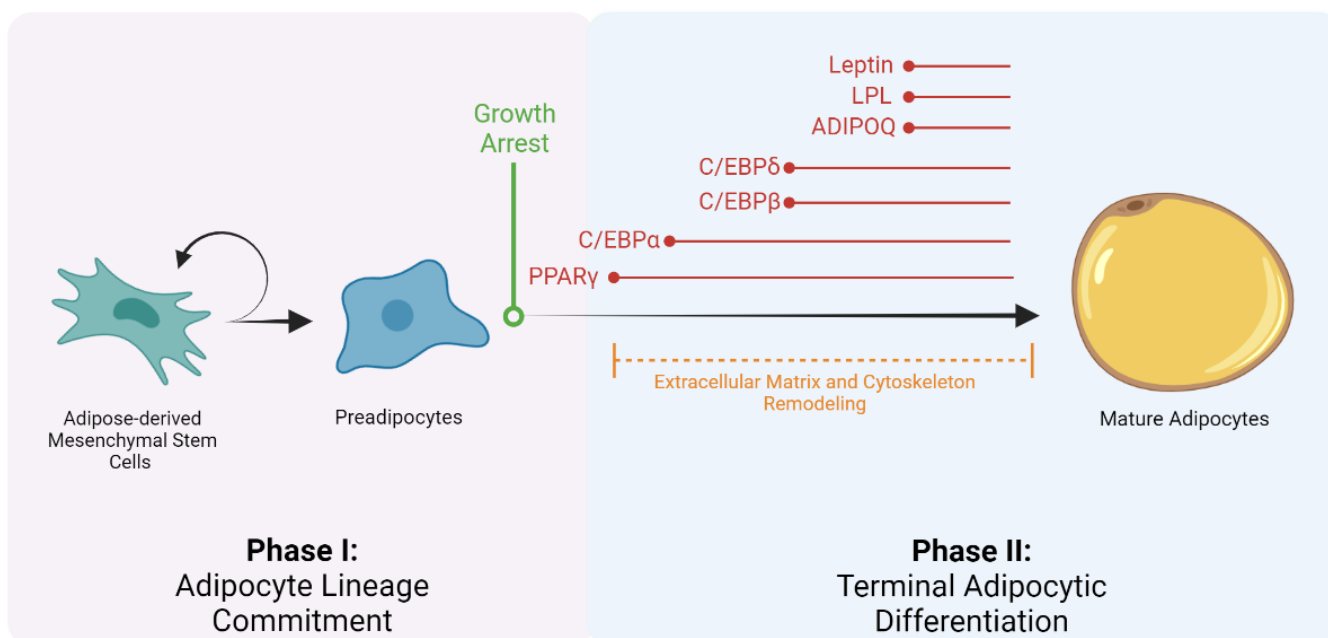


Figure 1.2: Basic overview of adipogenic differentiation. Adipose-derived stem cells (AD-MSCs) undergo asymmetric mitosis during adipocyte lineage commitment (Phase I), producing both a lineage-committed preadipocyte and a pluripotent AD-MSC. Following growth arrest, adipocytic genes (red) are expressed at varying stages throughout terminal adipocytic differentiation (Phase II). (Adapted from Bourgeois et al. 2019, created with BioRender.com). ADIPOQ – Adiponectin; C/EBP – CCAAT/enhancer-binding protein; FABP4 – Fatty acid-binding protein 4; LPL – Lipoprotein lipase; PPAR γ – Peroxisome proliferator-activated receptor gamma.

In many cell-culture based studies of adipose-derived stem cells and adipogenesis, investigators stimulate adipogenic differentiation *in vitro* by the addition of an adipogenic media cocktail. Comprising factors such as insulin which promotes the uptake of glucose for the synthesis of triglycerides, dexamethasone which stimulates the expression of C/EBP δ , 3-isobutyl-1-

methylxanthine (IBMX) which inhibits cAMP and cGMP and induce the expression of C/EBP β , and a PPAR γ agonist in the form of either indomethacin or a thiazolidinedione (TZD) to initiate adipogenesis and upregulate the adipogenic genes (Figure 1.2) ^{49–52}.

1.2.1 Thiazolidinediones

Thiazolidinediones (TZDs) are a class of drugs that were first introduced for the treatment of type II diabetes mellitus (T2DM) ⁵³. By selectively binding to the nuclear receptor peroxisome proliferator-activated receptor-gamma (PPAR γ), these insulin-sensitizers can improve and sustain glycaemic control through increased expression of glucose transporters ^{6,53–55}.

PPAR γ has measurable expression in tissues such as the liver, skeletal muscle, colon and heart but is expressed most abundantly in adipose tissue ⁵⁶. The ligand-based activation of PPAR γ in preadipocytes by addition of TZDs is frequently employed *in vitro* technique to induce adipogenesis, as PPAR γ is a key transcriptional mediator in preadipocytic growth arrest and differentiation ^{52,57–59}. PPAR γ activation consequently results in the recruitment of transcriptional co-activators and co-repressors which stimulate the expression of the early adipocyte differentiation markers C/EBP α , C/EBP β , and C/EBP δ (Figure 1.2) ^{57,59,60}.

In both human and animal studies, the use of TZDs such as pioglitazone, troglitazone, and rosiglitazone as a monotherapy has resulted in significant increases in adipose tissue mass, adipocyte size and adipocyte number ^{50,61–66}. A redistribution in adipose tissue was also observed in clinical studies, as the mass of the intra-abdominal adipose tissues decreased whilst the subcutaneous adipose tissues expanded ^{64–66}. This ability for tissue remodelling by TZDs can be used as a tool to elucidate the mechanisms behind adipose tissue plasticity and has been utilised in the project presented here.

1.3 Adipose Tissue Types

Whilst some similarities in the cellularity and structure of adipose tissue exist, in most animals adipose tissue is present in three forms, namely; brown (BAT), beige (BeAT), and white adipose tissue (WAT) which collectively constitute a dynamic, specialized, multicellular organ ^{24,67}. Each adipose tissue type is noted to perform specific metabolic functions which jointly contribute to the regulation of whole-body glucose homeostasis, insulin sensitivity, and lipid metabolism ^{24,68}.

1.3.1 Brown and Beige Adipose Tissue

Briefly, mature adipocytes in both BAT and BeAT, differ from white adipocytes in gene expression, secretome and phenotype ^{69,70}. When active, these cells often appear polygonal with a variable diameter and are referred to as multilocular, owing to the mature cell's granular cytoplasm containing many small lipid vacuoles ^{71,72}. Whilst the intracytoplasmic lipid vacuoles of the BAT and BeAT

adipocytes facilitate the storage of excess triglycerides, the storage capacity is significantly lower than that of WAT adipocytes⁷³. Brown and beige adipocytes also characteristically encompass an abundance of mitochondria which are solely responsible for maintaining homeothermy by the transformation of stored triglycerides into heat⁷⁴. This transformation process is mediated by uncoupling protein 1 (UCP1), a characteristic BAT protein located in the inner membranes of the adipocyte's multitude of mitochondria⁷⁵⁻⁷⁷. Typically within adipocytes, lipolysis and β -oxidation of stored triglycerides produces the active factors required for the intracytoplasmic mitochondria to generate ATP via oxidative phosphorylation^{78,79}. In brown and beige adipocytes the UCP1 protein (when activated) disrupts this process by uncoupling the proton gradient from the ATP-synthase enzyme which results in the generation of heat as opposed to ATP⁸⁰. During this process, large volumes of lipoprotein lipase (LPL) are released which degrade chylomicrons and very-low-density lipoprotein (VLDL) – a lipoprotein that functions to transport triglycerides throughout the body^{76,81,82}. The rate of glucose uptake by the adipocytes is also increased, leading to lower serum glucose levels⁸². As a result of the beneficial metabolic implications of the elevated energy expenditure of BAT and BeAT, these tissues have been recognised as a potential therapeutic target for the treatment of obesity and its associated metabolic disorder⁷³. This has been previously explored in rodents, with results indicating that the activation and/or expansion of brown adipocytes is associated with optimal levels of glucose, cholesterol, and triglyceride in the serum, effectively constituting a healthy metabolic phenotype⁸³⁻⁸⁵.

Although beige adipocytes share a similar morphology and the expression of some genes with brown adipocytes, studies have shown that they do not arise from the same myogenic factor 5 (Myf5)-expressing precursor cells and have distinct gene expression profiles⁸⁶⁻⁸⁸. BeAT will also generally remain inactive unless stimulated by exogenous cues such as a significant reduction in body temperature or by β 3 adrenergic stimulation^{89,90}. BAT is exclusively found in mammals and differs in both its abundance and position in every species^{71,75}. In most mammals, BAT is distributed around the perirenal, interscapular and cervical regions and is present in variable quantities throughout life cycle⁷⁴. It has previously been suggested that humans were the exception to this rule as it was thought that BAT was only present in discernible volumes as a foetus and new-born but gradually decreased to the point of becoming almost negligible as an individual progresses into adulthood^{24,31,71,72}. Studies conducted in the last decade have however identified BAT and BeAT depots in humans throughout their lives^{67,91-93}. Although the distribution of BAT differs between organisms, the apparent lack of anatomical boundaries between BAT and WAT is evident in all mammalian species with active brown and beige adipocytes being found interspersed within WAT depots (Figure 1.3)⁹⁴⁻⁹⁶.

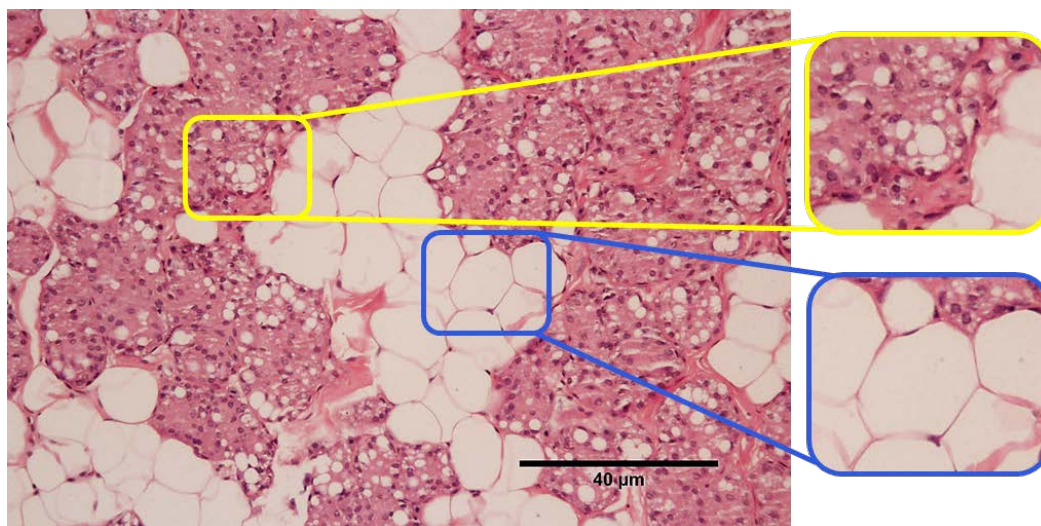


Figure 1.3: Intercalation of brown and white adipocytes within the inguinal adipose tissue of a male Wistar rat. Haematoxylin and eosin-stained inguinal adipose tissue showing intercalation of multilocular brown adipocytes (yellow) and unilocular white adipocytes (blue). The eosin-stained cytoplasm of each cell appears pink, and the dark purple spots indicate the haematoxylin-stained cell nuclei. Micrograph was taken at 20X magnification. Scale bar = 40 μm.

1.3.2 White Adipose Tissue

Prior to 1551, when BAT was discovered by Swiss researcher Konrad Gessner, as a result of its anatomical abundance, it was believed that WAT was the only type of adipose tissue⁷⁴. WAT functions as the foremost storage location for triglycerides, insulates the body from heat and cold, enables muscle bundles to move without friction, and provides a mechanical barrier to protect vital organs from trauma^{31,97}. Being the largest endocrine organ in the body, WAT has also been found to control appetite and fertility, modify blood pressure, induce thrombus formation, and influence immune responses through the secretion of bioactive peptides such as leptin and adiponectin^{98–101}. Mature white adipocytes are typically spherical and vary in size according to the volume of the single intracytoplasmic lipid droplet¹⁰². The quantity of WAT in humans is determined by several factors, some of which include age, sex, genetics, and environment¹⁰³. Whilst excessive accumulation of WAT has been associated with metabolic dysfunction^{5,104}, the location of the increased adiposity remains the key determinant in the WATs pathogenicity.

1.4 Subcutaneous and Visceral White Adipose Tissue

Both BAT and WAT are distributed in discrete depots throughout the body which can be broadly divided into either the subcutaneous adipose tissue (SAT) or visceral adipose tissue (VAT) depots. The SAT and VAT depots of humans and rodents are similar in relative size and position, with the exception that one of the greatest VAT depot in humans – the omental WAT – is undetectable in rodents^{24,105}. To compensate, rodents have a much larger perigonadal WAT depot (Figure 1.4)

24,105

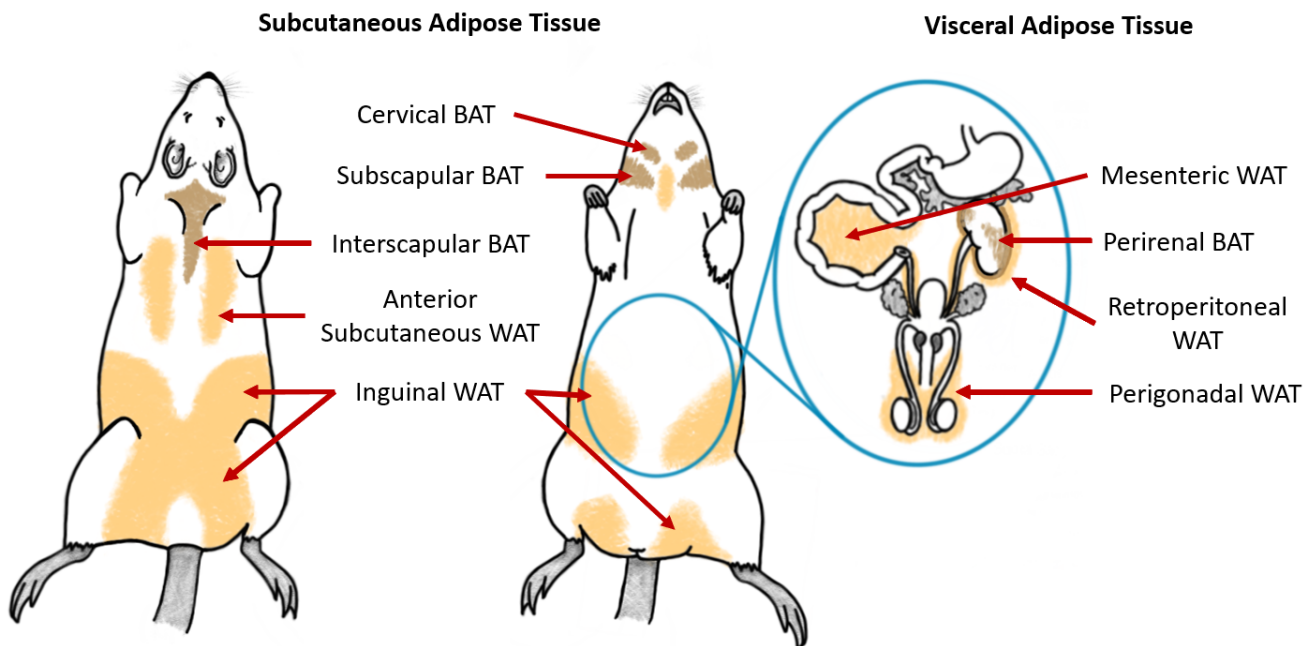


Figure 1.4: Distribution of brown and white adipose tissue within the subcutaneous and visceral depots of a male Wistar rat. (Adapted from Tchkonja et al. 2013). BAT – Brown adipose tissue; WAT – White adipose tissue.

Whilst the two distinct adipose depots share some similarities in structure and function (section 1.3.2), subcutaneous WAT (sWAT) and visceral WAT (vWAT) fundamentally differ in several aspects, besides their anatomical location. In particular, disparities in the molecular, physiological, clinical, and prognostic states of the sWAT and vWAT are repeatedly noted in studies on adipose tissue^{24,31,105,106}.

1.4.1 Subcutaneous White Adipose Tissue

Characteristically located between the dermis and skeletal muscle tissue, sWAT most notably accumulates around the hips, thighs, breasts, abdomen, and buttocks in humans and on the anterior side of the hind limbs in rodents¹⁰⁷. This adipose depot occupies approximately 80-85% of the total body fat in both lean and obese humans, therefore undisputedly constituting the largest adipose depot¹⁰⁸⁻¹¹¹. Subcutaneous adipocytes are known to be highly sensitive to insulin, less lipolytic, and more lipogenic than those of the vWAT depot¹¹²⁻¹¹⁵. These characteristics correspond with the often reported decreased expression of the lipolytic enzymes such as LPL and hormone-sensitive lipase (HSL), and the up-regulation of lipogenic genes such as leptin and adiponectin¹¹²⁻¹¹⁵. Despite its role in increasing an individual's BMI, prior studies have shown that an accumulation of lipids in sWAT depots is not as detrimental to metabolic health as the accumulation of vWAT¹¹⁶⁻¹¹⁹. In some cases, the accumulation of gluteofemoral sWAT has been associated with reduced cardiovascular and metabolic risk and a protective lipid and glucose profile¹²⁰. It has previously been hypothesised that the substantial quantities of brown adipocytes that are observed to be interspersed within the sWAT may contribute to the lack of associated pathogenicity in sWAT accumulation (Figure 1.3)

^{121,122}.

1.4.2 Visceral White Adipose Tissue

In humans, the vWAT depot encompasses the intra-abdominal mesenteric, retroperitoneal, perigonadal, and omental adipose tissues^{24,68}. Whilst, in most cases, this depot only constitutes a small proportion of the overall adipose load (~ 10%), visceral adiposity poses the highest risk for the onset of metabolic syndrome – a cluster of conditions that includes hyperglycaemia, hypertension, and dyslipidaemia^{123,124}. Many hypotheses exist to explain the pathogenicity of vWAT accumulation. One such hypothesis stems from the observation that vWAT has a substantial infiltration of monocytes and an elevated secretion level of pro-inflammatory cytokines such as tumour necrosis factor- α (TNF- α), resistin, and interleukin 6 (IL-6)^{125–128}. Due to its proximity to the vital organs, the accumulation of vWAT could cause widespread intra-abdominal inflammation which disrupts the homeostatic balance, leading to the development of metabolic syndrome^{127,129}. Another frequently cited hypothesis for the pathology of vWAT is referred to as the ‘portal theory’. Formed due to the proximal position of the vWAT to the hepatic portal vein, the portal theory suggests that the higher lipolytic activity and FFA turnover of vWAT results in the drainage of excess FFAs into the portal system^{125–128,130,131}. The delivery of the FFAs directly to the liver is thought to result in hepatic steatosis (fatty liver disease) and impaired suppression of glucose production (gluconeogenesis) as a result of hepatic insulin resistance^{125,128,132,133}.

1.5 Dynamics of Subcutaneous and Visceral Adipose Tissue Expansion

In vivo adipose tissue accumulation has been studied by using imaging techniques such as dual-energy X-ray absorptiometry (DEXA) scanning, computed tomography (CT) scanning, or magnetic resonance imaging (MRI)^{13,134–137} which indicate that during chronic excessive calorie intake, fat has the tendency to first accumulate in subcutaneous adipose depots, with visceral adiposity being subsequently expanded. Consequently, it has been suggested that triglyceride sequestration by adipose depots is hierarchical, with excess lipids primarily being deposited within the highly lipogenic subcutaneous adipocytes^{114,138–141}. It is believed that only after the subcutaneous adipocytes have become lipid replete, hypertrophic, and dysfunctional, that the triglycerides are diverted towards the visceral adipose depots^{138,140,141}.

It has been hypothesised that the level of insulin sensitivity of adipocytes in both the sWAT and vWAT determines the triglyceride storage capacity¹¹⁴. When compared to adipocytes found in sWAT, visceral adipocytes are known to exhibit a decreased sensitivity to the antilipolytic effects of insulin¹⁴². Thus, on the basis that increased insulin sensitivity leads to more triglyceride storage, lipids would preferentially accumulate in the more insulin sensitive subcutaneous adipocytes. The subcutaneous adipocytes would then become increasingly hypertrophic, progressively reducing their insulin sensitivity. Eventually, the subcutaneous and visceral adipocyte insulin sensitivities would be on par, at which point the visceral adipocytes would begin to sequester circulating triglycerides thus explaining the lag in vWAT accrual which is often observed¹⁴².

Whilst the mechanism behind the apparent switch in location of triglyceride accumulation remains unknown, speculation as to the role of intracellular signalling cascades in the determination of adipose tissue accrual is ongoing.

1.5.1 The Role of Intracellular Signalling in Adipose Tissue Accrual

All cells within adipose tissue have the ability to secrete soluble proteins, extracellular vesicles, lipids, and free nucleic acids^{68,99,143–145}. Collectively these factors are referred to as the cellular secretome. The primary role of the secretome is to facilitate communication locally, with neighbouring cells via paracrine signalling, or systemically, with cells of another tissue by endocrine signalling (Figure 1.3)

146–149

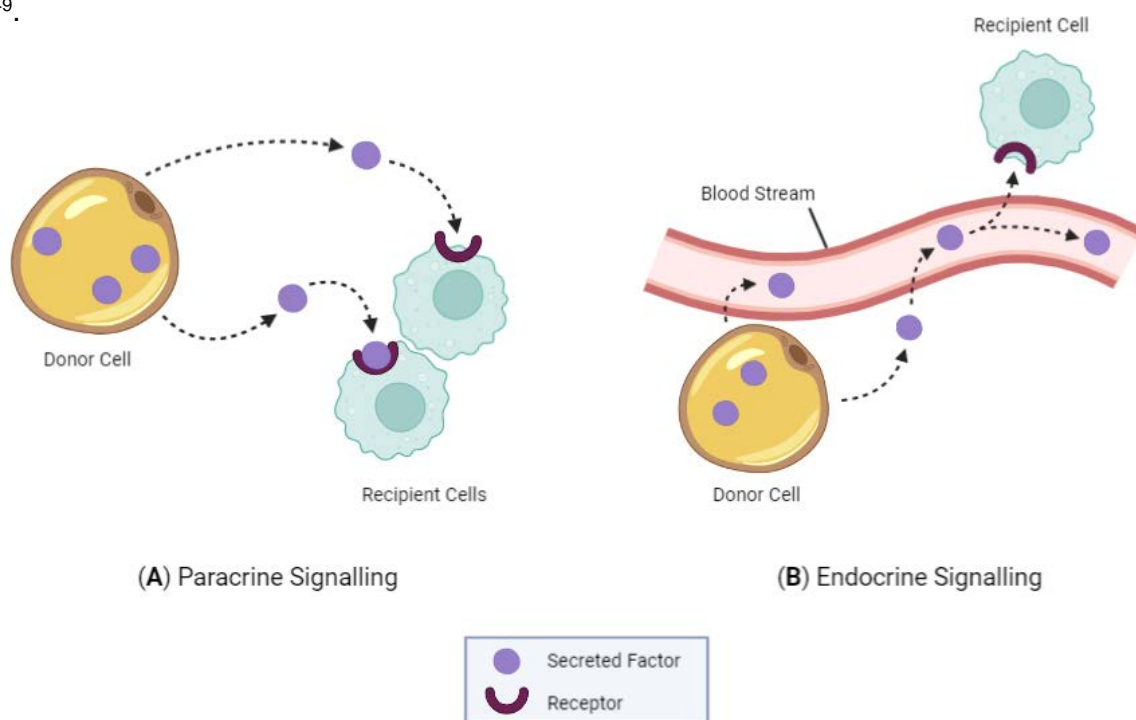


Figure 1.5: Paracrine and endocrine signalling. Factors are secreted by a donor cell and may induce responses (A) locally via paracrine signalling or (B) systemically via endocrine signalling (Adapted from Greensted et al. 2003, created with BioRender.com).

The discovery that adipocytes secrete leptin, an adipose-specific bioactive peptide (adipokines) which functions in the regulation of cellular energy expenditure and food intake, first revealed the endocrine signalling capacity of adipose tissue¹⁵⁰. Further investigation has identified several adipokines such as adiponectin, leptin, and hepatocyte growth factor (HGF) within the secretome of adipocytes, effectively defining the tissue's role as an endocrine organ^{68,94,115,151–153}. Adipocytes in both the subcutaneous and visceral adipose depots are known to secrete adipokines that participate in the maintenance of metabolic homeostasis^{24,139,146}.

Whilst the role of adipokines in the onset and progression of pathologies such as insulin resistance and inflammatory disorders like osteoarthritis has been extensively studied^{104,126,154–156}, the ability of these secreted factors to influence adipose tissue accumulation in specific depots is still under

investigation. A significant increase of intracytoplasmic lipid accrual in preadipocytes has been found to occur when these cells are directly co-cultured with mature adipocytes isolated from the same depot of origin ¹⁵⁷. This study made use of culture well inserts to prevent the preadipocytes and mature adipocytes from coming into direct contact with one another, thus ensuring that the effects were solely induced through the secretion of factors into the shared culture medium – suggesting paracrine induced lipid accrual ^{157–159}. By measuring the expression of glycerol-3-phosphate dehydrogenase (GPDH), a marker for adipogenesis and a key enzyme in the triglyceride biosynthesis pathway ¹⁶⁰, these researchers ensured that the lipid accumulation was induced by the occurrence of adipogenesis and was not solely due to the cells sequestering lipids from the media. When co-culturing AD-MSCs isolated from human subcutaneous adipose tissue with mature adipocytes of the same depot, Stacey *et al.* (2009) also concluded that the adipogenic paracrine signalling interactions occurred between the adipocytes and adipocyte progenitors ¹⁶¹.

Further experiments have used recipient AD-MSCs from lean rats to compare the adipogenic effects of secreted factors from adipocytes isolated from lean- and corpulent donor rats ¹⁶². This comparison examining the effects of increased adiposity on the paracrine signalling-induced lipid accrual found that mature adipocytes from genetically obese (cp/cp) rats are able to stimulate considerably more lipid accumulation in the naïve AD-MSCs as compared to the lean rat adipocytes ¹⁶². Shillabeer *et al.* (1990), the authors of this study, hypothesised that the disparities observed between the lean and obese rats were due to fewer differentiation factors being secreted by the lean adipocytes as a result of the diminished size of these cells ¹⁶².

The growing body of evidence for the paracrine signalling interactions between adipocytes and precursor cells has been extensively reviewed by Haylett and Ferris (2020) ¹⁶³. Only a few studies have, however, investigated the effects of the adipocyte secretome of one adipose tissue depot on progenitor cells isolated from an anatomically distant tissue. By culturing segments of subcutaneous adipose tissue and then transferring the secretome-conditioned media onto bone-marrow mesenchymal stem cells (BM-MSCs), Wu and colleagues were able to stimulate adipogenesis in the BM-MSCs ¹⁶⁴. These results highlight the ability of factors secreted by adipose tissue explants to stimulate adipogenesis in progenitors from discrete adipose depots, effectively providing evidence for the potential role of endocrine signalling in the determination of adipose tissue distribution ¹⁶⁴.

1.6 The Present Study

1.6.1 Rationale for Research

The volume, distribution, and functionality of adipose tissue has been identified as one of the key determinants of metabolic health in overweight and obese individuals ^{5,11}. Despite the link between visceral adiposity and the onset and progression of metabolic syndrome, the mechanisms behind visceral fat accrual remain elusive ¹⁶⁵.

We hypothesise that the frequently observed lag in visceral adipose tissue expansion could be due to the influence of endocrine factors secreted by the subcutaneous adipose stores. It is plausible that functional subcutaneous adipocytes secrete factors that suppress adipogenesis in the visceral AD-MSCs, but once adipocytic hypertrophy and dysfunction occur, the signalling ceases permitting the visceral AD-MSCs to differentiate. We suggest an alternative mechanism in which the hypertrophy and dysfunction of the subcutaneous adipocytes, which has previously been observed to increase adipokine secretion^{153,166,167}, induces the secretion of endocrine factors which stimulate adipogenesis in the visceral AD-MSCs. It is also unknown whether the visceral adipocytes, once fully differentiated, secrete factors that may down-regulate adipogenic genes in the subcutaneous AD-MSCs, consequently making the visceral depots the primary sites for triglyceride accrual.

Furthermore, as several factors are known to influence the cellular secretome, thereby impacting its signalling capacity, this study wishes to investigate how increased adiposity resulting from the chronic consumption of a high-caloric diet may affect the depot-depot interactions. In addition, as thiazolidinediones have been associated with adipose tissue redistribution in patients treated for insulin resistance, we hypothesise that these drugs may also affect intra-adipose depot communication. By investigating the endocrine communication between the adipocytes and AD-MSCs in the subcutaneous and visceral depots, the present study wished to elucidate some of the mechanisms which regulate visceral adiposity, consequently providing insight into the aetiology of obesity and its related comorbidities and potentially better disease management.

1.6.2 Aims and Objectives of the Present Study

This study primarily aimed to determine whether factors secreted by mature subcutaneous adipocytes have the ability to induce *in vitro* lipid accumulation in visceral AD-MSCs, and vice versa. It also sought to assess how the chronic consumption of a high-fat or elevated sugar diet affects the putative depot-depot endocrine communication, and evaluate the impacts of these diets on the *in vitro* AD-MSC morphology, proliferation, and capacity for adipocytic differentiation. Lastly, this study aimed to investigate the effects of rosiglitazone (a thiazolidinedione) on the ability of subcutaneous adipocytes to stimulate lipid accrual in visceral AD-MSCs, and vice versa.

In order to achieve the aims of this investigation, the following objectives were set forth:

- To feed either a control, high-fat diet (HFD), or elevated sugar diet (ESD) to groups of male Wistar rats (n = 7/ group) for 16-weeks and subsequently compare the final body weights, terminal fasting blood glucose levels, and weights of the excised inguinal and retroperitoneal adipose depots.
- To stain inguinal and retroperitoneal adipose tissues with haematoxylin and eosin to visualise and measure the sizes of the constituent adipocytes.

- To isolate and culture AD-MSCs from the excised inguinal and retroperitoneal adipose tissues.
- To characterise the proliferation, cell surface marker expression, and adipogenic capacity of AD-MSCs from inguinal- and retroperitoneal adipose depots of rats fed control, HFD, and ESD by examining growth curves, flow cytometric analyses, and adipocytic differentiation respectively.
- To assess whether the adipocytic secretome can induce lipid accrual in naïve, undifferentiated AD-MSCs by differentiating the control (n = 7), HFD (n = 7), and ESD (n = 7) inguinal and retroperitoneal AD-MSCs into adipocytes *in vitro* and collecting conditioned media (encompassing the adipocyte secretome) which would then be used to treat naïve recipient AD-MSCs from both depots for 14 days (n = 3/depot).
- To assess the adipogenic impacts of supplementing the inguinal and retroperitoneal conditioned media with 1 μ M Rosiglitazone (Rosi) before treating the naïve inguinal and retroperitoneal AD-MSCs (n = 3).
- To quantify the adipogenic effects of conditioned media treatments (with and without Rosi) by staining the cells with oil red O (ORO) and crystal violet, conducting *in-silico* micrograph analyses, and measure the absorbances of the eluted stains via spectrophotometry.

Methods and Materials

2.1 Materials and Reagents

Table 2.1: Reagents used throughout the present study.

Product	Supplier	Product Code
Reagents		
2-Propanol	Sigma-Aldrich	190764
3-isobutyl-1-methylxanthine (IBMX)	Sigma-Aldrich	15879
Bovine serum albumin - HyClone®	Roche	10735086001
Casein from bovine milk	Sigma-Aldrich	102248237
Horizon V450 conjugated anti-CD45 IgG	BD Biosciences	561587
Fluorescein isothiocyanate (FITC) conjugated Mouse anti-rat CD90	BD Biosciences	554897
Cholesterol	Sigma-Aldrich	1003027770
Collagenase Type I	Gibco	17100-017
Crystal Violet	Sigma-Aldrich	C0775
D-(–)-Fructose	Sigma-Aldrich	102291275
Dexamethasone	Sigma-Aldrich	D4902
Disodium hydrogen phosphate (Na ₂ HPO ₄)	Merck	1.06586.0500
Dulbecco's modified Eagle's medium	Lonza	BE12-604F/U1
Ethanol 99.9%	Merck	1.00983.2500
Ethanol 95%	Kimix	ALH955
Foetal bovine serum	Gibco	10493-106
Hank's balanced saline solution	Sigma-Aldrich	H6648
Indomethacin	Sigma-Aldrich	I7378
Insulin	Sigma-Aldrich	I9278
L-ascorbic acid	Sigma-Aldrich	1001297149

Oil Red O	Sigma-Aldrich	O0625
Penicillin/streptomycin	Lonza	DE17-602E
Potassium Chloride (KCl)	Merck	TA544033
Potassium dihydrogen orthophosphate (KH ₂ PO ₄)	BDH	10203
Rosiglitazone	Cayman Chemicals	71740
Sodium Chloride (NaCl)	Sigma-Aldrich	57653
Sodium pentobarbitone (Eutha-naze, Ref.No. 83/91)	Bayer (Pty) Ltd.	22079248DJ
Trypsin EDTA (200 mg/L Versene, Ethylenediaminetetraacetic acid)	Lonza	BE17-161E
Trypan Blue stain 0.4% - Invitrogen	Thermo Fisher Scientific	T10282

2.2 Ethical Approval

The following protocol was approved by the animal ethics review board of the University of Stellenbosch, Tygerberg Medical School (ACU-2020-6986) in compliance with the South African Animal Protection Act (Act No. 71 of 1962). All methods and procedures used to isolate adipose-derived mesenchymal stem cells (AD-MSCs) from murine adipose tissue have previously been optimised in our laboratory ¹⁶⁸.

2.3 General Overview of Study Methods

Inguinal subcutaneous and retroperitoneal visceral white adipose tissue isolated from male Wistar rats were used as the source of the adipose-derived mesenchymal stem cells (AD-MSCs) in the present study. The flow diagram in Figure 2.1 surmises the tissue and cell isolation processes, subculture, and cell characterisation techniques applied to cells isolated from a control group of rats (n = 7). These methods were repeated in two more groups of male Wistar rats following 16-weeks of being fed either a high-fat diet (n = 7) or an elevated sugar diet (n = 7) (section 2.4). Briefly, the AD-MSCs liberated from the subcutaneous and visceral adipose tissue were maintained under sterile cell culture conditions at previously optimised temperatures, humidity's, CO₂ levels, and pH's to simulate the *in situ* cellular environments. By maintaining a constant fresh supply of nutrients and co-factors by replacing the cell culture media regularly, the AD-MSCs were able to proliferate freely in culture until ~80% confluence was reached. At this stage, the cells were subcultured as per section 2.8 to prevent over-confluence from occurring as this could lead to contact inhibition and senescence. The cells were subcultured three times before they either were seeded into multi-well plates in triplicate to conduct growth curves (section 2.10), were used for flow cytometric analyses

(section 2.11), or underwent adipocytic differentiation prior to the collection of conditioned media (section 2.12 and 2.13).

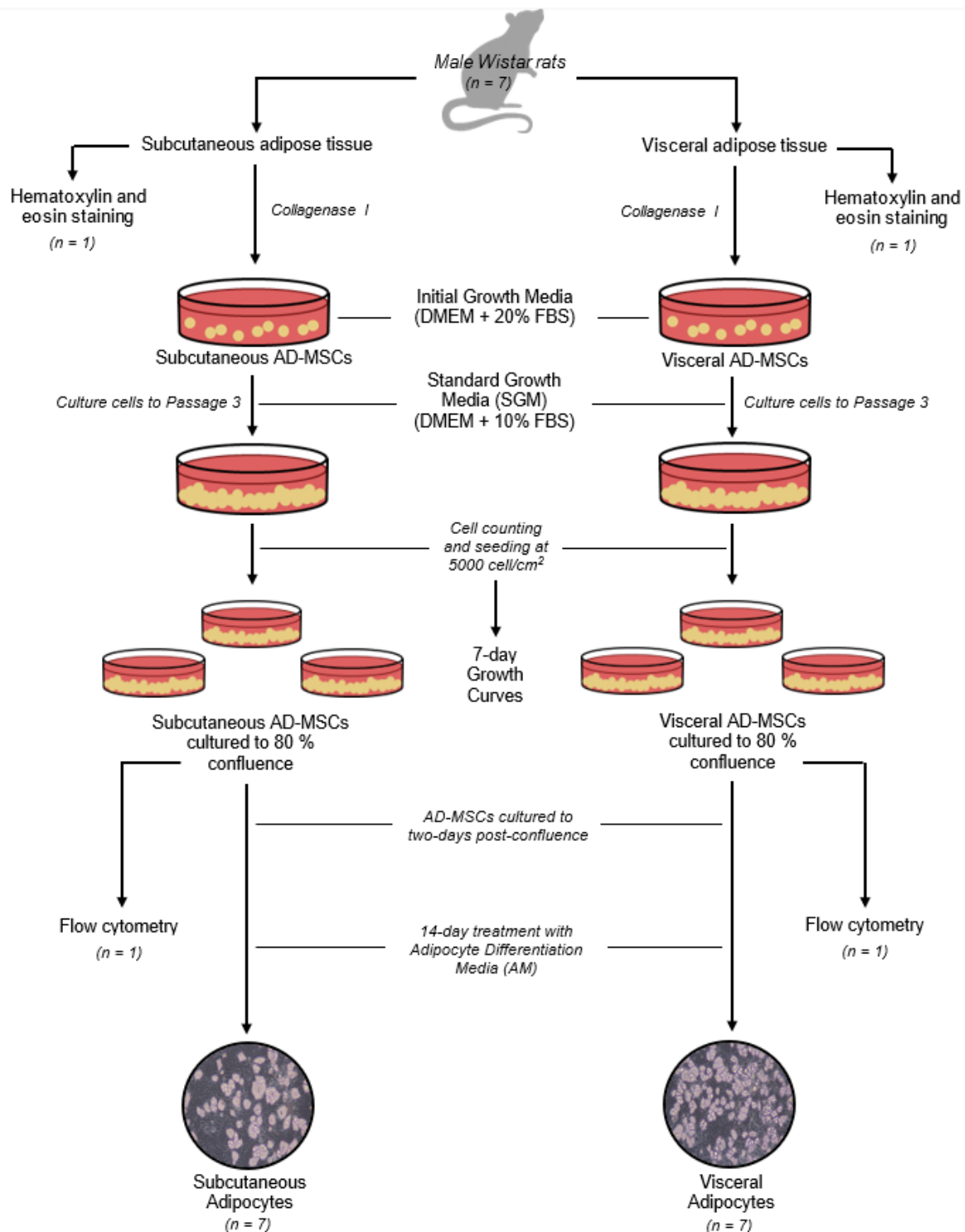


Figure 2.1: Isolation and purification of subcutaneous and visceral adipose-derived mesenchymal stem cells. AD-MSCs – Adipose-derived mesenchymal stem cells; DMEM – Dulbecco’s Modified Eagle Medium; FBS – Foetal bovine serum.

Following isolation, culture, and differentiation of the subcutaneous and visceral AD-MSCs, conditioned media (CM) – media containing factors secreted by the *in vitro* differentiated adipocytes – was collected from the adipocytes of each depot and pooled (Figure 2.2). The conditioned media

(CM) collection process is explained in further detail in section 2.13. The treatment groups, consisting of 100% CM or CM combined with equal parts of either standard growth media (SGM) or adipogenic media (AM), were added to the recipient subcutaneous- ($n = 3$) and visceral AD-MSCs ($n = 3$) for 14 days as explained in Results section 3.5. The effects of the conditioned media treatments were then qualitatively analysed by oil red O and crystal violet staining and microscopy, and quantitatively analysed by *in-silico* analyses and spectrophotometry (section 2.15). A full list of the treatment groups and their components can be found in Appendix Table D.1. This treatment and quantification process was then repeated with the 100% CM, 1:1 CM: SGM, and 1:1 CM: AM treatments being supplemented with 1 μM Rosiglitazone – a PPAR γ agonist known to stimulate adipogenesis.

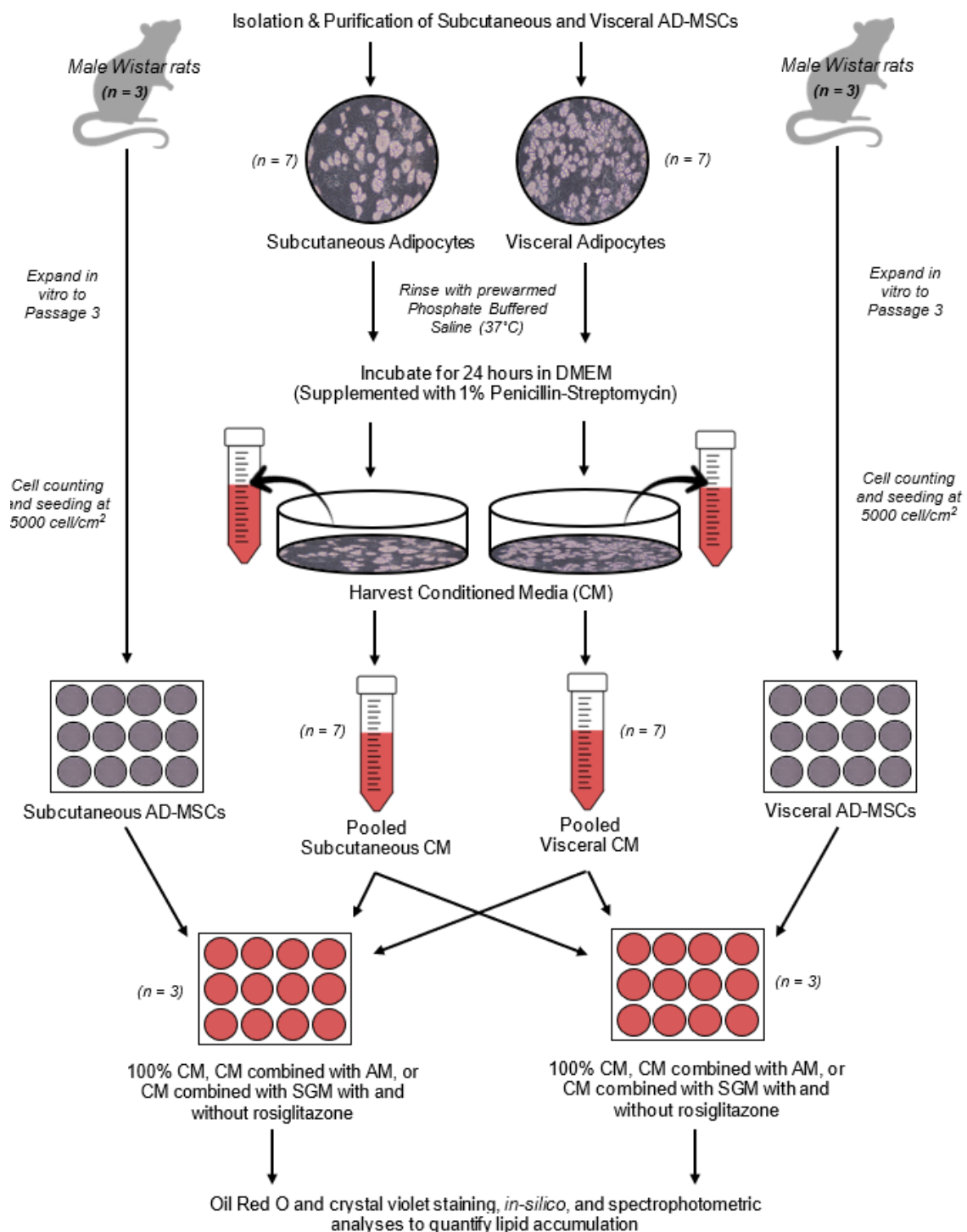


Figure 2.2: Collection of conditioned media from mature subcutaneous and visceral adipocytes and treatment of cells. AD-MSCs – Adipose-derived mesenchymal stem cells; AM – Adipogenic media; DMEM – Dulbecco's Modified Eagle Medium; SGM – Standard growth media.

2.4 Experimental Animals

The adipogenic potential of mesenchymal stem cells isolated from both male and female rats has been compared in prior studies. These investigations noted the pro-adipogenic effects of oestrogen, resulting in discrepancies in the efficiency of adipogenesis between the sexes^{169,170}. As the present project aims to assess the impact of certain factors on adipogenesis, male Wistar rats served as the sole source of adipose tissue, thus eliminating the potential confounding effects of fluctuating oestrogen levels. All rats used in this study were bred and housed at the University of Stellenbosch, Tygerberg Medical School's animal unit.

The animals were caged in groups of up to four in a Type 4 cage with a floor area of 1815 cm² covered in wood chip bedding. The ambient temperature was maintained at 22–25 °C for the duration of the study and the rats were subjected to a 12-hour light/dark cycle. A small control group (n = 3), fed autoclaved standard lab chow and double-distilled water (ddH₂O) *ad libitum*, were euthanised at 12-weeks-old by injection with 200 mg.kg⁻¹ sodium pentobarbitone (Eutha-naze Ref-83/91, #22079248DJ, Bayer, South Africa), followed by cardiac exsanguination to confirm death. The tissue harvested from these rats was used to conduct preliminary studies, growth curves, and underwent histological staining for comparison against the experimental adipose tissues.

The rats used in the diet study were weaned at 3 weeks of age and randomly split into three treatment groups of n = 7. A sample size of n = 7 was selected for this investigation as it would provide seven biological repeats for each adipose depot, effectively producing enough statistical power to ensure that any observed effect was not due to chance. The rats were then fed either (i) an elevated sugar diet (ESD n = 7), (ii) a high-fat diet (HFD n = 7) or (iii) a control diet (n = 7), the composition of which is outlined in Table 2.2. The HFD and ESD food was prepared weekly and replaced every two days for 16 weeks as per the protocol previously published by Salie *et al.* (2014) and Blignaut *et al.* (2019)^{171,172}. By starting the ESD, HFD, and control diets at 3 weeks of age and continuing them 16 weeks, this study ensured that the rats consumed the diets for a majority of their lives effectively mimicking the consumption of a high-calorie Western diet from childhood into adulthood in humans. The control animals were fed standard chow pellets (#US/RB2005, Rodent Breeder, LabChef Research Nutrition™, Stellenbosch, South Africa) for the duration of the study, with the food also being replaced every two days. During the study, the daily water and food consumption for each cage was monitored and the rats were weighed weekly so changes in body mass could be tracked. The fasting blood glucose levels of each rat were measured using a handheld glucometer (Accu-chek Instant, Roche, Germany) by obtaining a drop of blood via a tail prick following overnight fasting¹⁷³. These

levels were measured before the initiation of the diet, at 3 weeks old, and before euthanasia, at 19 weeks old.

Table 2.2: Nutritional composition of the control, high-fat diet, and elevated sugar diet.

Diet	Fat (g/100g)	Cholesterol (mg/100g)	Protein (%)	Carbohydrates (%)	Sugar (g/100g)	Fructose (g/100g)	Energy (kJ/100g)
Control	4.8	3	17.1	34.6	6.6	0.5	1272
HFD	27.9	6.4	14.6	29.5	13.3	11.0	1829
ESD	11.6	13	8.3	42	24.4	-	1354

ESD – Elevated-sugar diet; HFD – High-fat diet

At 19-weeks-old the HFD, ESD, and control rats were euthanised by injection with 200 mg.kg⁻¹ sodium pentobarbitone and subsequent cardiac exsanguination. The rat cadavers were then transferred to a sterile biosafety cabinet and adipose tissue from the subcutaneous and visceral adipose depots was isolated.

2.5 Adipose tissue isolation

White adipose tissue from the left and right posterior subcutaneous inguinal depots and bilateral retroperitoneal visceral depots were excised from the rat cadavers of each diet group. Immediately following excision, the tissue samples were sterilized by a brief rinsing in 70% ethanol followed by immersion in Phosphate Buffered Solution (PBS) (pH 7.4) to remove excess ethanol. Thereafter, the adipose tissue was placed into a centrifuge tube containing holding media (Dulbecco's modified Eagle medium (DMEM) supplemented with 1% penicillin-streptomycin (PenStrep)). The sample tubes were then transported on ice to the biosafety level 1 (BSL1) cell culture laboratory for further processing. All harvested fat pads were weighed before processing to enable a comparison of the mean differences in adipose depot mass between diet groups. The weights of the retroperitoneal and inguinal fat pads were also divided by the total body weights of each rat and expressed as a percentage to indicate the proportion of the respective depots within each individual. A representative ~3 g sample of inguinal and retroperitoneal adipose tissue from each diet group was placed directly into a 10% Neutral Buffered Formalin (NBF) solution (see Appendix Table C.1 for preparation) following excision. These samples, together with those isolated from the 12-week-old controls from the preliminary study, were left to undergo fixation for a minimum of ~48 hours at room

temperature. The NBF-fixed tissues were then subjected to further processing and stained with haematoxylin and eosin for morphological comparison between samples.

2.6 Histological Staining of Subcutaneous and Visceral Adipose Tissue

2.6.1 Tissue Processing for Histological Staining

The tissues excised from the cadavers were fixed in 10% NBF as described in section 3.5. To quantify hypertrophy (an increase in cell size) within the inguinal and retroperitoneal adipose tissue samples, the number and area of fat-depleted vesicles in which the lipids were present before fixation was measured. A formaldehyde-based fixative (NBF) was selected for use in this investigation as it is stable at room temperature, is known to penetrate adipose tissue well, and maintains the morphology of the tissue by means of cross-linking amino acid residues ¹⁷⁴.

The entire tissue processing and staining procedure was conducted in the Stellenbosch University Histology laboratory (Faculty of Medicine and Health Sciences) with assistance from Mr Reggie Williams. Following fixation, the tissue samples from each depot were sectioned into representative samples of approximately 2 mm thick and enclosed in labelled embedding cassettes ¹⁷⁵. Before any further processing could occur, the adipose tissues were dehydrated as the paraffin in which the tissues were to be embedded is hydrophobic thus preventing it from penetrating hydrated tissues. This was achieved by replacing the water within the tissues by submersion in a series of increasing concentrations of alcohol as shown in Table 2.3. Thereafter, the alcohol was replaced with xylene which acts as an intermediary solvent due to its miscibility with both ethanol and paraffin.

Table 2.3: Dehydration and xylene infiltration of adipose tissues for histological staining.

Step	Solution	Time
1	70% Ethanol	15 min
2	96% Ethanol	15 min
3	99% Ethanol	15 min
4	99% Ethanol	15 min
5	99% Ethanol	30 min
6	99% Ethanol	45 min
7	Xylene	20 min
8	Xylene	20 min
9	Xylene	45 min

Once the ethanol had been completely replaced by xylene, the specimen was embedded in paraffin wax at 60 °C using the Leica EG1160 embedder. After cooling at 20 – 25 °C, the solid paraffin blocks containing the adipose tissue specimens were cut into uniform 5 µm sections using a Leica RM 2125 RT microtome. The sections were transferred into a 40 °C water bath to stretch out any folds in the wax before being mounted onto frosted glass slides and labelled. The slides were then stained with haematoxylin and eosin (H&E).

2.6.2 Haematoxylin and Eosin staining of Adipose Tissue

H&E staining was selected for this study as it provides a comprehensive overview of the microanatomy of tissues. By staining the adipose tissue samples harvested from various depots, comparisons in the size, and configuration of adipocytes could be made. Haematoxylin binds to the negatively charged nucleic acids found in the nucleoli and heterochromatin of all eukaryotic cells whilst the eosin counterstains the anionic cytoplasmic components ¹⁷⁶.

To ensure the staining was reproducible and void of variation and human error, the following staining protocol took place within a Leica Auto Stainer XL. For the H&E stains to effectively penetrate the adipose tissue sections, they must first be deparaffinized, rehydrated, and cleared. These procedures were executed by completion of steps one to six in Table 2.4. Step one – the deparaffinization – was completed before the slides were inserted into the Auto Stainer by incubation in a freestanding 60 °C oven, as stated in subsection 2.6.1.

Table 2.4: Haematoxylin and Eosin staining protocol conducted within the Leica Auto Stainer XL.

Step	Solution	Time	Number of Repetitions
1	Oven (60°C)	2 min	1
2	Xylene	5 min	2
3	Ethanol (99%)	2 min	2
4	Ethanol (96%)	2 min	1
5	Ethanol (70%)	2 min	1
6	Water	2 min	1
7	Haematoxylin	8 min	1
8	Running water	5 min	1
9	Eosin	4 min	1
10	Running water	1 min	1
11	Ethanol (70%)	30 sec	1
12	Ethanol (96%)	30 sec	2
13	Ethanol (99%)	30 sec	1
14	Xylene	1 min	1

Once the staining protocol had been completed, the adipose tissue sections were mounted onto edge-frosted glass slides with glass coverslips using DPX Mountant and left to dry at room temperature for ~48 hours. Thereafter, the slides were imaged at 20X magnification using a Canon 600D camera mounted on an Olympus inverted phase-contrast microscope (CKX41, CACHN 20X/0.40 PhP objective).

2.6.3 *In silico* Analyses of H&E-Stained Adipose Tissue

Photomicrographs of the H&E stained inguinal and retroperitoneal adipose tissue harvested from 12-week-old control, 19-week-old control, HFD- and ESD fed rats (n = 3 per group) were imported into AdipoGauge (© Moussa Lab, Texas Tech University, November 25, 2020) for analyses (Figure 2.3) ¹⁷⁷. Following manual calibration by setting the scale of the images using a micrograph of the haemocytometer taken at the same magnification as the histology samples, the images were subjected to automated processing by AdipoGauge, as described in detail by Yosofvand *et al.* (2020). The calibration factor as determined by the software when inputting the known distance of the grids in the haemocytometer image was set at 0.074897 for all analysed images. Any adipocytes which had not automatically been identified by the algorithm as a result of cell membrane rupture during the staining process were manually defined in Microsoft Paint. Cells that were incomplete as a result of being on the micrograph's boundaries were excluded from the analyses. AdipoGauge was able to both count the number of adipocytes present in the micrographs and measure the area of each identified adipocyte. The outputs were then transferred into IBM SPSS Statistics for Windows (Version 27.0. Armonk, NY: IBM Corp) and the mean area and cell counts of the adipocytes were compared between age and diet groups to assess statistical significance. The adipocytes were also categorised by size (μm^2) and data were expressed as the frequency of adipocytes per category in relation to the total number of adipocytes counted in each micrograph (% total) ¹⁷⁸.

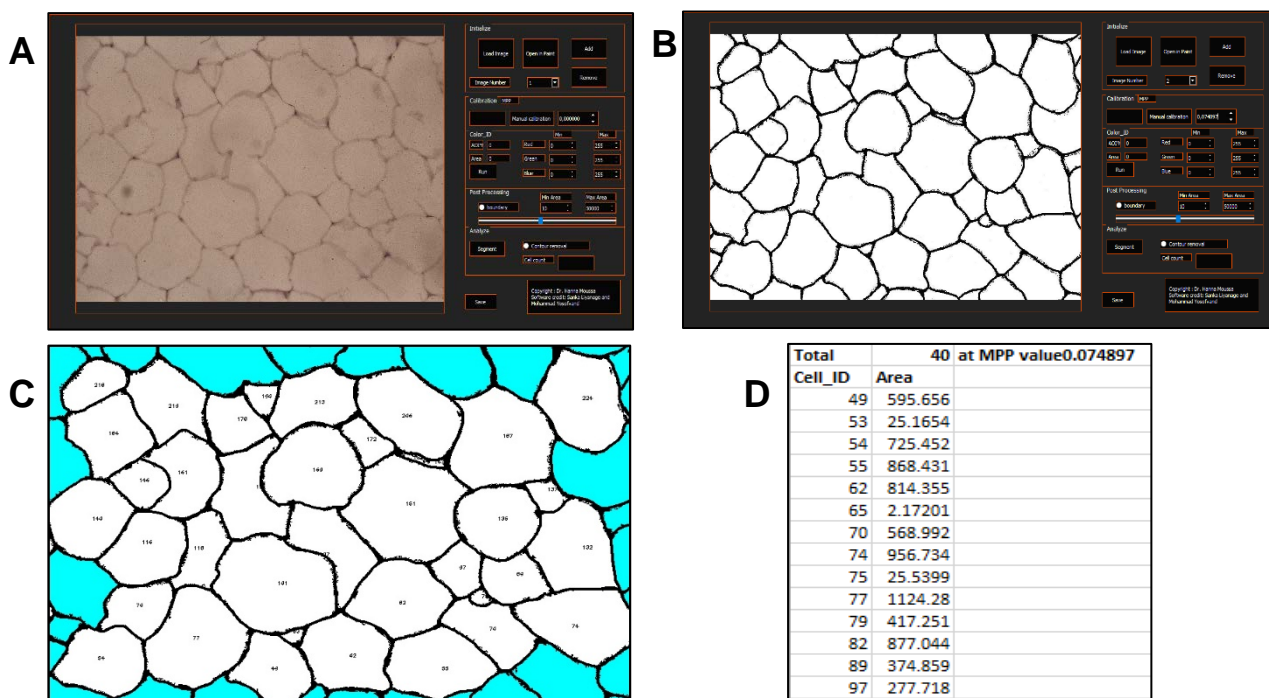


Figure 2.3: The process of analysing haematoxylin and eosin-stained adipose tissue using AdipoGauge software (© Moussa Lab, Texas Tech University, November 25, 2020). First (A) the micrograph of the H&E-stained adipose tissue is loaded onto the software, then using the calculated calibration factor of 0.074897, the image undergoes segmentation (B), any cell membrane ruptures are manually corrected using the linked Microsoft Paint and the corrected image is reloaded onto the user interface. (C) The segmented image can then be analysed, and boundary adipocytes (coloured blue) are excluded from the measurements in post-processing. (D) The software then provides a .csv output of the area (μm^2) of each adipocyte numbered according to the associated cell IDs of the analysed image

2.7 Isolation and Culture of Adipose-derived Mesenchymal Stem Cells (AD-MSCs)

2.7.1 Isolation of Subcutaneous and Visceral AD-MSCs from White Adipose Tissue

To liberate the component cells from the inguinal and retroperitoneal adipose tissues, the extracellular matrix, which maintains tissue integrity, had to undergo digestion. This digestion was initiated by shredding the tissues into $\sim 1 \text{ mm}^3$ pieces using sterile scalpel blades in 100 mm^2 culture dishes under sterile conditions within a laminar-flow biosafety cabinet. The shredded tissues, which exhibited an increased surface area, were then transferred into 15 mL centrifuge tubes containing 10 mL collagenase digestion solution (1.5 mL of 10% BSA in PBS + 1 mL 10 x collagenase type 1 stock solution + 7.5 mL HBSS). To aid the tissue's decomposition, the sample tubes were placed in a 37°C water bath for 30 minutes and were inverted intermittently. The digested samples were subsequently subjected to centrifugation at $400 \times g$ for 5 minutes, after which the cell pellet from each tube was carefully transferred into a clean 15 mL centrifuge tube using sterile plastic Pasteur pipettes. To rid the cell pellets of debris, 5 mL of prewarmed, sterile PBS (37°C) was added, and the samples were subjected to centrifugation again for 5 minutes at $400 \times g$. The PBS was then aspirated and discarded, taking care not to disturb the cell pellets which were then resuspended in 2 mL of Initial Growth Media (IGM), comprising holding media and 20% Foetal Bovine Serum (FBS). The cell suspensions were then seeded into 100 mm^2 culture dishes together with 9 mL of IGM.

Following 24 hours of incubation, the dishes were visualised under an Olympus light microscope (CKX41, CACHN 10X/0.25 PhP objective) to confirm cell adherence to the plate. Once cultures had been established, the media was changed by aspirating off the IGM, washing the adhered cells with prewarmed, sterile PBS (37°C) and finally, the addition of 10ml Standard Growth media (SGM) (holding media supplemented with 10% FBS).

2.7.2 Standard Cell Culture Conditions

All AD-MSC cultures were maintained in SGM and incubated at 37°C in a Forma Series II water-jacketed CO_2 incubator (Model 3111, Thermo Scientific) with 95% humidity and 5% CO_2 . The cells were visualised under an Olympus inverted phase-contrast microscope daily to monitor viability and growth. To ensure the cells received the required growth factors and nutrients to facilitate

proliferation, the SGM was replaced twice a week. When the cells had reached approximately 80% confluence, to prevent contact inhibition of proliferation from occurring, the cells were subcultured.

2.8 Subculturing Cells

To subculture the AD-MSCs, the SGM from each dish was aspirated and discarded and the cells were rinsed with prewarmed, sterile PBS (37°C) to remove excess media and cell debris. To facilitate cell detachment, 0.5% trypsin solution was added to the culture dish, followed by incubation at 37°C for 2 minutes. The 0.5% trypsin solution was then deactivated by adding twice the volume of SGM, as the constituent FBS contains α 1-antitrypsin – a protease inhibitor which arrests trypsinisation¹⁷⁹.

Prior studies have made use of a subculture ratio between 1:3 and 1:10 for this cell type^{52,168}. As a result, a ratio of 1:3 was selected for this study as this provided enough culture plates for experimentation without compromising cell density, where plating cells sparsely could affect cell viability. To achieve this, from the final 3 ml 0.5% trypsin / SGM cell suspension, 1 ml was removed and introduced to a new 100 mm² culture dish already containing 9 mL of SGM⁵². The cells, which had now been “passaged”, were maintained as per subsection 2.7.2. Once a confluence of ~80% had been reached by the cells in each culture dish, the above subculturing procedure was repeated until the cells reached passage three.

2.9 Cell Counting

Once the cells at passage two had reached ~80% confluence, trypsinisation occurred as above and the cell suspension was transferred into a 15 mL centrifuge tube and pelleted at 400 x g for 5 minutes. Thereafter, the supernatant was removed and discarded taking care not to disturb the cell pellet. SGM was then added to the pellet, so the final cell suspension volume was 1 mL. To quantify the number of cells present in this cell suspension, 10 μ L was transferred into a 0.5 mL microfuge tube to which 10 μ l of Trypan Blue was subsequently added. The 20 μ l Trypan Blue stained cell suspension was then transferred onto a Fuchs-Rosenthal haemocytometer and the cells were manually counted on the Olympus inverted phase-contrast microscope. Using this cell count, calculations were conducted as previously described¹⁸⁰ and the cells were subsequently seeded into culture plates at a density of 5000 cells/cm² – a seeding density frequently used in mesenchymal stem cell investigations^{181–183}.

2.10 Growth Curves

Growth curves were conducted to quantify and compare AD-MSC proliferation rates between anatomical locations (subcutaneous vs. visceral), ages (12-week-old vs. 19-week-old) and diet groups (Control vs. HFD vs. ESD). Once ~80% confluence had been established at passage two, the AD-MSCs were counted as per section 3.9 and seeded into 24-well plates in triplicate at a density

of 5000 cells/cm². Thereafter, the plates were incubated and the AD-MSCs were trypsinised and counted by haemocytometer on days 1, 4 and 7 post-seeding. The data points were imported into IBM SPSS Statistics (Version 27) for statistical analysis and the growth curves were plotted in GraphPad Prism v9.00 (GraphPad Software Inc., California, USA). To compare the resulting growth curves whilst compensating for the effect of small sample size, the differences in the proliferation rates of the inguinal and retroperitoneal AD-MSCs between diet groups were assessed by conducting a Compare Groups of Growth Curves (CGGC) permutation test using the 'compareGrowthCurves' function of the statmod software package for R (<http://bioinf.wehi.edu.au/software/compareCurves/>)^{184,185}. As recommended by the authors, a total of 10 000 permutations were conducted on the cell count data from each depot's AD-MSCs to ensure definitive results.

The population doubling times (PDT) for each depot were calculated to facilitate comparisons between the diet groups whilst controlling for potential outliers in cell count which may be present due to pipetting error in the triplicate wells.

Equation 1: Calculation of population doubling time (PDT).

$$PDT = \frac{t \times \log(2)}{\log(N_t) - \log(N_0)}$$

Where t represents the duration of culture, N_t is the final number of cells at the end of the culture period and N_0 is the initial concentration of cells seeded into each well^{186,187}. As a secondary measure to the results were compared against the PDT calculated by inputting the daily cell counts into Doubling Time – an online PDT calculator application¹⁸⁸.

2.11 Flow Cytometry

The present study exploited the characteristic plastic adherence of AD-MSCs by using serial passaging to purify the primary rat cells, to achieve a homogenous culture of stem cells by passage 3. To confirm the efficacy of this technique, flow cytometry was conducted with the assistance of Dr Dalene De Swardt from the Central Analytics Facility on Stellenbosch University's Tygerberg Campus. Mesenchymal stem cells (MSCs) typically express several selective cell surface markers including CD105, CD73, and CD90 and lack the expression of CD14, CD45, CD34, and CD79 α ¹⁸⁹. Thus, to effectively discriminate between AD-MSCs and any other vascular stromal cells which may be present in culture, a panel of conjugated antibodies should be selected. Unfortunately, because of the time constraints imposed on this study by the COVID-19 lock-down, a decision was made to conduct the flow cytometric analyses on the subcutaneous and visceral AD-MSCs using one positive and one negative AD-MSC marker, specifically CD90 (Thy-1) and CD45 (Table 2.6). The cell surface

marker expression of one sample of AD-MSCs from each depot isolated from the control, HFD, and ESD-fed rats was quantified.

Table 2.5: Fluorescently conjugated antibodies for use in the flow cytometric analysis of inguinal and retroperitoneal AD-MSCs.

Specificity	Fluorochrome	Isotype	MSC marker (+/-)
CD45	V450	Mouse (BALB/c) IgG1, κ	-
CD90	FITC	Mouse (BALB/c) IgG1, κ	+

To prepare the subcutaneous and visceral AD-MSCs for analysis by flow cytometry, the cells, which had been cultured to ~80% confluence at passage three, were rinsed with prewarmed, sterile PBS and liberated from the culture plate by addition of 0.5% Trypsin EDTA (section 2.8). A cell count was performed as described above in section 2.9. The suspension was then re-pelleted by centrifugation at 400 x *g* for 5 minutes, the supernatant discarded, and the cells resuspended in staining buffer (sterile filtered PBS supplemented with 20% FBS). Approximately 1 x 10⁶ cells/mL were transferred into each 5 mL Fluorescence-activated cell sorting (FACS) tube, 1 mL PBS was added to rinse the cells and the sample tubes were subjected to centrifugation at 400 x *g* for 5 minutes. The supernatant was discarded and 50 μ L of staining buffer was added to the cell pellet in each FACS tube.

Normally, an appropriate volume of each antibody would then be added to this cell suspension, however, to date no guidelines exist for use of the selected fluorescent conjugated antibodies (Table 2.5) on rat AD-MSCs. Thus, the optimal quantities of the two conjugated antibodies on each cell type were determined by performing titration experiments as the addition of excess antibody can cause low-affinity binding which will increase the background fluorescence, thus reducing the resolution of the results¹⁹⁰. This involved the serial dilution of each antibody from a primary concentration of 5% in cell suspension, down to a concentration of 0.156%. The cell suspension and antibody mix were homogenised through gentle trituration with a pipette, and the sample tubes were incubated in the dark at 4 °C for 30 minutes. Following incubation, 1 mL staining buffer was added to each FACS tube, and the tubes were subjected to centrifugation for 10 minutes at 250 x *g*. The supernatant, containing unbound fluorescent antibodies, was then gently removed, and discarded taking care not to disturb the cell pellet. The cells were subsequently resuspended in 200-500 μ L staining buffer and the samples were stored at 4 °C until they were run on the Beckman Coulter DxFLEX flow cytometer using CytExpert for DxFLEX Software (Version 2.0). An unstained control sample was included in each run for voltivation and gating and the resulting data were analysed using FlowJo Vx (Version 10.8.1, Treestar, Oregon, USA) software. To determine the optimal antibody concentrations, the

staining index (SI) values of each acquired sample was calculated using Equation 2, and the results were plotted.

Equation 2: Calculation of staining index following antibody titration. The ratio quantifies the difference between the positively stained and unstained cell populations following flow cytometric analyses.

$$\text{Staining Index} = \frac{MFI_{Pos} - MFI_{Neg}}{2 \times SD_{Neg}}$$

Where MFI_{Pos} represents the median fluorescent intensity of the antibody-stained cells, MFI_{Neg} is the median fluorescent intensity of unstained cells and SD_{Neg} is the standard deviation of unstained cells¹⁹⁰. The concentration of antibody that elicited the peak SI of the standard curve was selected for use in this study. The results reported display the SI curves for the anti-CD90 antibody titration as it is the positive MSC marker used in the present study. The optimal volumes of the anti-CD90 and anti-CD45 antibodies determined for each cell type were subsequently used when completing the above protocol on cells isolated from rats in each diet group.

2.12 Adipocytic Differentiation

Two days after the AD-MSCs had become confluent at passage three, adipogenesis was induced using the protocol previously reported by Jacobs et al. (2019)¹⁹¹. Adipocyte Differentiation media (AM) and the Vehicle Control media (VCM) were prepared immediately before use as per Appendix Table C.2. Notably, the AM used in this experiment included L-ascorbic acid – a relatively uncommon component. Ascorbic acid has been identified as a key cofactor in the biosynthesis and secretion of type I and type VI collagen, vital constituents of the extracellular matrix^{192–196}. It has also been proven to have an effect on the expression of cell adhesion molecules within the matrix which aids in the adherence of cells to the untreated, sterile culture dishes^{195,197,198}. Thus, by including L-ascorbic acid in the AM, the potential for detachment of the differentiating, fibroblastic adipocytes from the surface of the culture dish was reduced^{196,199}.

To ensure the replenishment of differentiation factors and prevent the expenditure of growth factors, both the AM and VCM were replaced every three days for two weeks. All culture dishes were observed daily with a phase-contrast microscope to monitor cellular health until the cells had terminally differentiated and large lipid droplets had developed. On day 14 of adipogenesis, the differentiation protocol was terminated and conditioned media, containing the adipocytic secretome, was harvested and stored.

2.13 Harvesting Conditioned Media from *in vitro* Differentiated Subcutaneous and Visceral Adipocytes

To harvest the conditioned media (CM), AD-MSCs were differentiated in 100 mm² culture dishes as per section 2.12. Once the adipocytes had terminally differentiated following 14 days of treatment, the AM was removed from the culture dishes and the cells were then rinsed briefly with pre-warmed PBS. The media was then replaced with serum-free DMEM, as per Park *et al.* (2020), and the dishes were incubated for 24 hours^{164,200,201}. The media was then harvested and subjected to centrifugation for 5 minutes at 400 x g to separate out any cell debris. Thereafter, the CM supernatant was transferred into a sterile, labelled centrifuge tube.

Due to the time constraints imposed upon this project as a result of the COVID-19 national lockdown in 2020, all recipient subcutaneous and visceral AD-MSCs (cells which would be incubated in CM) (n = 3) were collected at the same time. This presented a logistical challenge when it came to treating the recipient cells with CM collected from 21 rats (n = 7 in three diet groups) in terms of both incubator space and time. A decision was therefore made to pool the CM for each group i.e., all the samples from the same group and adipose depot were combined. Thus, one representative subcutaneous and visceral CM sample from the control, HFD, and ESD diet groups were composed by mixing the CM in equal parts. The pooled aliquots were then stored at -80°C until use. Once the CM had been collected, pooled, and stored, the lipid accumulation per cell in culture was quantified by intracellular staining with oil red O (ORO) and crystal violet, subsequent spectrophotometry of the eluted stains, and *in silico* micrograph analyses.

2.14 Preparation of Rosiglitazone for *in vitro* cell treatment

Rosiglitazone (Rosi) stock solutions were prepared as previously described in an article by van de Vyver *et al.* (2014)⁵². Briefly, 9.5 mM (w/v) stock solutions were prepared by dissolving Rosi in DMSO. These stocks were then aliquoted and stored at -20°C until use. Directly before treatment of the recipient cells, 100 µM working solutions of Rosi were prepared by diluting the stock solutions with PBS. An appropriate volume of Rosi working solution was then added to the treatment group to attain a final concentration of 1 µM Rosi. A 1 µM concentration of Rosi was selected for use in this study as it is the concentration most frequently utilised to stimulate adipogenesis *in vitro* and it represents the average serum concentration in individuals taking a dosage of 4 mg/day for the treatment of type II diabetes mellitus^{52,86,202,203}.

2.15 Quantification of Lipid Accumulation by Oil Red O and Crystal Violet Staining, Spectrophotometry, and *in-silico* Photomicrograph Analyses

ORO was utilized to quantify the intracytoplasmic lipid accumulation of the AD-MSCs as being a lysochrome, it preferentially binds to triglycerides²⁰⁴. A 1% (w/v) stock solution of ORO stain was

made by the addition of powdered ORO dye to isopropanol and the solution was stirred at low speed overnight by a magnetic stirrer at room temperature. The ORO was used at a concentration of 0.7% (w/v) in concurrence with previous studies^{205,206}. To achieve this, the 1% (w/v) stock solution was diluted with distilled H₂O and filtered immediately before use to remove all debris^{52,168}.

To begin the staining protocol, the media was aspirated from the plate and the cultured cells were fixed and stained with ORO solution for 30 minutes at room temperature. The stain was subsequently removed, and the cells were washed three times with distilled H₂O to remove any excess stain. The stained adipocytes were then submerged in distilled H₂O, viewed under the Olympus inverted phase-contrast microscope (CKX41) and micrographs were taken at 20X magnification (CachN 20X/0.40 PhP objective). Thereafter, the ORO stain was eluted from the adipocytes with 100% isopropanol and the absorbance of the solution was read in duplicate at 510 nm on a Multiskan Go microplate spectrophotometer (Thermo Fischer Scientific, Vantaa, Finland). Duplicate wells of 100% isopropanol were read at the same frequency as the samples so the absorbances could later be subtracted from the sample readings to remove any background introduced by the solvent.

To ensure the quantification of total lipid accumulation seen in the culture had not been confounded by reduced cell viability, the adipocytes were counterstained with crystal violet. As per Jacobs *et al.* (2018), a 1% (w/v) stock solution of crystal violet stain was prepared by dissolving crystal violet dye in distilled H₂O¹⁹¹. The solution was then diluted further to a concentration of 0.01% to prevent the stain from non-specifically binding to the intracellular glycoproteins once added to the cultured cells²⁰⁷. Thereafter, the diluted stain was added to each well and the adipocytes were incubated for 5 minutes at room temperature. As with the ORO staining, the crystal violet was eluted from the cells with isopropanol and the absorbances of each sample were measured in triplicate at 570 nm in the spectrophotometer. To establish the triglyceride content per cell in culture, the ORO absorption values were divided by the corresponding CV absorption values. The relative lipid accumulation per treatment was subsequently calculated by expressing the absorption readings relative to the negative control – cells treated with non-adipogenic SGM.

Photomicrographs of the ORO-stained inguinal and retroperitoneal adipose tissue harvested from control, HFD- and ESD fed rats were imported into Fiji ImageJ software (Version 1.53c, National Institute of Health, US) for analysis²⁰⁸. By thresholding the images based on hue, saturation, and brightness using the Colour Thresholding plugin, the region of interest was selected, and the ORO-stained area was then measured as shown in Figure 2.4. The resulting measurements were expressed as a percentage of ORO-stained surface area. Three representative images of each sample were analysed and means from each treatment group were compared in IBM SPSS Statistics for Windows.

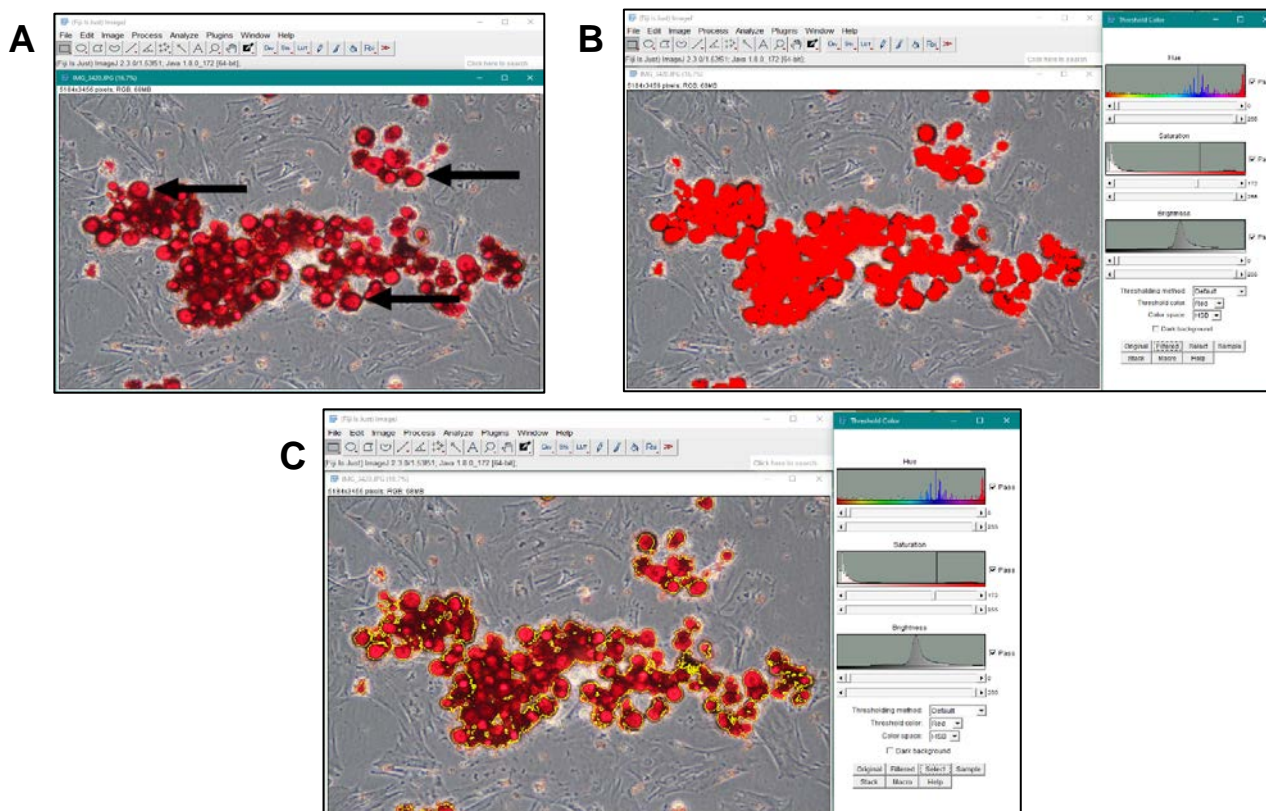


Figure 2.4: Quantification of oil red O (ORO) staining by thresholding based on hue, saturation, and brightness in ImageJ Fiji. (A) The input image of ORO-stained lipid droplets (indicated by black arrows) in control retroperitoneal adipocytes following 14 days of adipocytic differentiation (20X magnification), (B) Thresholding to select ORO-stained region of interest in red (C) Region of interest outlined in yellow. The region of interest was then measured and the percentage of ORO-stained area of each micrograph was then calculated.

2.16 Statistical Analyses

Dr Michael McCaul, a professional statistician from the Division of Epidemiology and Biostatistics on Stellenbosch University's Tygerberg Campus was consulted during this study. All statistical analyses were performed using IBM SPSS Statistics for Windows (Version 27.0. Armonk, NY: IBM Corp). Either a one-way or two-way analysis of variance (ANOVA) was used for the comparison of means as applicable. If statistical significance was detected within a dataset, a Bonferroni or Dunnett's post-hoc analysis for multiple comparisons were then performed. To ensure the assumptions of these parametric statistical tests were satisfied, the normality of each dataset was confirmed by conducting both a Shapiro-Wilk and Kolmogorov-Smirnov test. All results are expressed as the mean \pm standard error of the mean (SEM) and differences were considered to be significant when $p < 0.05$.

Results

The results of this project are reported in this chapter and will then be discussed further in Chapter 4. The salient findings are initially given in brief, followed by the data in detail.

No significant differences were noted in the final body weights of the control, high-fat diet (HFD), and the elevated sugar diet (ESD) fed Wistar rats at the end of the 16-week feeding period. Both the HFD and ESD diets did, however, increase the mass of the inguinal subcutaneous and retroperitoneal visceral adipose tissue depots and induce hypertrophic expansion in the constituent adipocytes. Prior to the initiation of further experiments, the adipose-derived mesenchymal stem cells (AD-MSCs) isolated from the inguinal and retroperitoneal adipose tissues were characterised *in vitro*. This was accomplished by assessing the *in vitro* morphology, proliferation rate, adipogenic potential, and expression of mesenchymal stem cell (MSC) surface markers of the cells. The results of these analyses indicate that intrinsic differences exist between the cells isolated from the inguinal- and those isolated from the retroperitoneal adipose tissues (section 3.3).

A preliminary study was then conducted to determine the lowest concentration of adipogenic media (AM) required to promote adipogenesis, below which terminal differentiation would not occur (section 3.4). This was done to ensure that the effects of conditioned media (CM) on differentiation (either positive or negative) could still be observed in recipient cells when mixed with adipogenic media (AM). The outcomes of this study confirmed the findings of prior literature as concentrations of 25% AM and 50% AM had comparable adipogenic effects. Thus, a concentration of 50% AM was selected for use in subsequent studies as less CM would then be used, preserving the store of CM for proteomic profiling in future studies.

The main aim of this project was to quantify the effects of CM from subcutaneous adipocytes on visceral AD-MSCs and vice versa. The additional impacts of the HFD and ESD on the secretory profiles of the adipocytes and consequently any changes these diets may have on the possible endocrine / paracrine modulation of AD-MSC differentiation was also considered. Subcutaneous and visceral CM samples from *in vitro* differentiated control, HFD, and ESD adipocytes were, therefore, added on their own or in 1:1 combination with either standard growth media (SGM) or AM to inguinal and retroperitoneal AD-MSCs that had been maintained and purified in culture to passage three (section 3.5). The effects of the CM treatments were then quantified by oil red O (ORO) and crystal violet staining, *in-silico* analysis of ORO-stained areas, and spectrophotometry of the eluted stains. The findings of these experiments revealed that whilst the visceral CM collected from the control and HFD retroperitoneal adipocytes were able to stimulate adipogenesis in the visceral recipient cells,

the CM collected from the ESD visceral adipocytes had the greatest adipogenic effect on the visceral recipient cells, producing statistically significant results when added to the cells in all three formulations (100% CM, 1:1 CM: SGM, and 1:1 CM: AM). Adipogenesis was also effectively stimulated by the subcutaneous CM harvested from the control, HFD, and ESD inguinal adipocytes, however, the lipid accrual was only found to be statistically significant when the subcutaneous CM was combined with 50% AM. Although some adipogenesis was qualitatively and quantitatively observed, no statistical differences were identified between any of the CM treatments when added to the inguinal recipient AD-MSCs.

Further investigations were then conducted to evaluate the impact of additional supplementation of the subcutaneous and visceral CM samples with rosiglitazone (Rosi) – a peroxisome proliferator-activated receptor- γ (PPAR γ) agonist known to instigate adipogenesis (section 3.6). As performed in the CM experiments, the control, HFD, and ESD subcutaneous and visceral CM samples were added to control recipient AD-MSCs isolated from both adipose depots as either a 100% CM, 1:1 CM: SGM, or 1:1 CM: AM treatment. Each treatment group was, however, supplemented with 1 μ M Rosi. Following 14 days of treatment, the effects of the treatment groups on adipogenesis within the recipient cells was quantified by ORO and crystal violet staining, *in-silico* analysis, and spectrophotometry (section 2.15). The results of the *in-silico* ORO staining quantification identified the control and HFD CM's from both the subcutaneous and visceral adipose depots as having the most significant adipogenic effects when treating the retroperitoneal visceral recipient AD-MSCs. Treatment of the inguinal subcutaneous recipient AD-MSCs with the 1 μ M Rosi supplemented CM treatments did not induce any more lipid accumulation than observed within the CM experiments.

3.1 Diets

The 21 male Wistar rats in this study were weighed weekly during the 16-week diet period so any increase or decrease in total body weight could be monitored. The rat's progressive weight gain can be seen in Figure 3.1, where control rats ($n = 7$) gained weight at a faster rate than the HFD and ESD fed rats for the first seven weeks, whereafter the weight of the rats began to plateau whilst weights of the HFD and ESD rats gradually continued to increase.

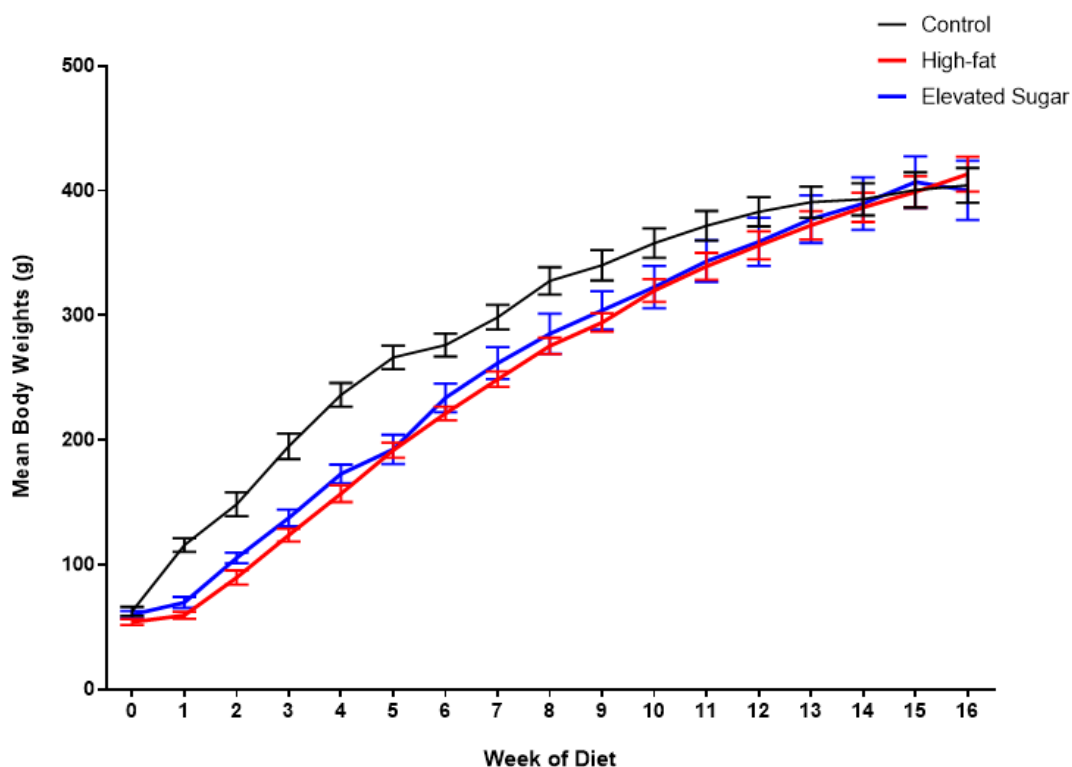


Figure 3.1: Bodyweight growth curve of the control ($n = 7$), high-fat diet ($n = 7$), and elevated-sugar diet ($n = 7$) fed male Wistar rats over the 16-week diet feeding period. Data are represented as mean \pm SEM.

The biometric data indicates the lack of substantial differences in the average daily food consumption between the three diet groups during the 16-week diet period, but the control rats were noted to have a considerably higher water intake per day ($p = 0.005$) (Table 3.1). Though the HFD and ESD fed rats were, on average, heavier than the control group at the end of the 16-week diet period, the differences in final body weights between the diet groups were not significant (404.17 ± 14.06 g Control vs. 412.74 ± 14.44 g HFD vs. 413.31 ± 20.23 g ESD, $p > 0.05$). The endpoint fasting blood glucose (FBG) results indicated that the HFD rats had the highest mean FBG (4.86 ± 0.14 mmol/l), which was significantly higher than that of the ESD group's endpoint FBG (4.27 ± 0.08 mmol/l, $p = 0.017$) but not of the control rat's (4.6 ± 0.16 mmol/l, $p > 0.05$).

When comparing the weights of the inguinal adipose depots, both the HFD (10.54 ± 0.72 g) and ESD (11.56 ± 1.39 g) rats had higher mean inguinal fat pad weights than the control group (7.77 ± 0.58 g). Nevertheless, only the ESD group's inguinal adipose depot was significantly heavier ($p = 0.038$).

than the controls and constituted a substantial proportion of body weight ($2.76 \pm 0.24\%$, $p = 0.013$). Retroperitoneal fat pads from the HFD (15.66 ± 1.24 g, $p = 0.001$) and ESD (15.28 ± 1.72 g, $p = 0.002$) fed rats were, however, significantly larger than those of the control rats (8.06 ± 0.44 g) and constituted $3.78 \pm 0.24\%$ ($p = 0.0002$) and $3.66 \pm 0.32\%$ ($p = 0.0003$) of the HFD and ESD groups, respectively, which were significantly higher than the $2.00 \pm 0.12\%$ of retroperitoneal fat within the control rats.

Table 3.1: Biometric data generated during and after the feeding of a control, high-fat, and elevated sugar diet to male Wistar rats (n = 21). Results for each biometric parameter were produced by conducting one-way ANOVAs with Bonferroni post-hoc tests (n = 7). All data are expressed as mean \pm SEM.

Biometric parameter	Control (n = 7)	HFD (n = 7)	ESD (n = 7)
Food consumption (g/cage/day)	78.48 \pm 5.54	60.15 \pm 3.06	74.04 \pm 9.26
Water intake (ml/cage/day)	100.17 \pm 21.69*	49.44 \pm 3.28	48.52 \pm 3.01
Final body weight (g)	404.17 \pm 14.06	412.74 \pm 14.44	413.31 \pm 20.23
Basal fasting blood glucose (mmol/l)	3.29 \pm 0.27	4.40 \pm 0.24**	3.97 \pm 0.11
Endpoint fasting blood glucose (mmol/l)	4.6 \pm 0.16	4.86 \pm 0.14#	4.27 \pm 0.08
Inguinal fat weight (g)	7.77 \pm 0.58	10.54 \pm 0.72	11.56 \pm 1.39**
Retroperitoneal fat weight (g)	8.06 \pm 0.44	15.66 \pm 1.24***	15.28 \pm 1.72***
Proportion of inguinal fat (% body weight)	1.93 \pm 0.15	2.54 \pm 0.12	2.76 \pm 0.24**
Proportion of retroperitoneal fat (% body weight)	2.00 \pm 0.12	3.78 \pm 0.24*	3.66 \pm 0.32*

HFD – High-fat diet; ESD – Elevated sugar diet

* $p \leq 0.005$ versus HFD and ESD; ** $p \leq 0.05$ versus control; *** $p < 0.005$ versus control; + $p < 0.0005$ versus control; # $p < 0.05$ versus ESD

3.2 Histological Staining of Subcutaneous and Visceral White Adipose Tissue

Haematoxylin and eosin (H&E) staining, and subsequent microscopic analysis of the inguinal subcutaneous and retroperitoneal visceral adipose tissues revealed no distinct differences in general morphology and distribution of unilocular white adipocytes between the four experimental groups. Subcutaneous adipose tissue is characteristically heterogeneous, with the intercalated multilocular

brown adipocytes (yellow arrows) being seen in the 12-week-old inguinal adipose tissue sample and more connective tissue being visible in all the inguinal micrographs as compared to the retroperitoneal images (black arrows) (Figure 3.2). More micrographs showing the high level of heterogeneity of this depot can be seen in Appendix Figure D.1. These images were not included in the quantitative analyses as only the size and number of the white adipocytes within each depot in response to the diets were of interest in the present study. The large, unilocular white adipocytes within the retroperitoneal adipose tissue samples are more uniform in size and number in all diet groups. Qualitative analysis of micrographs in Figure 3.2 shows that the visceral adipocytes of the 12-week-old control, 19-week-old control, and ESD groups are comparably larger than the subcutaneous adipocytes of the same donors. Conversely, the adipocytes in both adipose depots of the HFD donor appear to be similar in size and number.

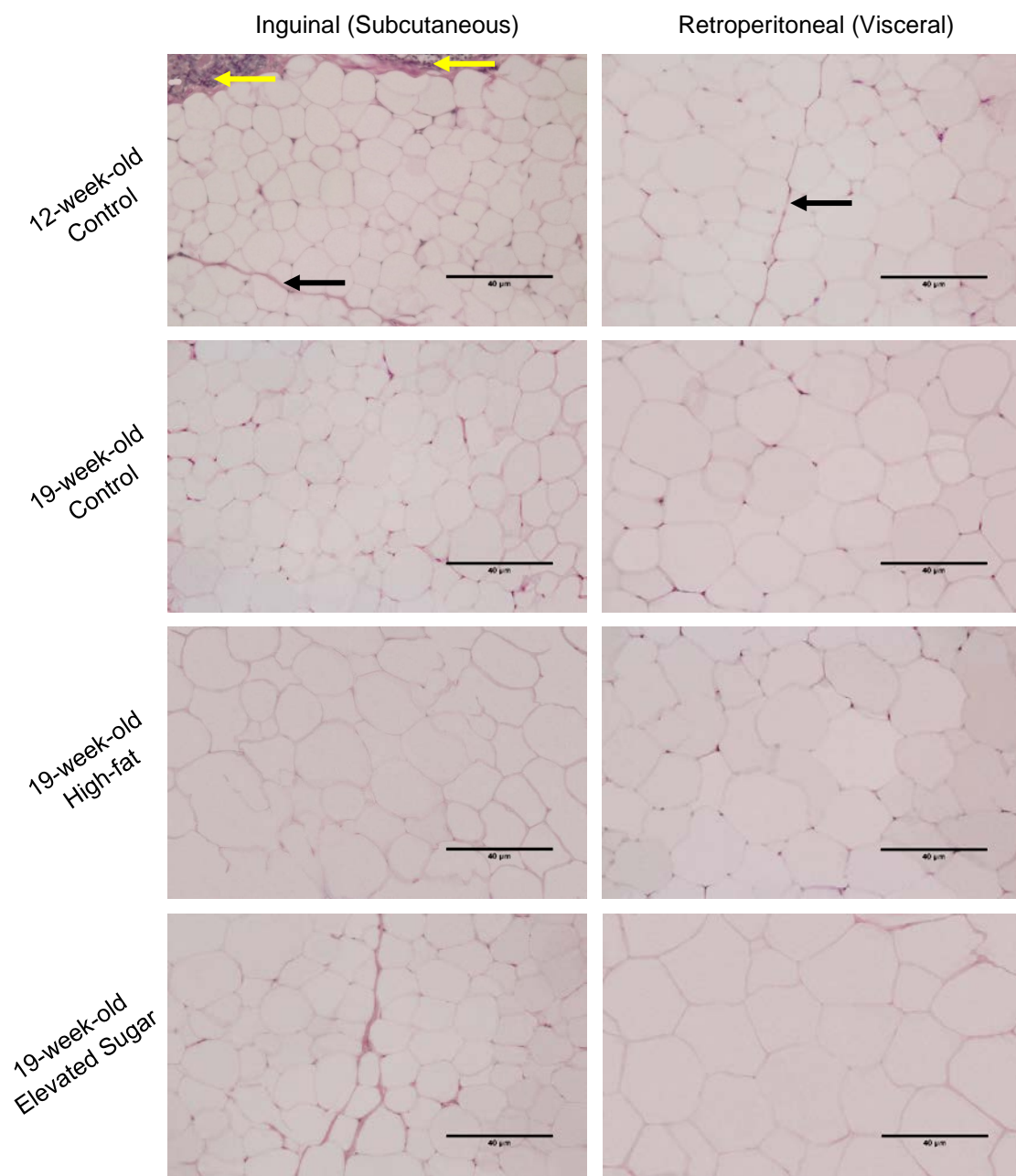


Figure 3.2: Haematoxylin and eosin-stained inguinal subcutaneous and retroperitoneal visceral white adipose tissue harvested from 12-week-old control, 19-week-old control, high-fat diet- and elevated-sugar diet-fed male Wistar rats. Micrographs were taken using a Canon 600D camera mounted on an Olympus inverted phase-contrast microscope at 20 X magnification. Scale bar = 40µm.

Quantification of cellular size showed that the adipocytes within the inguinal adipose tissue of the 19-week-old control ($178.0 \pm 8.17 \mu\text{m}^2$) were markedly bigger than those of the younger 12-week-old control donor ($120.42 \pm 3.78 \mu\text{m}^2$, $p < 0.0001$) (Figure 3.3 A). Conversely, when enumerating the adipocytes present in the micrographs, the 12-week-old control sample (178 ± 13.86) had more inguinal adipocytes per μm^2 than the 19-week-old control sample (119 ± 1.00 , $p = 0.0036$). Statistical analysis of the retroperitoneal adipocyte areas indicated that the 19-week-old donor ($520 \pm 31.61 \mu\text{m}^2$) had significantly larger adipocytes than the younger controls ($357.6 \pm 16.36 \mu\text{m}^2$, $p < 0.0001$) (Figure 3.3 A), however, no statistical differences were noted in the number of retroperitoneal adipocytes between either of the groups (Figure 3.3 B).

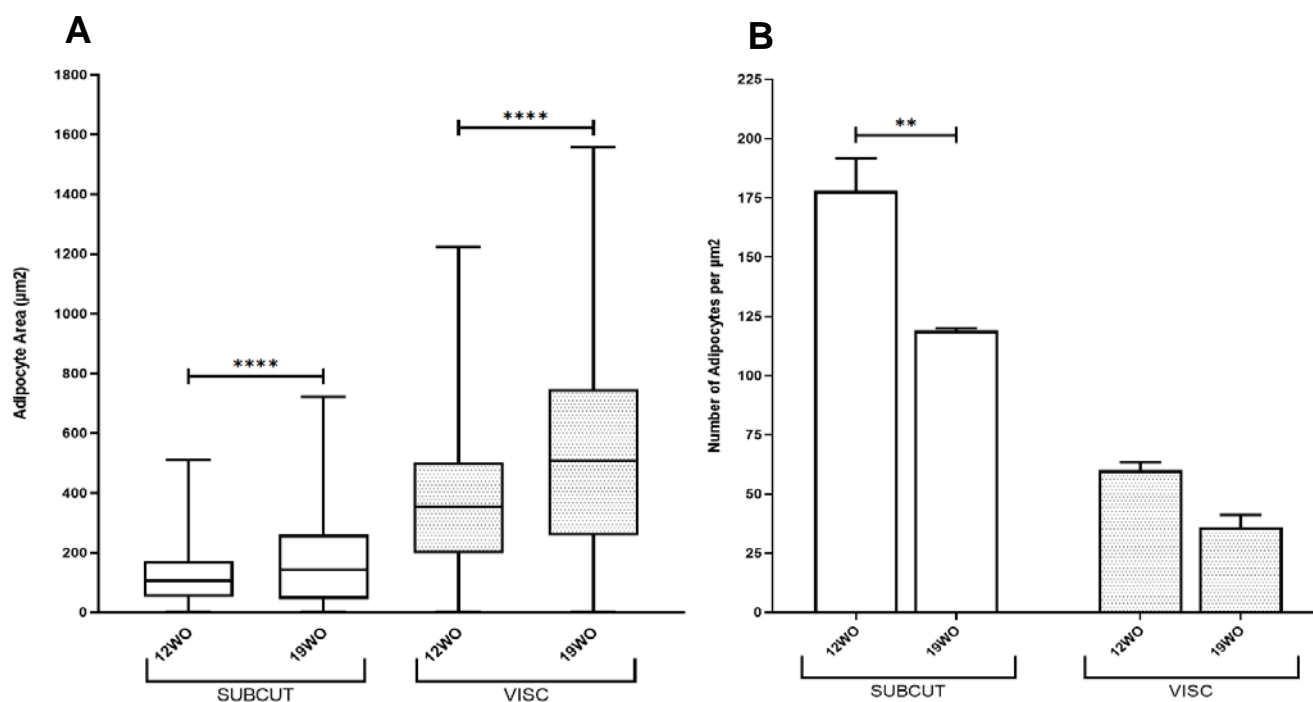


Figure 3.3: Morphometric indices of haematoxylin and eosin-stained inguinal and retroperitoneal white adipocytes within adipose tissue samples isolated from 12-week-old- and 19-week-old control male Wistar rats. Representative micrographs taken of the inguinal and retroperitoneal adipose samples ($n = 3$ per experimental group) were analysed using AdipoGauge Software with a calibration factor of 0.074897. (A) The areas (μm^2) of the inguinal and retroperitoneal adipocytes were measured and are presented as box and whisker plots, with the box representing the upper and lower quartiles, the central line being the mean and the whiskers indicating the highest and lowest recorded areas. (B) The number of adipocytes per μm^2 in each of the inguinal and retroperitoneal adipose sample micrographs were also quantified, and are represented as mean \pm SEM. All analysed micrographs were taken at 20 X magnification. One-way ANOVAs were conducted

to assess statistical significance, and the differences between treatment groups were tested with a Bonferroni post-hoc (** $p < 0.005$; **** $p < 0.0001$). WO – Week old; SUBCUT – Subcutaneous; VISC – Visceral.

Quantification of the adipocyte cell size (area) in the age-matched diet-fed rats showed that the HFD adipose tissue had the largest mean inguinal adipocyte size of all three samples ($393.40 \pm 25.49 \mu\text{m}^2$, $p < 0.0001$) (Figure 3.4 A). High statistical significance was also observed when comparing the inguinal adipocyte areas of the ESD donor ($223.60 \pm 9.98 \mu\text{m}^2$) to those of the control group ($178 \pm 8.37 \mu\text{m}^2$, $p < 0.0001$). The retroperitoneal adipocytes were, on average, predominantly larger than the inguinal adipocytes within all three experimental groups, this being especially evident in the ESD donor ($1005 \pm 79.64 \mu\text{m}^2$). This inherent hypertrophic expansion led to a high level of statistical significance ($p < 0.0001$) when comparing the ESD retroperitoneal adipocytes to those of the control ($520.30 \pm 31.61 \mu\text{m}^2$) and HFD ($580.60 \pm 43.18 \mu\text{m}^2$) groups.

When enumerating the inguinal and retroperitoneal adipocytes within the representative micrographs (20X magnification), it became apparent that the size of the adipocytes directly impacted the number of adipocytes per μm^2 (Figure 3.4 B). Due to the enlarged HFD inguinal adipocytes, the lowest density of adipocytes (number per μm^2) was recorded for this depot (HFD 50.67 ± 5.24 vs. Control 119 ± 1 , $p < 0.0001$; HFD 50.67 ± 5.24 vs. ESD 93 ± 15.28 , $p = 0.0032$). In addition, the ESD group was noted to have had the smallest mean quantity of retroperitoneal adipocytes per μm^2 (19 ± 1.16) as compared to both the control (36.00 ± 5.29 , $p = 0.032$) and the HFD (36.67 ± 1.76 , $p = 0.027$).

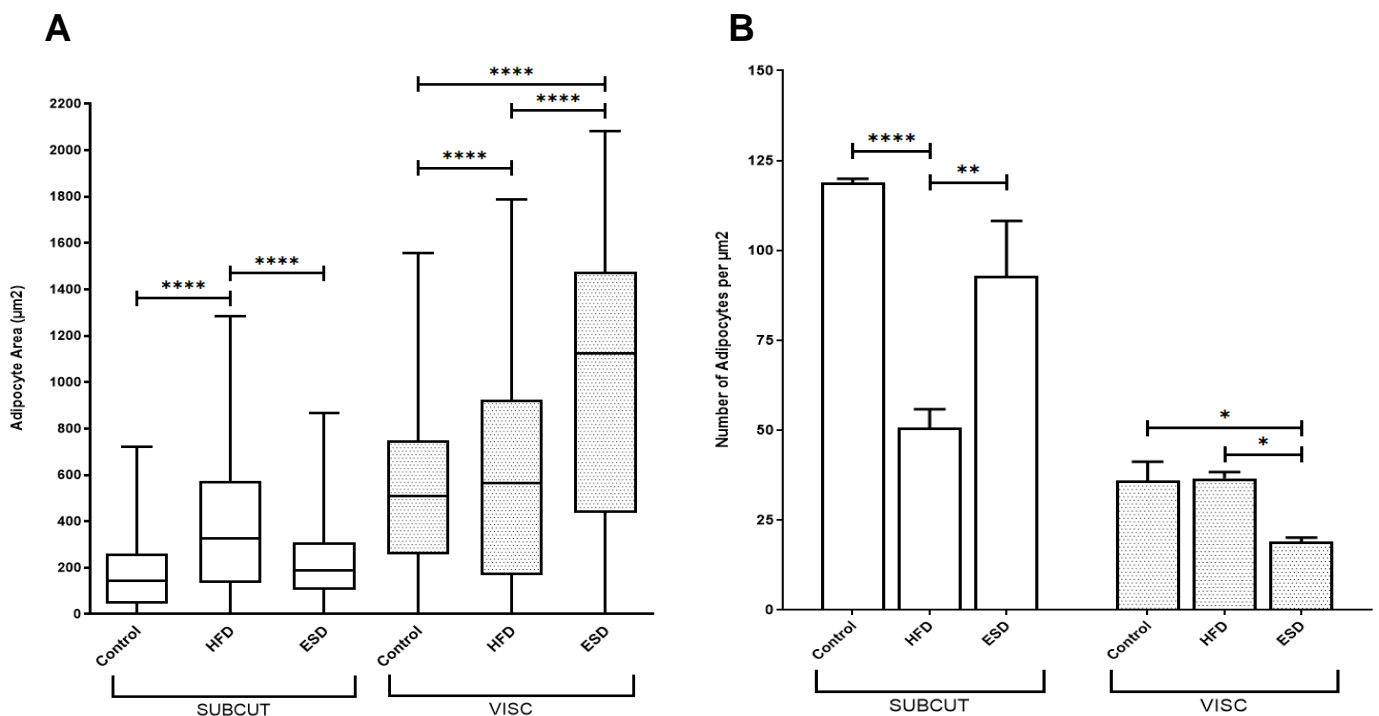


Figure 3.4: Morphometric indices of haematoxylin and eosin-stained inguinal and retroperitoneal adipocytes within adipose tissue samples isolated from age-matched 19-week-old control, high-fat diet-, and elevated sugar diet-fed male Wistar rats. Representative micrographs taken of the inguinal and

retroperitoneal adipose samples ($n = 3$ per experimental group) were analysed using AdipoGauge Software with a calibration factor of 0.074897. **(A)** The areas (μm^2) of the inguinal and retroperitoneal adipocytes were measured and are presented as box and whisker plots, with the box representing the upper and lower quartiles, the central line being the mean and the whiskers indicating the highest and lowest recorded areas. **(B)** The number of adipocytes per μm^2 in each of the inguinal and retroperitoneal adipose sample micrographs were also quantified, and are represented as mean \pm SEM. All analysed micrographs were taken at 20 X magnification. Two-way ANOVAs where depot and diet were represented the independent variables were conducted to assess statistical significance, and the differences between treatment groups were tested with a Bonferroni post-hoc (** $p < 0.005$; **** $p < 0.00001$). ESD – Elevated sugar diet; HFD – High-fat diet; SUBCUT – Subcutaneous; VISC – Visceral.

By grouping the adipocytes according to size and calculating the number of adipocytes present in each group as a percentage of total adipocytes counted, the size distribution of the adipocytes can be visualized (Figure 3.5). In inguinal adipose samples (Figure 3.5 A) as there is a higher number of small adipocytes ($1 - 50 \mu\text{m}^2$) and fewer large adipocytes ($>801 \mu\text{m}^2$) in all groups. Over 25% of the adipocytes in the 12-week-old control sample were $< 51 \mu\text{m}^2$, with the largest adipocyte in this depot being $401.89 \mu\text{m}^2$. The 19-week-old control inguinal adipocytes featured a wider range in size as 28% were between $1 - 50 \mu\text{m}^2$ but adipocyte areas of up to $722.38 \mu\text{m}^2$ were also recorded. The HFD inguinal sample was, however, an exception as adipocytes were recorded in all 14 size groupings, with the highest percentage of adipocytes being $>801 \mu\text{m}^2$.

The distribution of adipocytes in the retroperitoneal adipose tissue samples (Figure 3.5 B) is relatively even until the adipocytes reach above $601 \mu\text{m}^2$, thereafter the number of 19-week-old control, HFD, and ESD adipocytes increase rapidly. Forty-three percent of the adipocytes measured in the 19-week-old control's retroperitoneal adipose sample, and 47% of those measured in the HFD sample were $>601 \mu\text{m}^2$. The ESD group had the highest volume of large constituent adipocytes as 62% were $>936 \mu\text{m}^2$, the largest ESD adipocyte having had an area of $2079.89 \mu\text{m}^2$.

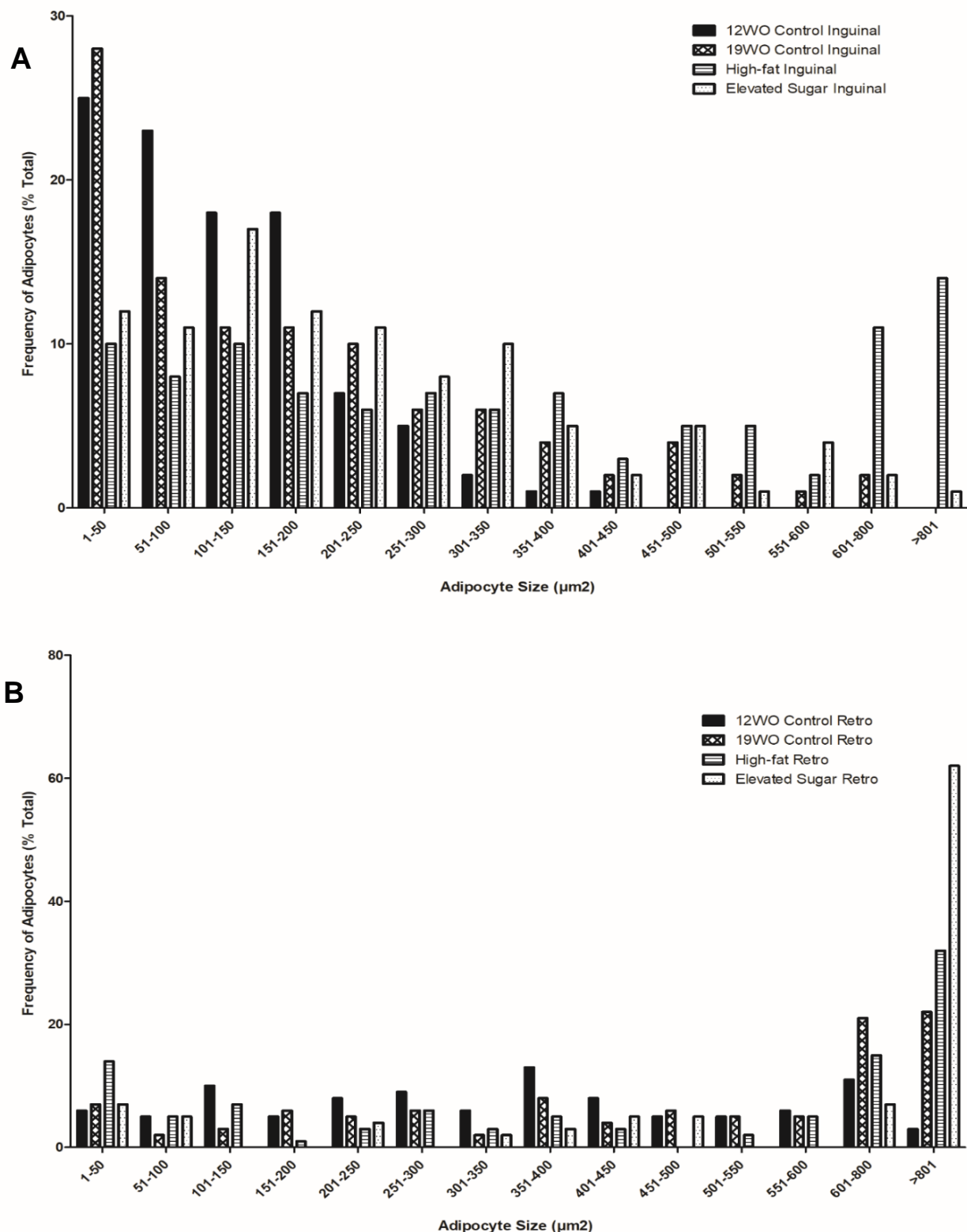


Figure 3.5: Frequency of adipocytes present in various size classes within haematoxylin and eosin-stained (A) inguinal and (B) retroperitoneal adipose tissue samples isolated from 12-week-old control, 19-week-old control, high-fat diet-, and elevated sugar diet-fed male Wistar rats. Measurements were made using AdipoGauge Software with a calibration factor of 0.074897. All analysed micrographs were taken at 20 X magnification. Data are represented as % total, relative to the number of adipocytes counted in each sample. Retro – Retroperitoneal; WO – Week old.

3.3 Characterisation of Inguinal and Retroperitoneal AD-MSCs from Control, HFD, and ESD fed rats

Plastic adherence and fibroblastic morphology are two distinguishing features of mesenchymal stem cells when cultured *in vitro*²⁰⁹, as seen in the micrographs of Figure 3.5. There are slight differences in morphology between the two isolated AD-MSC types, with protracted extensions from the cell bodies of inguinal AD-MSCs, which appear to be lacking in the broader retroperitoneal AD-MSCs. When conducting cell counts using a Fuchs-Rosenthal haemocytometer after trypsinisation to liberate adherent cells from the culture dish, the discrepancies in the cell sizes of the inguinal and retroperitoneal AD-MSCs are evident (Figure 3.6 C and D).

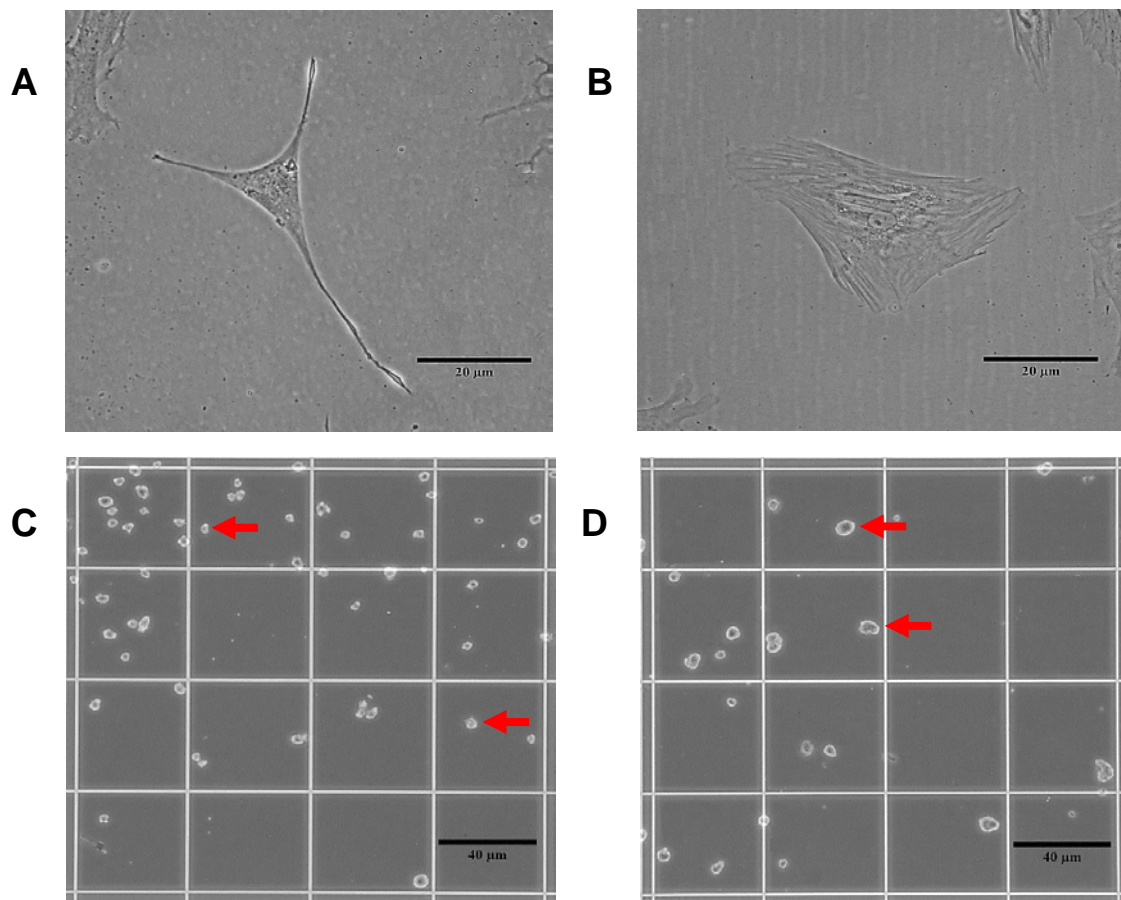


Figure 3.6: Representative micrographs showing the *in vitro* adherent morphology and the non-adherent size of inguinal and retroperitoneal AD-MSCs isolated from male Wistar rats. The (A) inguinal AD-MSCs are observed to be stellate, fibroblastic cells with elongated processes, whilst the (B) retroperitoneal AD-MSCs generally have broader cell bodies and processes (20X magnification, scale bar = 20 µm). When in suspension and placed onto a haemocytometer for cell counting, the size differences between the (C) inguinal and (D) retroperitoneal AD-MSCs (shown by the red arrows) can be seen (10X magnification, scale bar = 40 µm). Micrographs were taken using a Canon 600D camera mounted on an Olympus inverted phase-contrast microscope.

Both the inguinal and retroperitoneal AD-MSCs are observed to proliferate until cell-cell contact has been achieved and a monolayer of cells has been established, at this point contact inhibition, preventing further proliferation, may occur. Only once the proliferation has ceased and the cells are 100% confluent (Figure 3.7), can adipocytic differentiation be induced as the inhibition of proliferation is permissive for the differentiation process.

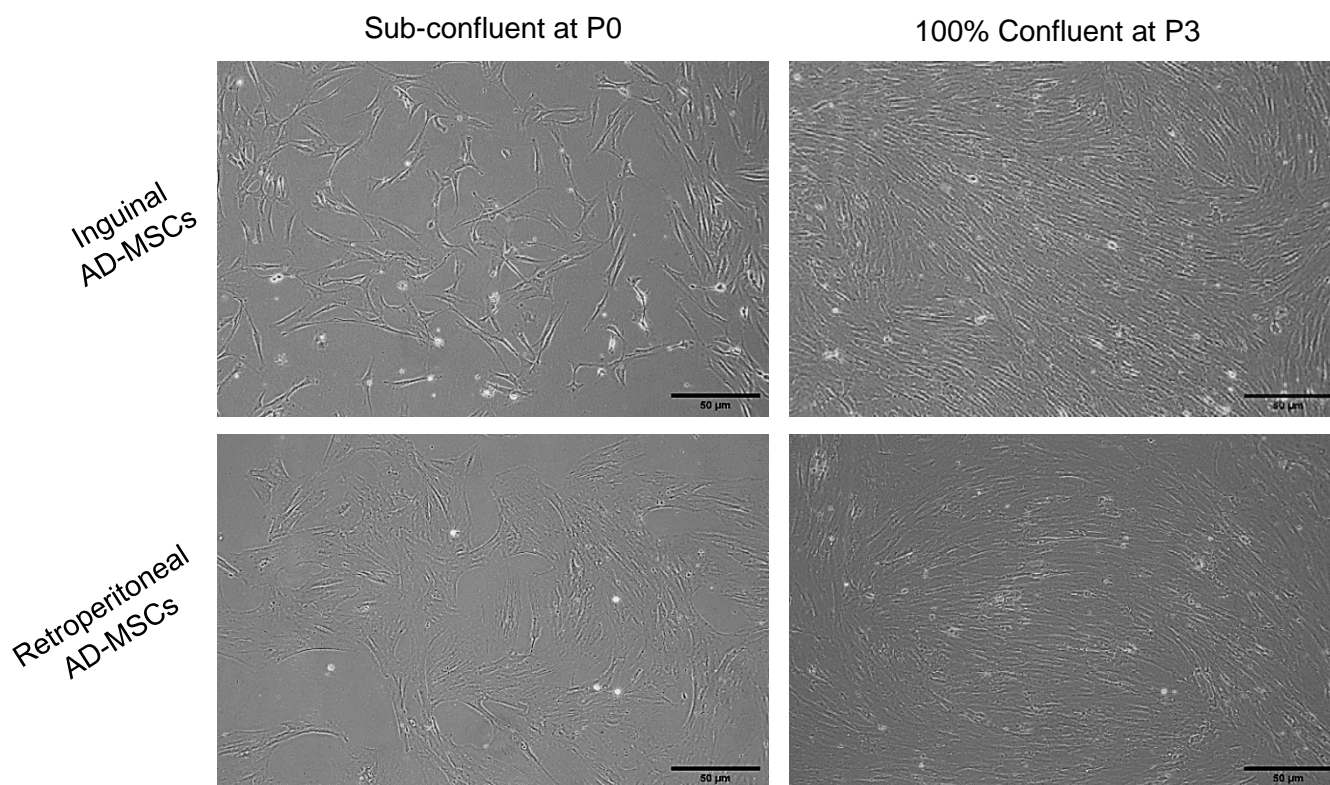


Figure 3.7: Aggregation of inguinal and retroperitoneal AD-MSCs at P0 and P3 following purification by serial subculture. Inguinal and retroperitoneal AD-MSCs were isolated and expanded *in vitro*. The fibroblastic morphologies of both cell types are displayed in the sub-confluent P0 images on the left. The images on the right show the unidirectional growth of the AD-MSCs when the cells have fully aggregated and have reached 100% confluence at P3. Images taken at 10X magnification with a Canon 600D camera mounted on an Olympus inverted phase-contrast microscope (CachN 10X/0.25 PhP ∞ /-FN22 objective). Scale bar = 50 μ m. P0 = Passage 0; P3 – Passage 3; AD-MSCs – Adipose-derived mesenchymal stem cells.

3.3.1 Growth Kinetics of Subcutaneous and Visceral AD-MSCs

The proliferation rates of AD-MSCs were measured by counting the cells (section 2.9) grown *in vitro* to passage 3 and trypsinised at time points 1-, 4- and 7-days post-seeding. Cells were from animals fed with either a control diet, HFD or ESD. Inguinal AD-MSCs isolated from the 12-week-old control, 19-week-old control, HFD and ESD groups consistently had a higher proliferation rate than the retroperitoneal AD-MSCs (Figure 3.8). Due to the small sample size ($n = 2$) and the resulting high standard error, no significant differences were observed in the proliferation rates of the inguinal or retroperitoneal AD-MSCs in any of the diet groups.

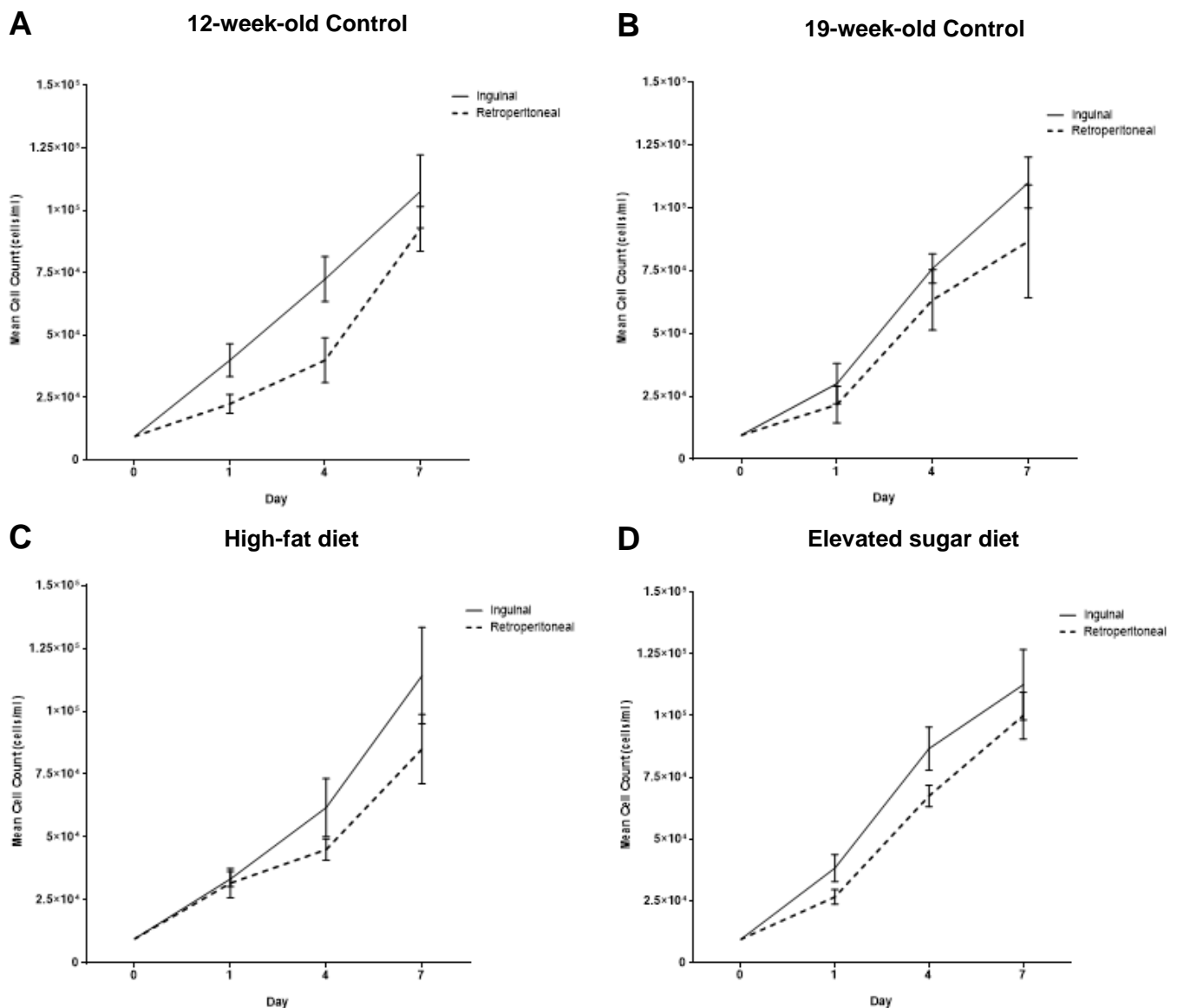


Figure 3.8: 7-day growth curves of subcutaneous and visceral AD-MSC of inguinal and retroperitoneal AD-MSCs isolated from (A) 12-week-old control, (B) 19-week-old control, (C) high-fat- and (D) elevated sugar diet-fed male Wistar rats. Cell counts ($n = 2$ per depot per diet group) were performed in triplicate on days 1, 4, and 7 post-seeding in 24-well cell culture treated plates. Data are represented at mean \pm SEM.

To establish whether there were significant differences in the proliferation rates between the inguinal and retroperitoneal AD-MSCs of each diet group, comparing groups of growth curves (CGGC) permutation tests were conducted as described in section 2.10. When comparing the growth curves of the inguinal AD-MSCs between the four experimental groups, no statistical significance was found with the multiple comparison permutations, with adjusted p values > 0.05 . Similarly, no differences were detected in the retroperitoneal AD-MSC proliferation rates between diet or age groups.

Another way to quantify the intrinsic growth properties of cells is the calculation of the population doubling time (PDT) (Figure 3.9). Analysis of the mean PDT (hours) of the inguinal and retroperitoneal AD-MSCs isolated from the 12-week-old control, 19-week-old control, HFD- and

ESD-fed Wistar rats by one-way ANOVA, showed no significant differences ($p > 0.05$), consistent with the CGGC permutation test results. It should, however, be noted that the PDTs of the retroperitoneal AD-MSCs generally appear to be higher than those of the inguinal AD-MSCs in all diet groups, with the lowest PDT of all four groups being the HFD AD-MSCs with a mean PDT of 14.95 hours.

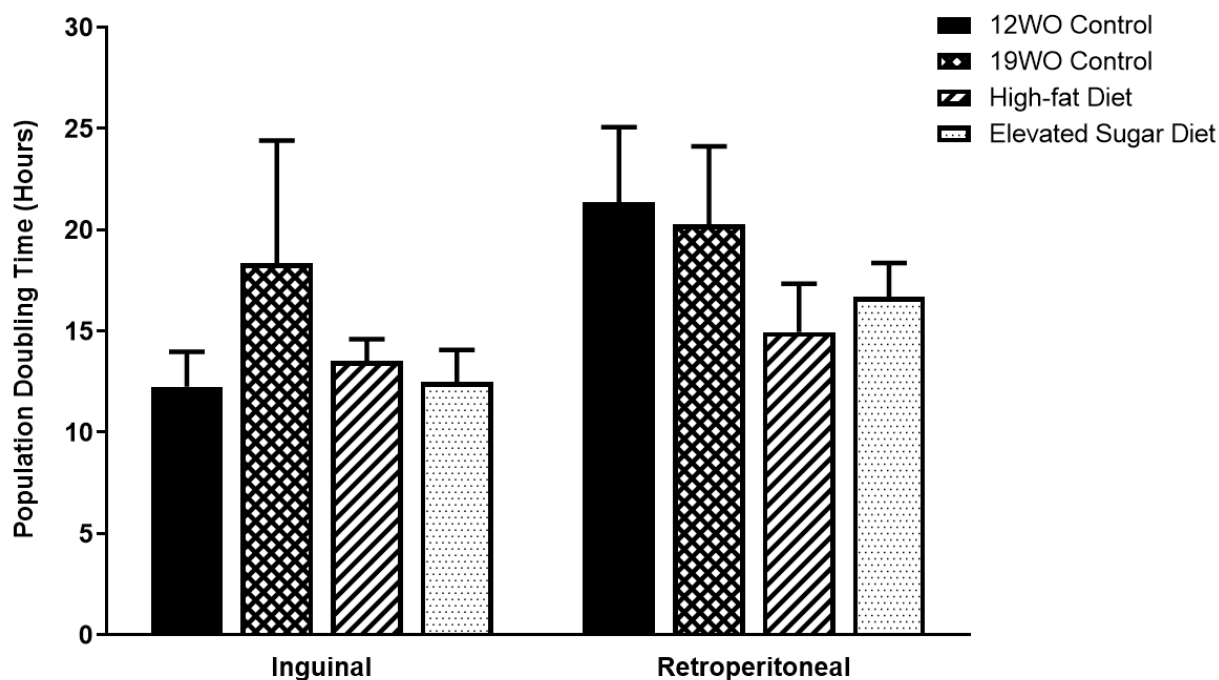


Figure 3.9: Population doubling times (hours) of inguinal and retroperitoneal AD-MSCs isolated from 12-week-old control, 19-week-old control, high-fat- and elevated-sugar diet-fed male Wistar rats. The bars are representative of each diet group ($n = 2$) and the data are expressed as mean \pm SEM.

3.3.2 Flow Cytometric Analyses

i. Antibody Titrations

Antibody titrations were conducted on samples of both the inguinal and retroperitoneal AD-MSCs prior to the flow cytometric analyses to ascertain the optimal antibody concentrations of the anti-CD90 and anti-CD45. This was done as, to our knowledge, no published guidelines for use of these antibodies against rat inguinal and retroperitoneal AD-MSCs exist. A serial dilution of anti-CD90 and anti-CD45 from a primary concentration of 5% down to a concentration of 0.156% was prepared, to which the cell suspensions of each depot were added (section 2.11). The staining index (SI) values for each titre was calculated (Equation 2) and graphed (Figure 3.10), with the optimal concentrations of the anti-CD90 being 1.25% and 1% for the inguinal and retroperitoneal AD-MSCs, respectively.

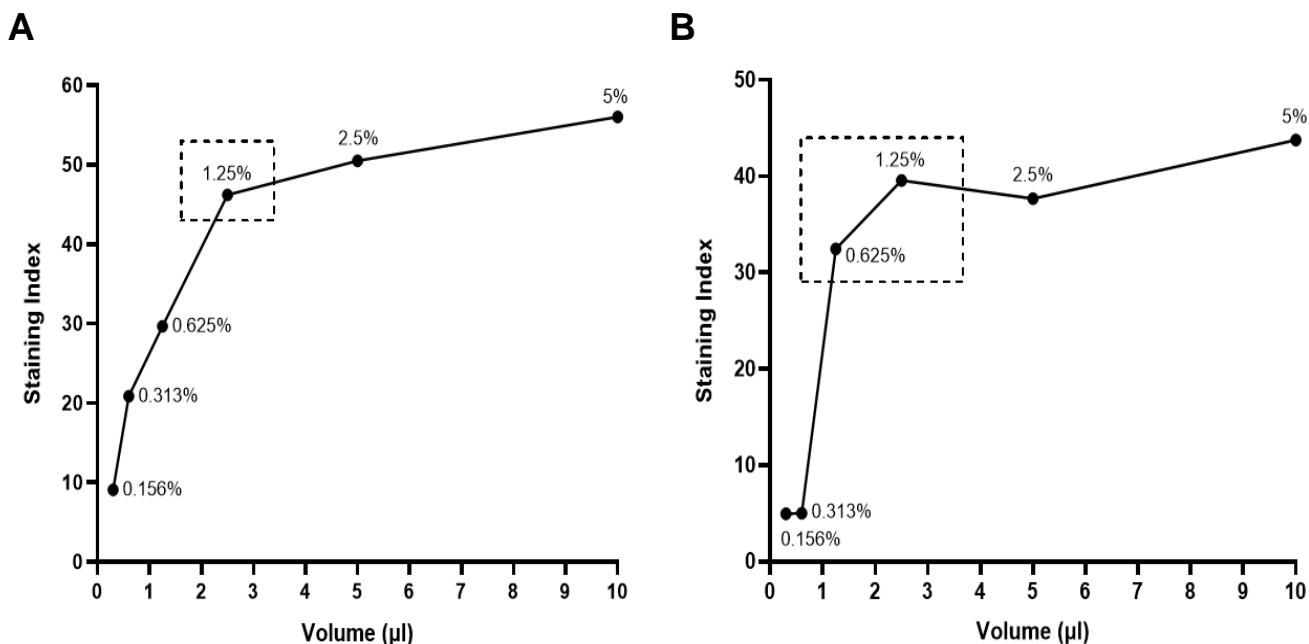


Figure 3.10: Titration of CD90 in rat inguinal and retroperitoneal adipose-derived mesenchymal stem cells (AD-MSCs). Inguinal subcutaneous and retroperitoneal visceral AD-MSCs were stained with FITC-conjugated CD90 at decreasing dilutions, and the staining index value for each titre was calculated and plotted. The optimal separation of the positively stained and unstained cell populations was observed at an SI of 46.19 (1.25%) in the (A) inguinal AD-MSCs and between 39.59 (1.25%) and 32.47 (0.625%) in the (B) retroperitoneal AD-MSCs. Optimal SI's for each cell population are indicated with a box.

ii. Mesenchymal Stem Cell Surface Marker Expression in Inguinal and Retroperitoneal AD-MSCs

Prior to the quantification of the mesenchymal cell surface marker expression, unstained samples of the subcutaneous and visceral AD-MSCs from each diet group were acquired on the Beckman Coulter DxFLEX flow cytometer so that the cells of interest could be distinguished by gating. Gating based on the forward-scatter (FSC) vs. side-scatter (SSC) density plot excluded extracellular debris based on the size and granularity of the AD-MSCs within the sample (Figure 3.11 A). Of the 50,000 events recorded in each sample, >98% of the cells were included in the FSC vs. SSC gate. Single-cell, also referred to as singlet, gating further differentiated the AD-MSCs within the sample by excluding any non-single cells in the form of doublets, or clumps (Figure 3.11 B). Of the >49,000 events recorded after gating for FSC vs. SSC, approximately 17,700 singlets were identified in each sample which therefore represented the cells of interest within which the expression levels of the selected antigens would be measured. The FSC vs. SSC and singlet plots of all subcutaneous and visceral control, HFD, and ESD samples are presented in Appendix Figure D.2.

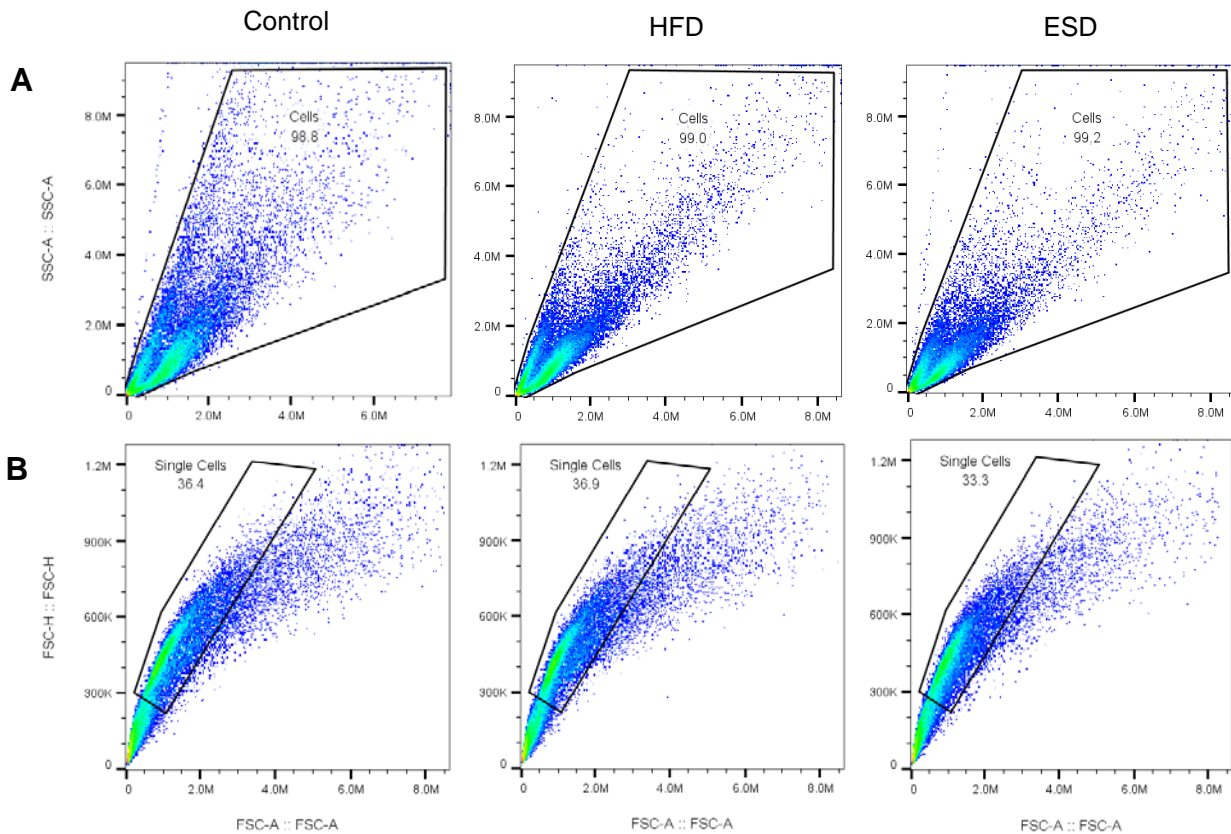


Figure 3.11: Representative forward-scatter vs. side-scatter and single-cell plots showing the gating strategies used for the control, high-fat diet, and elevated sugar diet AD-MSCs. (A) The size and granularity of the homogenous control, HFD, and ESD AD-MSC samples. (B) Gating of single cells based on the forward-scatter area vs. forward-scatter height.

Positive staining of the mesenchymal stem cell marker CD90 was exhibited by both the subcutaneous and visceral AD-MSCs (Figure 3.12 and Figure 3.13). Within the control diet group, the subcutaneous AD-MSCs (93.9%) expressed a higher percentage of CD90 than the visceral AD-MSCs (70.7%). The CD90 expression in the HFD AD-MSC samples did not appear to differ, with the subcutaneous AD-MSCs exhibiting 99.2% positivity and the visceral AD-MSCs exhibiting 98.7% positivity. Expression of CD90 in the ESD samples was very low in comparison to the positive expression percentages measured in the other two diet groups. Only 64.4% of the ESD subcutaneous AD-MSCs and 24.6% of the ESD visceral AD-MSCs expressed CD90. All subcutaneous and visceral AD-MSCs expressed low levels (< 0.33%) of the haematopoietic marker CD45.

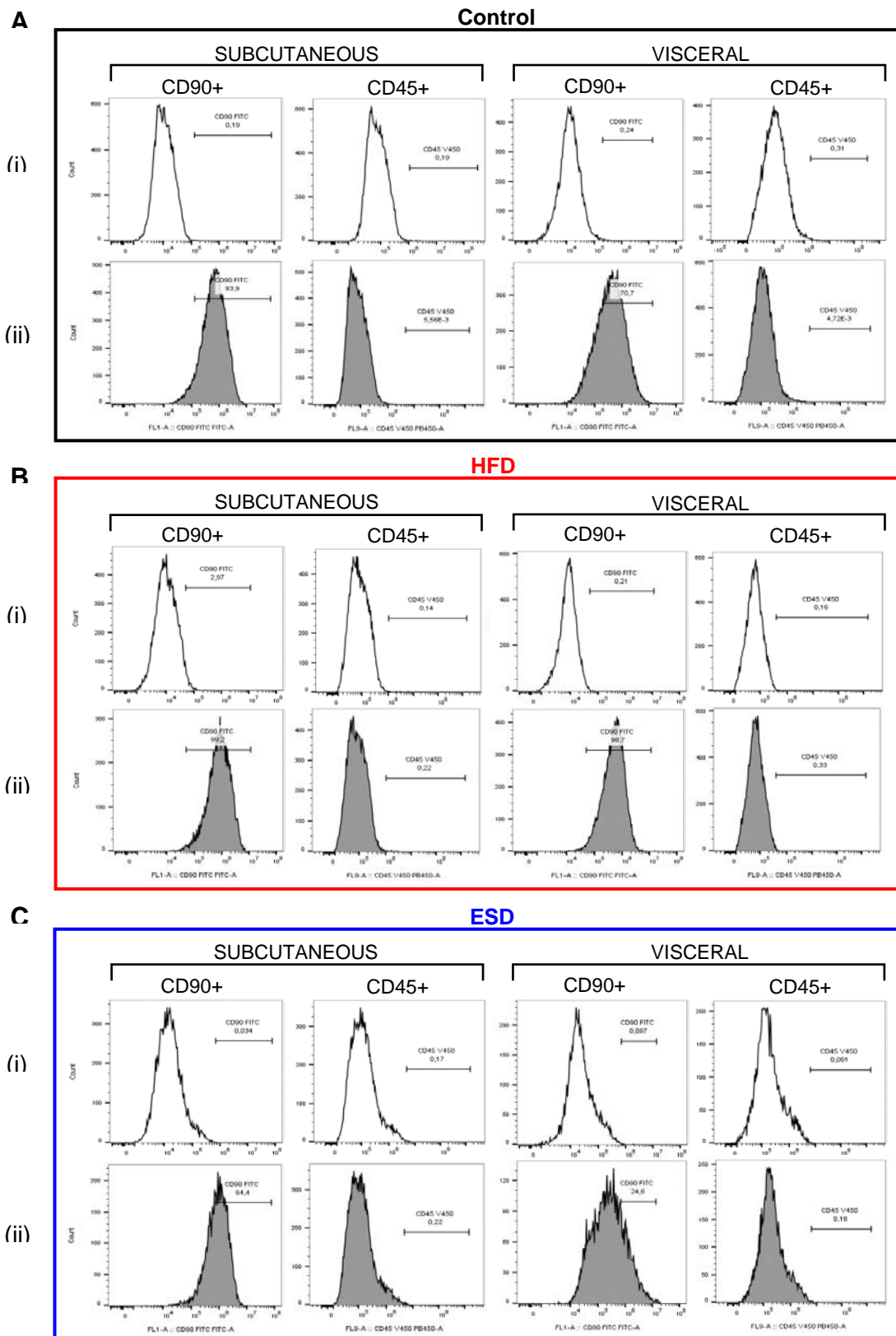


Figure 3.12: Mesenchymal cell surface marker expression profile of inguinal subcutaneous and retroperitoneal visceral AD-MSCs isolated from control, high-fat diet-, and elevated sugar diet-fed male Wistar rats. Subcutaneous and visceral AD-MSCs were isolated, expanded, and purified through serial subculture until passage 3 at which point, once ~80% confluence had been reached, they were labelled with either CD90-FITC or CD45-V450 fluorescent conjugated antibodies. Histograms of (A) Control, (B) high-fat

diet, and (C) elevated sugar diet (i) unlabelled control subcutaneous and visceral AD-MSCs and (ii) subcutaneous and visceral AD-MSCs labelled with the mesenchymal stem cell marker CD90 and haematopoietic stem cell marker CD45. For each experiment, 50,000 events were recorded of which 17,000 were gated and analysed using FlowJo Vx software (Version 10.8.1, Treestar, Oregon, USA). The data are representative of one biological repeat of the subcutaneous and visceral AD-MSCs from each diet group. HFD – High-fat diet; ESD – Elevated sugar diet.

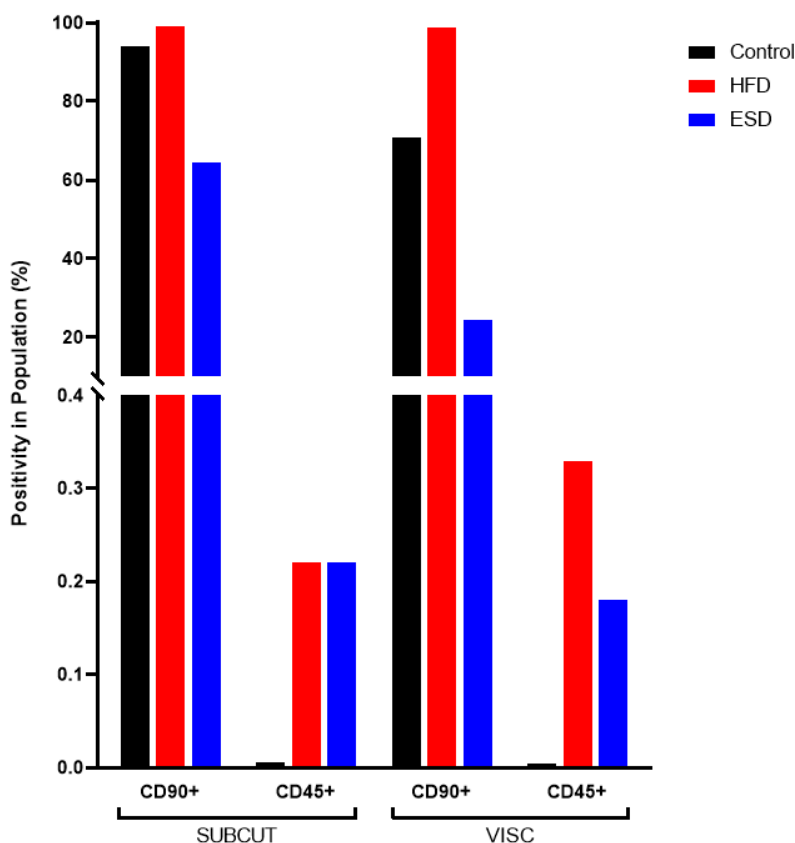


Figure 3.13: Percentage of control, high-fat diet, and elevated sugar diet subcutaneous and visceral AD-MSCs demonstrating positive expression of mesenchymal stem cell marker CD90 and haematopoietic marker CD45. Subcutaneous and visceral AD-MSCs were isolated, expanded, and purified through serial subculture until passage 3 at which point, once ~80% confluence had been reached, they were labelled with either CD90-FITC or CD45-V450 fluorescent conjugated antibodies. The data are representative of one biological repeat of the subcutaneous and visceral AD-MSCs from each diet group. HFD – High-fat diet; ESD – Elevated sugar diet.

3.3.3 Adipogenic Potential of Control, HFD and ESD Subcutaneous and Visceral AD-MSCs

Adipogenesis was initiated in AD-MSCs two days post-confluence at passage three (section 2.12), and after 14 days of adipogenesis conditioned media (CM) was collected from the culture plates (section 2.13) and the intracellular lipids stained with oil red O (ORO) (section 2.15). The control subcutaneous AD-MSCs exhibited widespread lipid accumulation, (Figure 3.14 A) with the lipids formed being numerous and disseminated (Figure 3.14 Aii and Aiii). In contrast, control visceral AD-MSCs differentiated into dense clusters of adipocytes with large intracellular lipids (Figure 3.14 B). The *in vitro* differentiated subcutaneous and visceral adipocytes from the HFD and ESD groups did not deviate from these adipogenic morphologies.

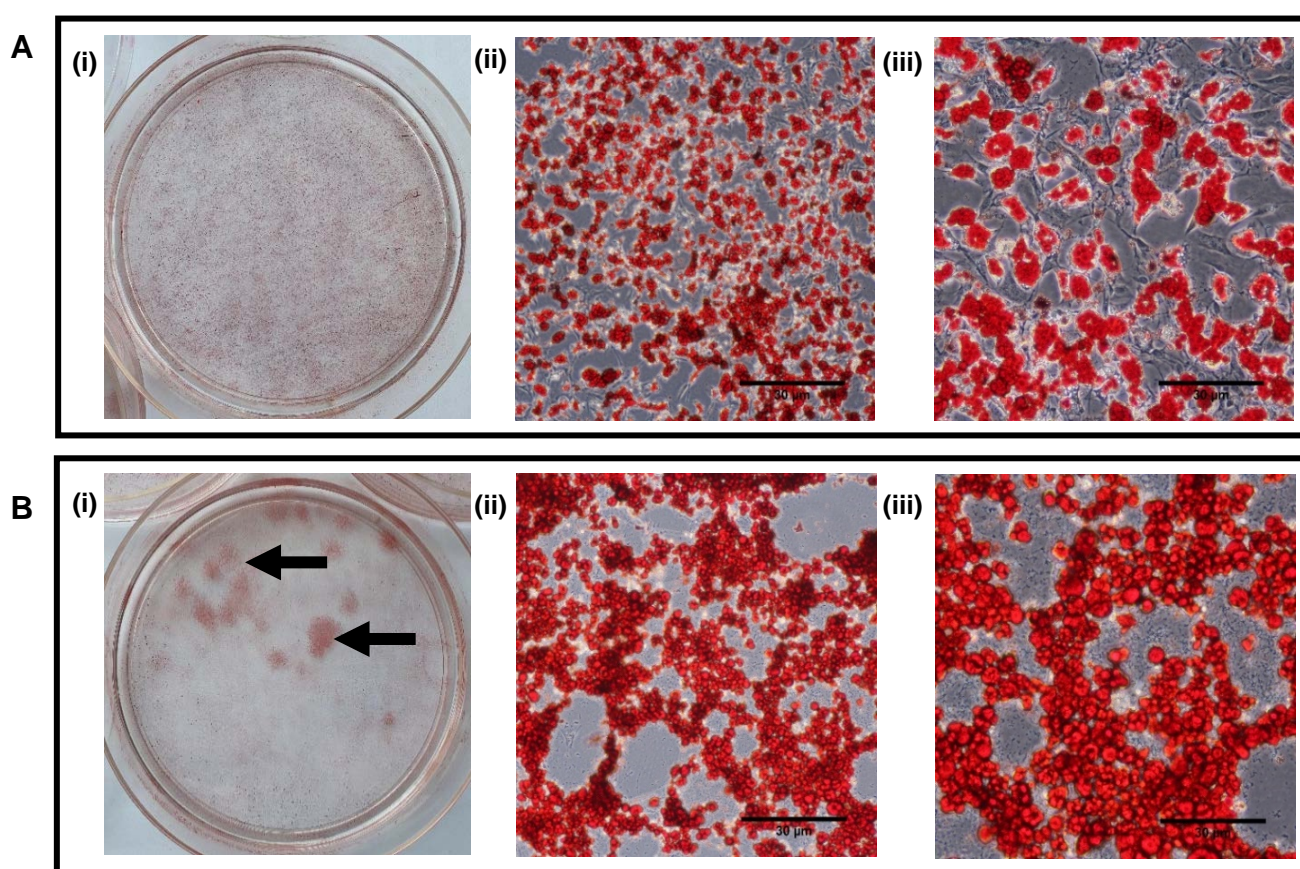


Figure 3.14: Representative images of oil red O-stained lipid droplets accumulated *in vitro* by inguinal subcutaneous and retroperitoneal visceral AD-MSCs following 14 days of adipogenesis. Inguinal and retroperitoneal AD-MSCs were isolated and expanded *in vitro* until two days post-confluence at passage three, and subsequently underwent adipocytic differentiation for 14 days. Dense clusters of lipid accumulation are highlighted by the black arrows. Micrographs in **A(ii)** and **B(ii)** were taken at 10X magnification, and micrographs in **A(iii)** and **B(iii)** were taken at 20X magnification. Scale bars = 30 µm.

To quantify the amount of adipogenesis induced within the AD-MSC cell populations, the cells were stained with ORO – a lysochrome which preferentially binds to the intracytoplasmic lipids

accumulated as a characteristic marker of adipogenesis – and crystal violet, so that the *in vitro* cell density could be accounted for when analysing the results. The eluted stains were subsequently analysed via spectrophotometry (section 2.15). These analyses revealed that the mean percentage of lipid accumulation per cell in culture was 58.38% and 79.71% in the control inguinal (n = 7) and control retroperitoneal (n = 7) cell populations, respectively. Similar volumes of adipocytic differentiation were observed in the HFD and ESD AD-MSCs samples from both adipose depots. This suggests that the adipocyte differentiation protocol was successful in inducing adipogenesis in control, HFD, and ESD AD-MSCs in both cell populations.

This project aimed to establish whether mature adipocytes within subcutaneous adipose tissue can induce adipogenesis in visceral AD-MSCs through endocrine communication, and vice versa. The ability to induce a high degree of adipogenesis within the AD-MSCs *in vitro* increases the likelihood that the CM collected from differentiated cells encompass a substantial proportion of the adipocyte secretome. Thus, as a majority of the AD-MSCs were observed to have accumulated lipids – a characteristic marker of adipogenesis – the CM collected from these cells was acceptable for use in the CM experiments to follow.

3.4 Impacts of Varying Concentrations of Adipogenic Media – A Preliminary Study

3.4.1 Introduction to Preliminary Investigation

As a result of the 24-hour incubation period when harvesting CM (section 2.13), the metabolic activities of the cells lead to the depletion of the amino acids, vitamins, cofactors, and carbohydrates present in the DMEM ²¹⁰. The addition of this media to recipient cells without supplementation would, therefore, result in reduced proliferation and potentially cell death as the factors within the DMEM are required for the maintenance of a healthy intracellular metabolism. To circumvent this issue when studying the effects of CM on various recipient cells, prior studies have combined equal parts CM and adipogenic media (AM) or standard growth media (SGM) ^{92,211}. In this study, to establish whether this 50/50 mix is optimal for the assessment of the effects of CM on adipocytic differentiation of AD-MSCs, preliminary experiments were conducted.

Subcutaneous and visceral AD-MSCs isolated from ~12-week-old male Wistar rats (n = 3) served as the recipient cells for this preliminary experiment. To determine the cut-off concentration of AM which induces adipogenesis below which no terminal differentiation occurs, thus permitting the effects of CM to be observed, the cells were treated with varying concentrations of AM. Concurrently, the impact of 24-hour serum starvation was also assessed as many published articles make use of this technique to synchronise the cell cycles of the AD-MSCs before the initiation of adipogenesis, rather than waiting for them to reach two days post-confluence as our protocol dictates ^{212–215}.

Semi-confluent inguinal and retroperitoneal AD-MSCs (~80%) at passage two, were trypsinised and seeded into 20 wells of a 24-well culture plate at the recommended 5000 cells/cm² as per the plate

set up in Appendix Figure D.3 ²¹⁶. The plates were then incubated at 37°C, 5% CO₂ with the SGM being replaced every two to three days until the AD-MSCs of both depots were two days post-confluence at passage three. Half of each plate was then serum-starved for 24-hours by removing the SGM from 10 of the wells and replacing it with serum-free DMEM (supplemented with 1% PenStrep). The control cells were maintained in SGM. Subsequently, the media was removed from all 20 wells, the cells were rinsed with prewarmed PBS, and either 100%, 75%, 50%, or 25% AM together with a vehicle control (VC) (Appendix Table C.2) was added to the serum-starved (SS) and non-serum starved (NSS) AD-MSCs in duplicate. To prevent the decreasing volumes of FBS in the varying concentrations of AM from impacting cell viability, the concentration of FBS was maintained at 10% throughout the treatment groups. The media was changed twice a week for 14 days (section 2.12).

Following 14 days of treatment, the media was aspirated from the plates and the cells stained with ORO and CV to evaluate the lipid accumulation qualitatively and quantitatively by microscopy, spectrophotometry, and *in-silico* analyses (section 2.15). The resulting data were compared using a two-way ANOVA, where serum level and AM concentration were the two independent variables and Dunnett post-hoc test to determine the optimal concentration of AM for use in the CM experiments.

3.4.2 Results of Preliminary Investigation

After 14-days, representative micrographs of each treatment group were taken using a Canon 600D camera mounted on an Olympus inverted phase-contrast microscope (Figure 3.15 and 3.16 A). The mean ORO-stained areas (%) were computed from the micrographs (n = 3 for each treatment) using Fiji ImageJ Software (Figure 3.15 and 3.16 B). Thereafter, the cells were counterstained with CV and spectrophotometry was conducted on the eluted stains. The absorbance readings were analysed and are expressed as a ratio of relative lipid content per cell in culture (ORO/CV) (Figure 3.15 and 3.16 C).

There is an increase in the quantity of ORO staining with increasing concentrations of AM in inguinal AD-MSC (Figure 3.15). Specifically, the cells treated with 100% AM had the largest measured ORO-stained areas (Figure 3.15 B; SS 22.54 ± 7.11% and NSS 25.96 ± 3.61%), and relative lipid accumulation (Figure 3.15 C; SS 0.67 ± 0.10 and NSS 0.70 ± 0.09), respectively. The 25% AM duplicates in all three biological repeats exhibited the least lipid accumulation of the four AM treatment groups, having had a mean ORO-stained area of 1.34 ± 0.41% (SS) and 4.7 ± 2.12% (NSS), and a relative ORO/CV ratio of 2.59 ± 2.97 (SS) and 3.76 ± 0.31 (NSS). No significant differences were noted in the results of the SS and NSS treatment groups.

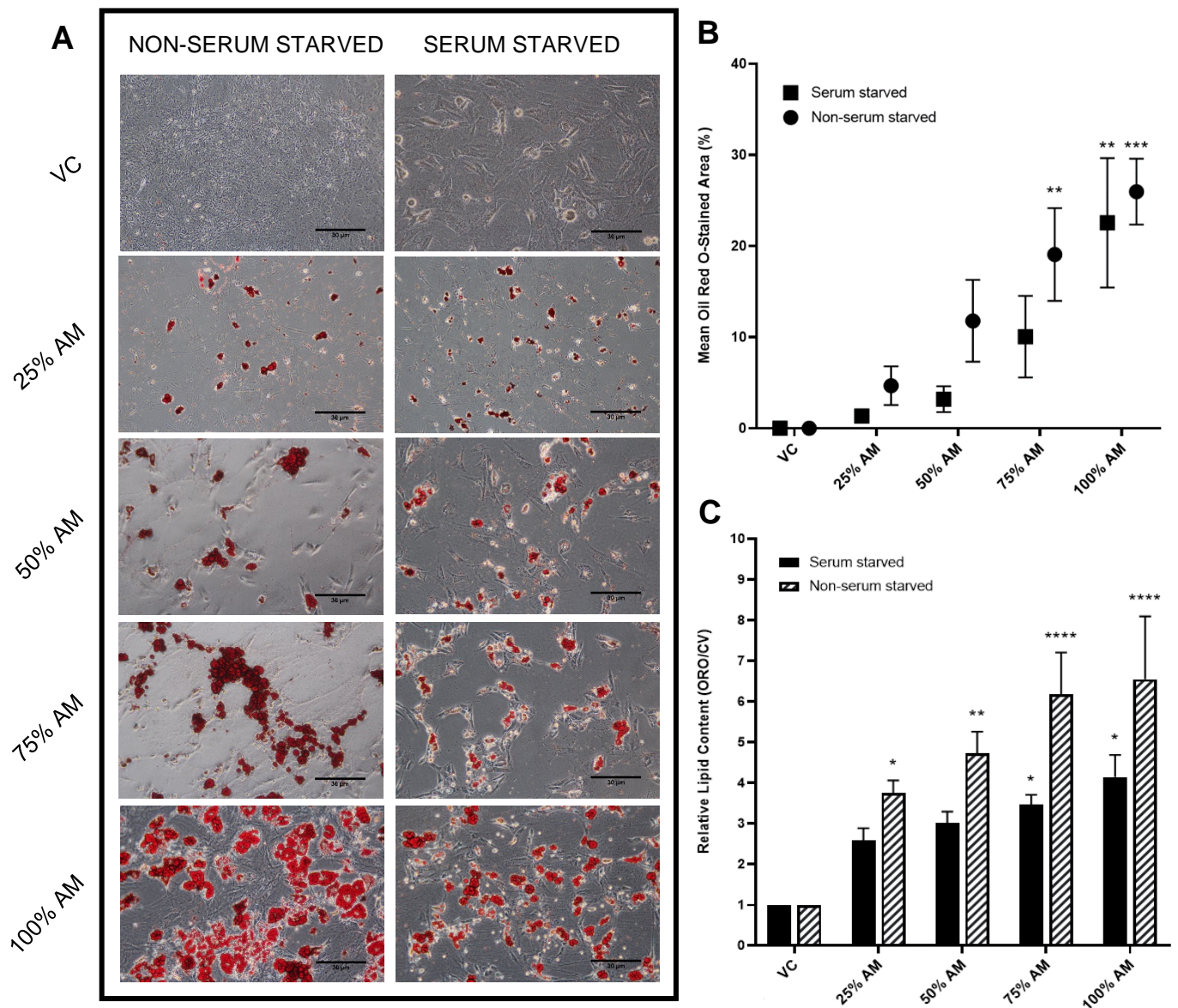


Figure 3.15: Micrographs, in-silico lipid quantification and spectrophotometric analysis of inguinal AD-MSCs subjected to 14-day treatment with varying concentrations of adipogenic media (AM). Representative micrographs (A) taken at 20X magnification of oil red o (ORO). The data generated by in-silico analyses of $n = 3$ micrographs per treatment using Fiji ImageJ v1.53c (B) are expressed as a mean percentage of ORO-stained area. From the spectrophotometric analyses of eluted ORO and crystal violet cytology stains from the inguinal adipocytes, the relative lipid contents were calculated and are represented as a ratio of ORO/CV relative to the VC which was set to 1 (C). Data are representative of three independent biological repeats which were performed in duplicate and are displayed as mean \pm SEM. A two-way ANOVA where serum level and AM concentration were the two independent variables and Dunnett post-hoc test were implemented to assess statistical significance (* $p < 0.05$ vs. VC; ** $p < 0.01$ vs. VC; *** $p < 0.001$ vs. VC; **** $p < 0.0001$ vs. VC). AM – Adipogenic media; VC – Vehicle control.

The lipid accumulation appears to correspond with the concentration of AM with which the cells were treated. The retroperitoneal adipocytes were, however, qualitatively observed to accumulate larger

lipid droplets than the inguinal cells during adipogenesis. The SS and NSS 75% AM ($p < 0.0001$) and 100% AM treatments ($p < 0.0001$) displayed a marked increase in ORO-stained area compared to the VC (Figure 3.16 B). The relative lipid accumulation of the 75% AM and 100% AM were also noted to have increased significantly vs. the VC (SS and NSS 100% AM, $p < 0.01$; SS and NSS 75%, $p < 0.05$).

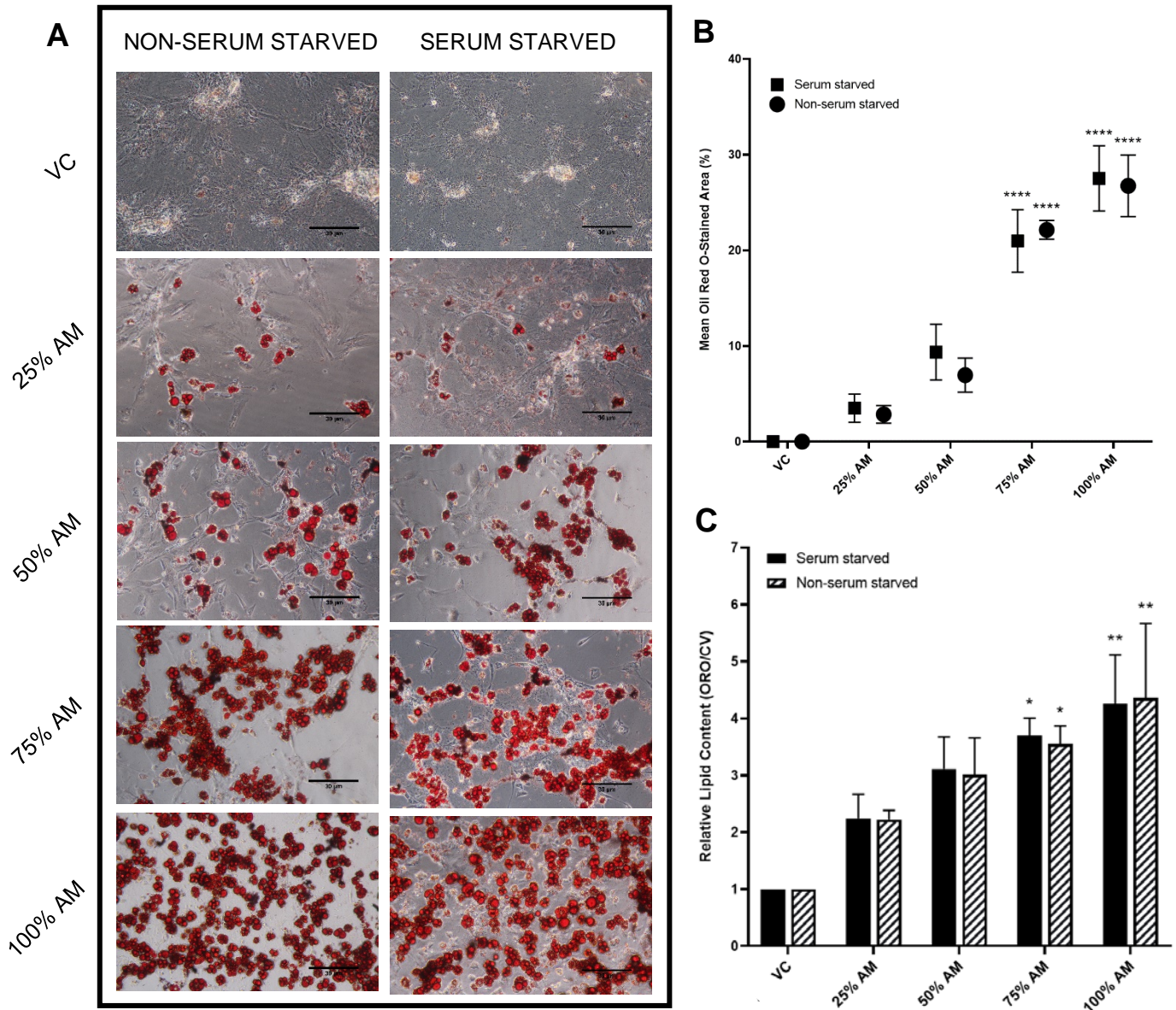


Figure 3.16: Micrographs, in-silico lipid quantification and spectrophotometric analysis of retroperitoneal AD-MSCs subjected to 14-day treatment with varying concentrations of adipogenic media. Representative micrographs (A) of oil red o (ORO) stained lipid droplets (20X magnification). The data generated by in-silico analyses of $n = 3$ micrographs per treatment using Fiji ImageJ v1.53c (B) are expressed as a mean percentage of ORO-stained area. The relative lipid contents of each duplicate were calculated from spectrophotometric analyses of eluted ORO and crystal violet stains from the retroperitoneal adipocytes and are expressed as a ratio of ORO/CV relative to the VC which was set to 1 (C). Data are representative of three independent biological repeats which were performed in duplicate and are displayed as mean \pm SEM. A two-

way ANOVA where serum level and AM concentration were the two independent variables and Dunnett post-hoc test were implemented to assess statistical significance (* $p < 0.05$ vs. VC; ** $p < 0.01$ vs. VC; **** $p < 0.0001$ vs. VC). AM – Adipogenic media; VC – Vehicle control.

When added to the cells of both depots, the 25% AM and 50% AM treatments induced the least adipogenesis, but lipid accumulation was still observed in all duplicate treatments within the $n = 3$ biological repeats. Based on these results, having not found a statistically significant difference between the effects of the 25% AM and 50% AM groups in either of the quantification methods employed, a concentration of 50% AM was selected for use in this study. This concentration, as a result of the addition of a slightly higher volume of AM compared to 25% AM, when combined with the CM during treatments, will conserve the limited pool of CM for further analyses in subsequent studies. A 50% mixture of AM and CM has also been frequently used in prior studies^{92,211}.

3.5 Effects of Control, HFD and ESD Conditioned Media on the Adipocytic Differentiation of Subcutaneous and Visceral AD-MSCs

3.5.1 Introduction to the Conditioned Media Study

To evaluate the impact of subcutaneous and visceral CM on adipogenesis in AD-MSCs, the control CM, HFD CM, and ESD CM samples – collected and prepared as described in section 2.13 – were added to cells *in vitro*. Inguinal and retroperitoneal AD-MSCs isolated from age-matched, 19-week-old control male Wistar rats were used as the recipient cells for this study. Three biological repeats were intended for use in this investigation, however, the retroperitoneal AD-MSCs isolated from one of the rats exhibited irregular proliferation rates and morphologies following subculture at passage three. For these reasons, a decision was made to exclude those cells from the study as the results obtained from using them as recipients for the CM treatments would not have been reliable. The treatments were, therefore, added to $n = 3$ inguinal and $n = 2$ retroperitoneal AD-MSCs in duplicate. Statistical analyses were performed on the *in-silico* ORO quantification and spectrophotometry results regardless of the low biological repeat number in the retroperitoneal samples. Consequently, these results must be regarded as preliminary upon which future studies may expand.

The CM samples were added to the cells in three formulations, namely, (i) as 100% CM control, (ii) combined 1:1 with standard growth media (iii) combined 1:1 with adipogenic media. All treatments were supplemented with 10% FBS (final concentration) to sustain an equal level of attachment factors, hormones, and nutrients so that potential deficiencies in these factors could not confound the results (Appendix Table D.1). The treatments were initiated once the cells had reached two days post-confluence at P3 (section 2.12) and were composed directly before use. The treatment groups were replaced twice a week for two weeks prior to analysis, at which point one well of each duplicate was stained with ORO and CV and lipid accumulation quantified (section 2.15). Ribonucleic Acid (RNA) was extracted from cells in the second well of each treatment duplicate using the RNeasy

Mini kit® RNA isolation kit (Qiagen) as per the manufacturer's instructions so that gene expression analyses can be conducted in the future ²¹⁷.

3.5.2 Quantitative Analyses of Photomicrographs of Conditioned Media Treated Inguinal and Retroperitoneal Recipient AD-MSCs by In-silico Oil Red O Quantification and Spectrophotometry

Oil red O staining of the 14-day treated subcutaneous (n = 3) and visceral (n = 2) AD-MSCs were quantified through the *in-silico* analysis of triplicate photomicrographs taken of each treatment well (Figure 3.14). The images were analysed using Fiji ImageJ software (Version 1.53c, National Institute of Health, US) (section 2.15), with the outputs indicating the percentage of each micrograph that has been stained with ORO. The ORO stain was subsequently eluted and the AD-MSCs stained with crystal violet (CV) to account for any variation in cell densities (section 2.15). The absorbances of the eluted dyes were measured via spectrophotometry and the ORO/CV ratios were calculated relative to the negative control for each treatment. One-way ANOVAs with a Dunnett's post-hoc were conducted to detect statistical significance in relative lipid accumulation between each treatment as compared to the respective negative control.

Very few lipid droplets were observed to have developed in the inguinal recipient AD-MSCs treated with 100% CM (Figure 3.17 A), with the only visible lipids being in the elevated sugar visceral CM (ESVCM) treated cells. Analysis by one-way ANOVA revealed that, when compared against the negative VC, no statistical significance in the ORO-stained area was noted in any of the treatment groups. In addition, low levels of differentiation occurred in the visceral recipient AD-MSCs in all of the control CM treatments (Figure 3.17 A), with the highest recorded mean ORO-stained area (Figure 3.17 B) being in the ESVCM treated cells with $0.79 \pm 0.42\%$ ($p = 0.013$ vs. SGM).

Spectrophotometric analyses (Figure 3.17 C) of all CM treatment groups in AD-MSC recipient cells from both depots exhibited no statistical differences in relative lipid accumulations. None of the CM-treated inguinal recipient cells had a relative lipid accumulation that exceeded the negative SGM control. All the calculated relative lipid contents of the retroperitoneal recipients were, however, higher than the negative SGM control, with the highest measurement being 2.00 ± 0.49 in the cells exposed to the high-fat subcutaneous CM (HFSCM).

The effects of each CM treatment were not compared between the inguinal and retroperitoneal recipient cells as drawing these comparisons would reduce the statistical power of this investigation as a result of the small sample sizes. It was therefore decided that the most important comparison to be made was between the CM treatments and the negative control in each experiment to assess the effects of the treatments.

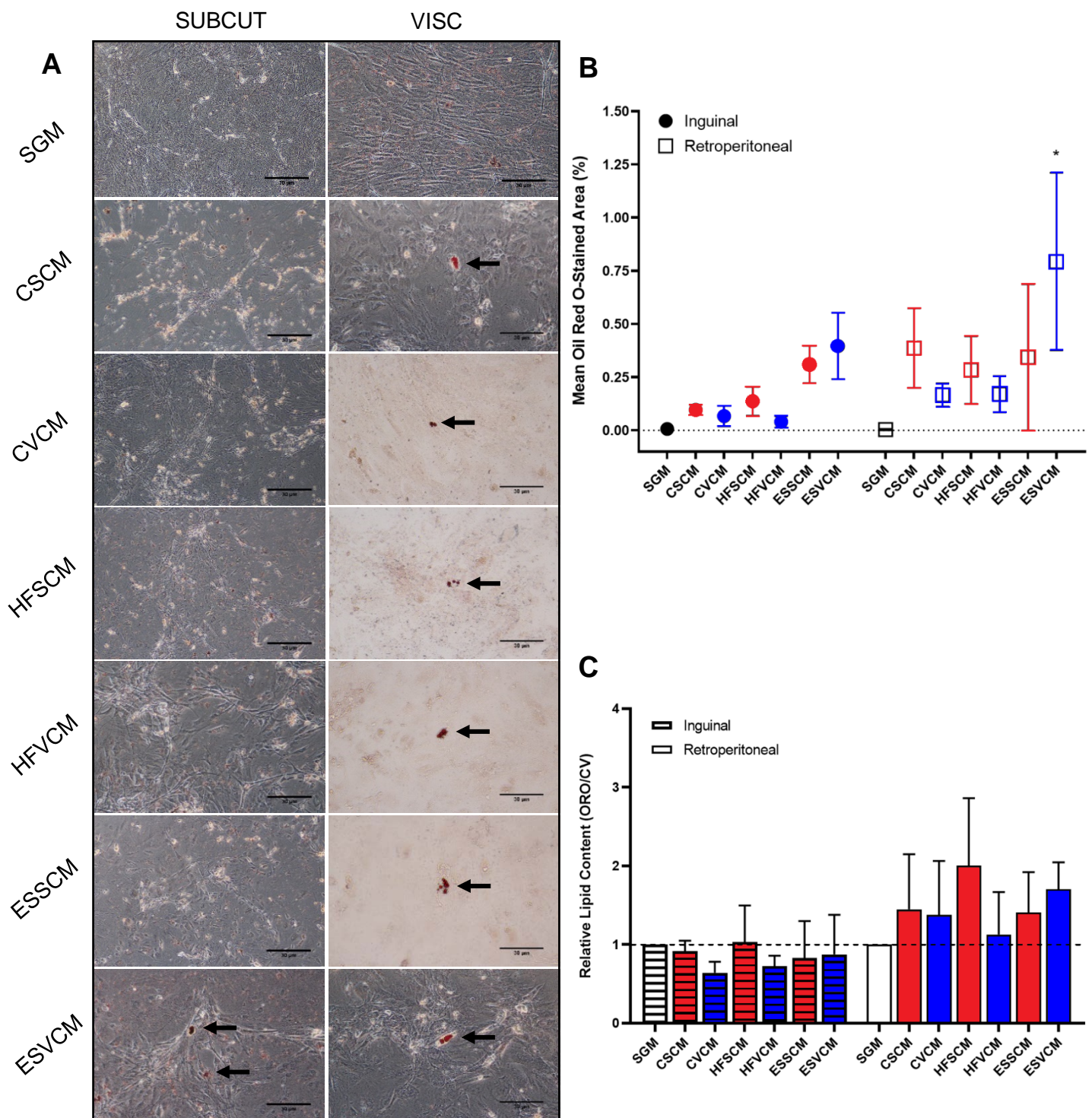


Figure 3.17: Representative micrographs, in-silico, and spectrophotometric quantification of oil red O-stained inguinal subcutaneous and retroperitoneal visceral AD-MSCs treated with conditioned media harvested from control, high-fat diet, and elevated sugar diet-fed rats. Conditioned media (CM) was collected from *in vitro* differentiated subcutaneous and visceral adipocytes isolated from control, high-fat- and elevated-sugar diet-fed male Wistar rats. The CM samples were then added to subcutaneous ($n = 3$) and visceral ($n = 2$) recipient AD-MSCs isolated from age-matched, 19-week-old control male Wistar rats for 14 days, with the treatments being changed twice a week. Black arrows (A), indicate differentiation in CM treated AD-MSCs. Subcutaneous CM treatment groups are delineated by red lines and visceral CM by blue lines.

(B) Three representative micrographs were taken of the subcutaneous and visceral cells in each treatment group and the mean ORO-stained areas were measured in Fiji ImageJ for Windows. (C) Spectrophotometric analyses of the eluted ORO and crystal violet stains were performed in triplicate and are represented as mean \pm SEM for each depot. Subcutaneous CM treatment groups are delineated by red bars and the visceral CM by blue bars. A one-way ANOVA with Dunnett's post-hoc test was used to test statistical significance ($*p < 0.05$ vs. SGM). Micrographs were taken at 20X magnification. Scale bars = 30 μ m. CSCM – Control subcutaneous conditioned media; CVCM – Control visceral conditioned media; ESSCM – Elevated sugar subcutaneous conditioned media; ESVCM – Elevated sugar visceral conditioned media; HFSCM – High-fat subcutaneous conditioned media; HFVCM – High-fat visceral conditioned media; SGM – Standard growth media; SUBCUT – Subcutaneous (inguinal); VISC - Visceral (retroperitoneal).

The addition of SGM to the CM treatment samples was performed to replace depleted nutrients, amino acids and vitamins required to sustain cell viability *in vitro*. Lipid accumulation was identified in all the inguinal (n = 3) and retroperitoneal AD-MSCs (n = 2) treated with a combination of CM and SGM (Figure 3.18 A). *In-silico* quantification of ORO-staining in the inguinal recipient AD-MSCs (Figure 3.18 B) revealed that, though higher than all other treatment groups, the mean area of the ESVCM+SGM group ($0.48 \pm 0.22\%$) did not differ significantly from the mean area of the SGM negative control ($0.003 \pm 0.003\%$). Similarly, spectrophotometry of the eluted ORO and CV stains revealed that the ESVCM+SGM (0.77 ± 0.1 , $p > 0.05$) had the highest relative lipid accumulation (ORO/CV) outputs within the inguinal recipient AD-MSCs.

The retroperitoneal recipient cells displayed a considerable increase in mean ORO-stained area (Figure 3.18 B) as compared to the negative SGM control ($0.007 \pm 0.003\%$) when treated with both the control visceral CM + SGM (CVCM+SGM) ($0.18 \pm 0.04\%$, $p = 0.028$) and ESVCM+SGM ($0.28 \pm 0.09\%$, $p = 0.0007$). This trend was also noted in the spectrophotometry outputs from the visceral recipient cells as both the HFSCM+SGM (1.41 ± 0.42) and ESVCM+SGM (1.63 ± 0.1) treatment groups had the highest mean relative lipid accumulations ($p > 0.05$).

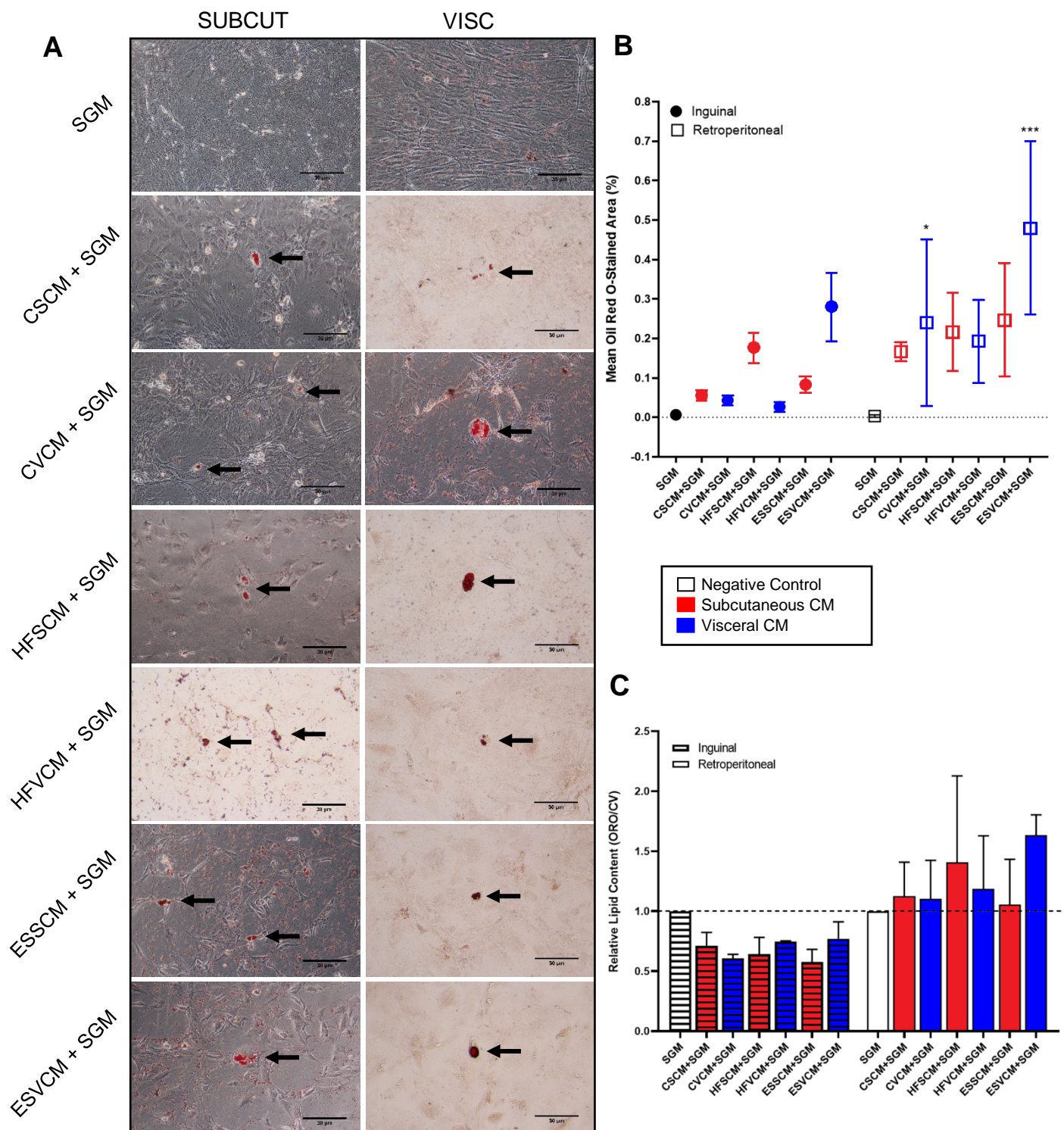


Figure 3.18: Representative micrographs, in-silico, and spectrophotometric of oil red O-stained inguinal subcutaneous and retroperitoneal visceral AD-MSCs treated with a combination of conditioned media and standard growth media. Conditioned media (CM) was collected from *in vitro* differentiated subcutaneous and visceral adipocytes isolated from control, high-fat- and elevated-sugar diet-fed male Wistar rats. The CM samples were then added to subcutaneous ($n = 3$) and visceral ($n = 2$) recipient AD-MSCs isolated from age-matched, 19-week-old control male Wistar rats for 14 days, with the treatments being changed twice a week. Black arrows (A), indicate differentiation in CM treated AD-MSCs. Subcutaneous

CM treatment groups are delineated by red lines and the visceral CM treatments by blue lines. (B) Three representative micrographs were taken of the subcutaneous and visceral cells in each treatment group and the mean ORO-stained areas were measured in Fiji ImageJ for Windows. (C) Spectrophotometric analyses of the eluted ORO and crystal violet stains were performed in triplicate and are represented as mean \pm SEM for each depot. Subcutaneous CM treatment groups are delineated by red bars and the visceral CM treatments by blue bars. A one-way ANOVA with Dunnett's post-hoc test was used to test statistical significance ($*p < 0.05$ vs. SGM; $***p < 0.001$ vs. SGM). Micrographs were taken at 20X magnification. Scale bars = 30 μ m. CSCM – Control subcutaneous conditioned media; CVCM – Control visceral conditioned media; ESSCM – Elevated sugar subcutaneous conditioned media; ESVCM – Elevated sugar visceral conditioned media; HFSCM – High-fat subcutaneous conditioned media; HFVCM – High-fat visceral conditioned media; SGM – Standard growth media; SUBCUT – Subcutaneous (inguinal); VISC - Visceral (retroperitoneal).

To assess whether further supplementation of the CM with adipogenic factors may potentiate CM-induced adipogenesis, AM was combined at a 1:1 ratio (determined through preliminary experimentation in 3.4) with the CM from the various diet groups. Micrographs of the inguinal recipient AD-MSCs (Figure 3.19 A) show that the cells are capable of accumulating clusters of lipids as seen in the AM positive control. Although a few more lipids may be visible in these images when compared to those in Figure 3.17 and Figure 3.18, the CM+AM treatments do not appear to have substantially increased the quantity of adipogenesis in the subcutaneous treatment cells. When assessing the *in-silico* ORO quantification outputs from the inguinal recipient cells (Figure 3.19 B), the control subcutaneous conditioned media + AM (CSCM+AM) ($2.21 \pm 1.14\%$) and the AM positive control ($1.15 \pm 0.55\%$) treatments had the highest and second-highest ORO-stained areas, respectively, of all seven treatment groups. Nevertheless, these differences were not statistically significant. In contrast, the spectrophotometry results of the subcutaneous recipients indicate that the AM positive control (4.13 ± 0.643 , $p = 0.046$), CSCM+AM (4.26 ± 0.43 , $p = 0.027$) and ESVCM+AM (3.89 ± 0.74 , $p = 0.028$) had significantly higher relative lipid accumulations as compared to the VC.

Due to the large volume of lipid accumulation apparent in the micrographs of the retroperitoneal recipient cells (Figure 3.19 A), substantial statistical significance was detected in both the *in-silico* ORO quantification (Figure 3.19 B) and the spectrophotometry (Figure 3.19 C). Following statistical analysis of the ORO-stained areas, when treating the visceral AD-MSCs all seven treatment groups attained a calculated p-value of < 0.0001 when compared to the VC. The CSCM+AM treatment group had the highest mean ORO-stained area overall, with $22.79 \pm 3.85\%$ of the analysed micrographs being stained and had the highest relative lipid accumulation as determined by spectrophotometry (8.11 ± 2.16 , $p < 0.0001$).

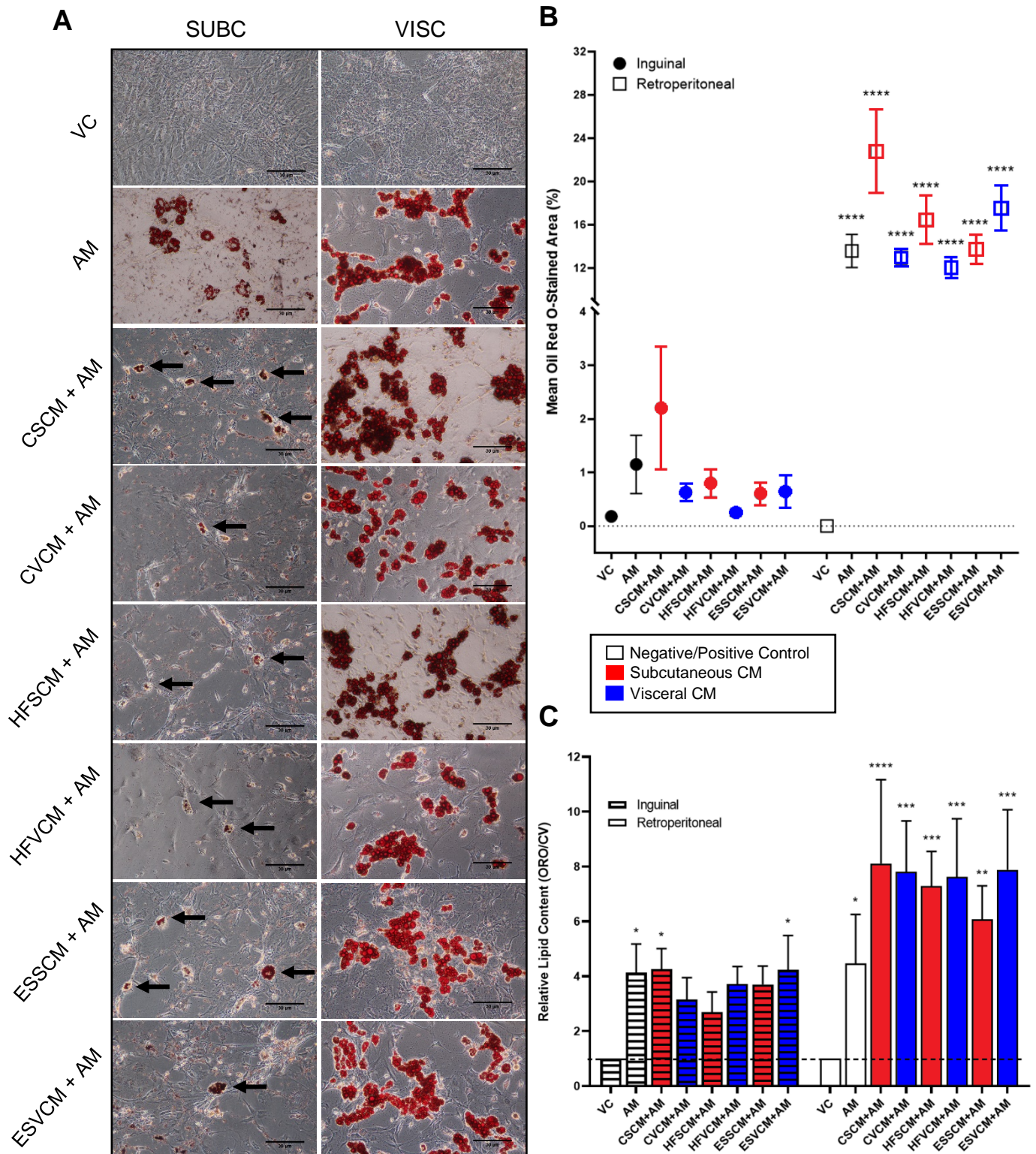


Figure 3.19: Representative micrographs, in-silico, and spectrophotometric quantification of oil red O-stained inguinal subcutaneous and retroperitoneal visceral AD-MSCs treated with a combination of conditioned media and adipogenic media. Conditioned media (CM) was collected from *in vitro* differentiated subcutaneous and visceral adipocytes isolated from control, high-fat- and elevated-sugar diet-fed male Wistar rats. The CM samples were then added to subcutaneous ($n = 3$) and visceral ($n = 2$) recipient AD-MSCs isolated from age-matched, 19-week-old control male Wistar rats for 14 days, with the treatments being changed twice a week. Black arrows (A), indicate differentiation in CM treated AD-MSCs. Subcutaneous CM

treatment groups are delineated by red lines and the visceral CM treatments by blue lines. (B) Three representative micrographs were taken of the subcutaneous and visceral cells in each treatment group and the mean ORO-stained areas were measured in Fiji ImageJ for Windows. (C) Spectrophotometric analyses of the eluted ORO and crystal violet stains were performed in triplicate and are represented as mean \pm SEM for each depot. Subcutaneous CM treatment groups are delineated by red bars and the visceral CM treatments by blue bars. A one-way ANOVA with Dunnett's post-hoc test was used to test statistical significance (* $p < 0.05$ vs. VC; ** $p < 0.01$ vs. VC; *** $p < 0.001$ vs. VC; **** $p < 0.0001$ vs. VC). Micrographs were taken at 20X magnification. Scale bars = 30 μ m. AM – Adipogenic media; CSCM – Control subcutaneous conditioned media; CVCM – Control visceral conditioned media; ESSCM – Elevated sugar subcutaneous conditioned media; ESVCM – Elevated sugar visceral conditioned media; HFSCM – High-fat subcutaneous conditioned media; HFVCM – High-fat visceral conditioned media; SGM – Standard growth media; SUBCUT – Subcutaneous (inguinal); VC – Vehicle control; VISC – Visceral (retroperitoneal).

Conditioned media harvested from control, HFD, and ESD adipocytes were able to induce lipid accumulation in the retroperitoneal recipient AD-MSCs without supplementation (Figure 3.17) and enhanced the adipogenesis when combined with AM (Figure 3.19). Once depleted nutrients, amino acids and hormones had been replenished with the addition of SGM, a positive effect in the lipid accumulation of the subcutaneous recipient cells was also observed in the micrographs (Figure 3.18 A) despite no statistical significance being reported. Overall, the ESD visceral CM induced the most lipid accumulation when added to the recipient AD-MSCs of both depots as a 100% CM, 1:1 CM:SGM, and 1:1 CM:AM treatment.

3.6 Effects of Control, HFD, and ESD Conditioned Media Supplemented with Rosiglitazone on the Adipocytic Differentiation of Subcutaneous and Visceral AD-MSCs

To investigate the effects of supplementing subcutaneous and visceral CM with a well-known pro-adipogenic drug, a concurrent study was conducted wherein the CM treatments displayed (Table 3.2) were repeated with the addition of Rosiglitazone (Rosi). Rosi induces adipogenesis through stimulation of peroxisome proliferator-activated receptor- γ (PPAR γ), a nuclear receptor abundant on the cell membranes of adipocytes due to its role in regulating catabolic and metabolic processes during adipogenesis²¹⁸. The PPAR γ 2 isoform is a particularly pivotal transcription factor in adipogenesis, yet activation alone does not provoke full differentiation²¹⁹. It was therefore questioned whether the CM could provide enough additional factors to stimulate the AD-MSCs to terminal adipocytic differentiation and lipid accrual. The control, HFD, and ESD subcutaneous and visceral CM samples were, therefore, added to the cells in three formulations, namely, (i) as a CM control supplemented with 10% FBS and Rosi, (ii) CM combined 1:1 with standard growth media, 10% FBS and Rosi (iii) CM combined 1:1 with adipogenic media, 10% FBS and Rosi. A Rosi concentration of 1 μ M was selected for use as it is frequently employed in *in vitro* studies for the

induction of adipogenesis and it represents the average serum concentration in individuals taking a dosage of 4 mg/day for the treatment of type II diabetes mellitus (section 2.14) ^{52,218,220,221}.

The same age-matched control subcutaneous (n = 3) and visceral (n = 2) AD-MSCs described in section 3.4 were used as the recipient cells for this investigation. The CM+Rosi treatments were prepared directly before use and changed twice weekly for 14 days, following which the recipient cells were ORO and crystal violet stained, with triplicate micrographs subjected to *in-silico* analyses, and the eluted stains quantified by spectrophotometry.

3.6.1 Quantitative Analyses of Photomicrographs of Conditioned Media and 1 μ M Rosiglitazone Treated Inguinal and Retroperitoneal Recipient AD-MSCs by *In-silico* Oil Red-O Quantification and Spectrophotometry

Rosiglitazone (Rosi), being a peroxisome proliferator-activated receptor γ (PPAR γ) agonist, has documented pro-adipogenic effects when added to cells *in vitro* ^{52,59,218,222}. The effects of supplementing the control, HFD, and ESD CM samples with 1 μ M Rosi (Figure 3.20 A) on inguinal recipient cells results in induced low-level adipogenesis in all six CM treatment groups. The *in-silico* quantification of the ORO-stained micrographs (n = 3 per treatment) showed that the mean ORO-stained areas were higher than that of the SGM + Rosi ($0.017 \pm 0.007\%$). Although no statistical significance was detected between the treatment groups, the high-fat subcutaneous CM plus Rosi (HFSCM+Rosi) treatment had the largest mean ORO-stained area at $1.39 \pm 0.72\%$. Similarly, the highest relative lipid accumulation in the inguinal recipient cells was recorded in the HFSCM+Rosi group (0.75 ± 0.22), however, none of the treatments had a measured ORO/CV ratio that exceeded the SGM + Rosi negative control thus, no statistical significance was detected.

Wide-spread adipocytic differentiation was observed in all CM+Rosi treated retroperitoneal AD-MSCs (Figure 3.20 A), but the lipids accumulated in these cells were uncharacteristically small for this cell type (section 3.3.3). The outcomes of the *in-silico* ORO quantification complement the micrographs as a majority of the CM treatments had substantially higher mean ORO-stained areas than the negative control (Figure 3.20 B). These groups, namely the CSCM+Rosi ($4.14 \pm 1.59\%$, p = 0.0018), CVSCM+Rosi ($3.76 \pm 1.09\%$, p = 0.0047), HFSCM+Rosi ($4.01 \pm 0.9\%$, p = 0.0025), and HFVCM+Rosi ($3.68 \pm 1.02\%$, p = 0.0058) all surpassed the mean ORO-stained area of the SGM+Rosi treatment group ($0.003 \pm 0.003\%$). The CM collected from both the subcutaneous and visceral elevated sugar diet AD-MSCs did induce more lipid accumulation than the negative control but the differences, as calculated by a Dunnett's post-hoc test, were not significant (SGM+Rosi $0.003 \pm 0.003\%$ vs. ESSCM+Rosi $2.53 \pm 0.67\%$ vs. ESVCM+Rosi $1.57 \pm 0.49\%$, p > 0.05). Spectrophotometry of the eluted ORO and CV stains indicate no considerable differences in the relative lipid accumulation between the CM+Rosi treatment groups and the negative control regardless that all treatments had higher mean ORO/CV ratios than the negative control. The highest of which, consistent with the results of the *in-silico* analyses, is the CSCM+Rosi group (1.58 ± 0.07).

As stated above, comparisons were drawn between responses of the subcutaneous and visceral adipose recipient cells to each treatment group to prevent a reduction in statistical power.

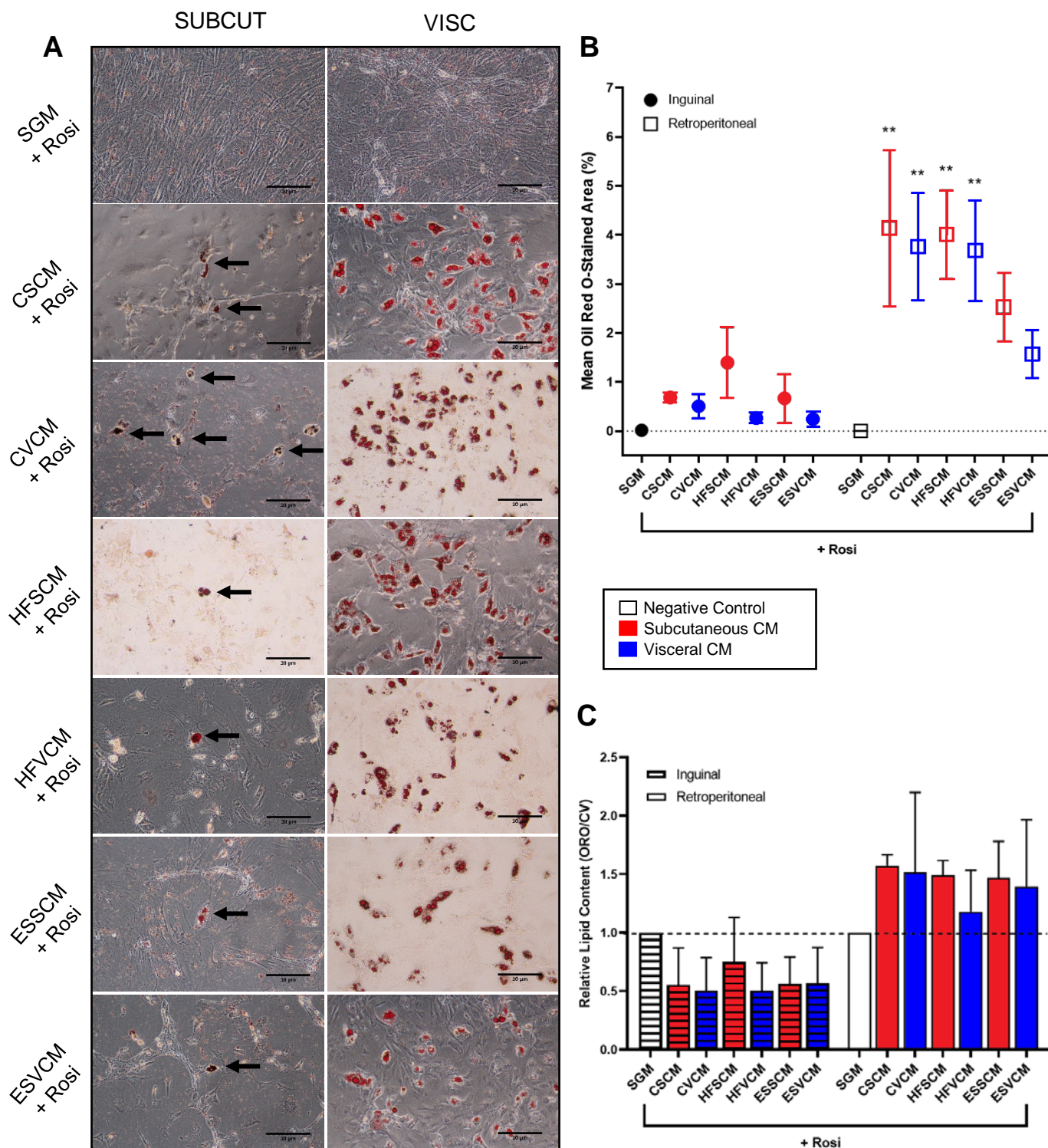


Figure 3.20: Representative micrographs, in-silico, and spectrophotometric quantification of oil red O-stained inguinal subcutaneous and retroperitoneal visceral AD-MSCs treated with conditioned media harvested from control, high-fat diet, and elevated sugar diet-fed rats supplemented with 1 μM Rosiglitazone. Conditioned media (CM) was collected from in vitro differentiated subcutaneous and visceral adipocytes isolated from control, high-fat- and elevated-sugar diet-fed male Wistar rats. The CM samples were

then combined with 1 μ M Rosiglitazone added to subcutaneous ($n = 3$) and visceral ($n = 2$) recipient AD-MSCs isolated from age-matched, 19-week-old control male Wistar rats for 14 days, with the treatments being changed twice a week. **(A)** Black arrows highlight the individual lipid droplets; large clusters of adipocytes are stained red and are evident in all visc CM + Rosi treated cells. Subcutaneous CM treatment groups are delineated by red lines and the visceral CM treatments by blue lines. Three representative micrographs were taken of the **(B)** subcutaneous and visceral cells in each treatment group and the mean ORO-stained areas were measured in Fiji ImageJ for Windows. **(C)** Spectrophotometric analyses of the eluted ORO and crystal violet stains were performed in triplicate and are represented as mean \pm SEM for each depot. Subcutaneous CM treatment groups are delineated by red bars and visceral CM treatments by blue bars. A one-way ANOVA with Dunnett's post-hoc test was used to test statistical significance ($*p < 0.05$ vs. SGM). Micrographs were taken at 20X magnification. Scale bars = 30 μ m. AM – Adipogenic media; CSCM – Control subcutaneous conditioned media; CVCM – Control visceral conditioned media; ESSCM – Elevated sugar subcutaneous conditioned media; ESVCM – Elevated sugar visceral conditioned media; HFSCM – High-fat subcutaneous conditioned media; HFVCM – High-fat visceral conditioned media; Rosi – Rosiglitazone; SGM – Standard growth media; SUBCUT – Subcutaneous (inguinal); VC – Vehicle control; VISC - Visceral (retroperitoneal).

Supplementation of the CM+SGM treatments with 1 μ M Rosi appears to have produced similar results to those of the CM+Rosi treatments (Figure 3.20), with lipid accumulation observed in all experimental recipient AD-MSCs, especially in the retroperitoneal cells. The *in-silico* analysis results show that whilst all CM+SGM+Rosi treatments elicited a higher mean ORO-stained area than the negative SGM+Rosi control ($0.07 \pm 0.01\%$), statistically, the outcomes did not differ. The spectrophotometric analyses were similar to the *in-silico* results, having identified no statistical differences in lipid accumulation in any of the treatment groups as compared to the SGM+Rosi.

The ORO quantification outcomes of the retroperitoneal recipient cells treated with CM+SGM+Rosi show an increase in mean ORO-stained area in all treatment groups in comparison to the SGM+Rosi. Notably, the visceral recipient cells treated with visceral CM harvested from the control (CVCM+SGM+Rosi $3.03 \pm 0.20\%$), HFD (HFVCM+SGM+Rosi $2.11 \pm 0.37\%$), and ESD cells (ESVCM+SGM+Rosi $1.72 \pm 0.24\%$) had the highest mean ORO-stained areas ($p < 0.0001$). This indicates that whilst the subcutaneous CM samples did elicit significant responses in lipid accumulation within the visceral recipient cells, the visceral CM samples were more successful in inducing adipogenesis when supplemented with SGM and Rosi. The CVCM+SGM+Rosi treatment's relative lipid accumulation was also the highest overall at 1.67 ± 0.76 , but the difference as compared to the SGM+Rosi control was statistically insignificant.

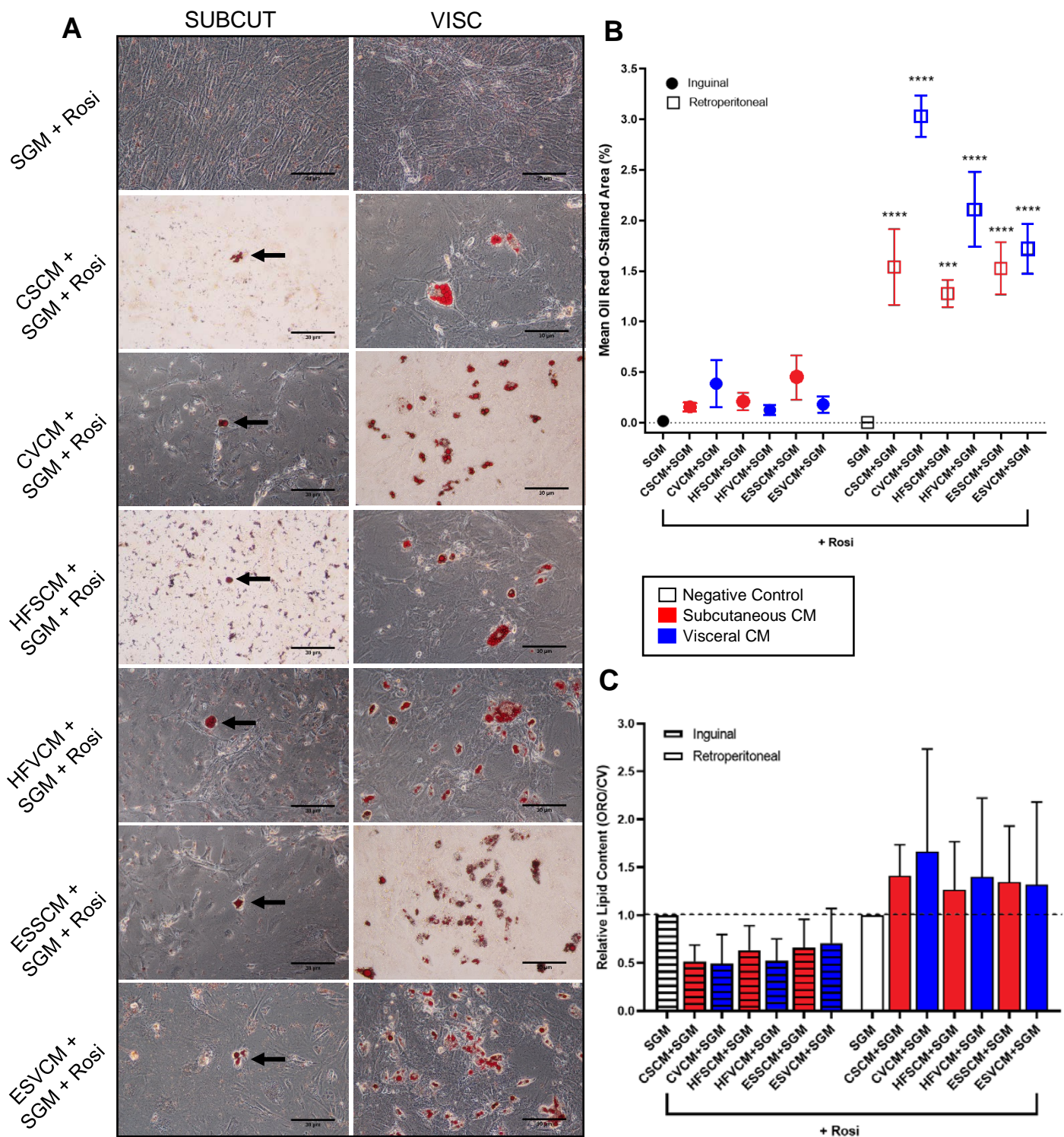


Figure 3.21: Representative micrographs, in-silico, and spectrophotometric of oil red O-stained inguinal subcutaneous and retroperitoneal visceral AD-MSCs treated with a combination of conditioned media, standard growth media, and 1 μ m Rosiglitazone. Conditioned media (CM) was collected from in vitro differentiated subcutaneous and visceral adipocytes isolated from control, high-fat- and elevated-sugar diet-fed male Wistar rats. The CM samples were combined at a ratio of 1:1 with standard growth media (SGM) and added to subcut and visc recipient AD-MSCs isolated from age-matched, 19-week-old control male Wistar rats for 14 days, with the treatments being changed twice a week. (A) Black arrows

highlight the individual lipid droplets; large clusters of adipocytes are stained red and are evident in all visc CM + Rosi treated cells. Subcutaneous CM treatment groups are delineated by red lines. Three representative micrographs were taken of the (B) subcutaneous and visceral cells in each treatment group and the mean ORO-stained areas were measured in Fiji ImageJ for Windows. (C) Spectrophotometric analyses of the eluted ORO and crystal violet stains were performed in triplicate and are represented as mean \pm SEM for each depot. Subcutaneous CM treatment groups are delineated by red bars. A one-way ANOVA with Dunnett's post-hoc test was used to test statistical significance (* $p < 0.05$ vs. SGM; *** $p < 0.001$ vs. SGM). Micrographs were taken at 20X magnification. Scale bars = 30 μ m. CSCM – Control subcutaneous conditioned media; CVCM – Control visceral conditioned media; ESSCM – Elevated sugar subcutaneous conditioned media; ESVCM – Elevated sugar visceral conditioned media; HFSCM – High-fat subcutaneous conditioned media; HFVCM – High-fat visceral conditioned media; Rosi – Rosiglitazone; SGM – Standard growth media; SUBCUT – Subcutaneous (inguinal); VISC - Visceral (retroperitoneal).

Adipogenesis is evident in the micrographs of all CM+AM+Rosi treatments (Figure 3.22 A). All CM+AM+Rosi treatment groups had elevated levels of adipogenesis as compared to the VC+Rosi control when added to the inguinal AD-MSCs (Figure 3.22). The AM+Rosi positive control treatment appears to have elicited the biggest response in the inguinal recipient cells, having the largest ORO-stained area ($1.65 \pm 0.79\%$) and relative lipid accumulation (4.49 ± 0.29 , $p = 0.009$). This was the only treatment group to have elicited a statistically significant result in the inguinal AD-MSCs.

Lipid accumulation was observed in the retroperitoneal AD-MSCs treated with VC+Rosi. As no adipogenesis occurred in the SGM+Rosi treatments (see Figure 3.20 or Figure 3.21) the combination of the dimethylsulfoxide (DMSO), ethanol, and 1 μ M Rosi within the VC group is thought to be responsible for the apparent lipid accumulation. When assessing the mean ORO-stained areas of the CM+AM+Rosi treated retroperitoneal AD-MSCs *in-silico*, high significance was determined in all treatment groups ($p < 0.0001$). The highest mean ORO-stained areas of these treatments were measured in the CVCM+AM+Rosi ($20.94 \pm 2.99\%$) and ESVCM+AM+Rosi ($20.01 \pm 0.14\%$) treatment groups. Following a one-way ANOVA and Dunnett's test on the relative lipid accumulation data generated following the spectrophotometric analyses, p -values of < 0.01 were reported in all CM treatment groups. The CVCM+AM+Rosi (4.63 ± 0.14), ESSCM+AM+Rosi (5.88 ± 0.84), and ESVCM+AM+Rosi (6.18 ± 0.89) treatment groups had the greatest measured increase in relative lipid accumulation in the visceral recipient AD-MSCs ($p < 0.001$).

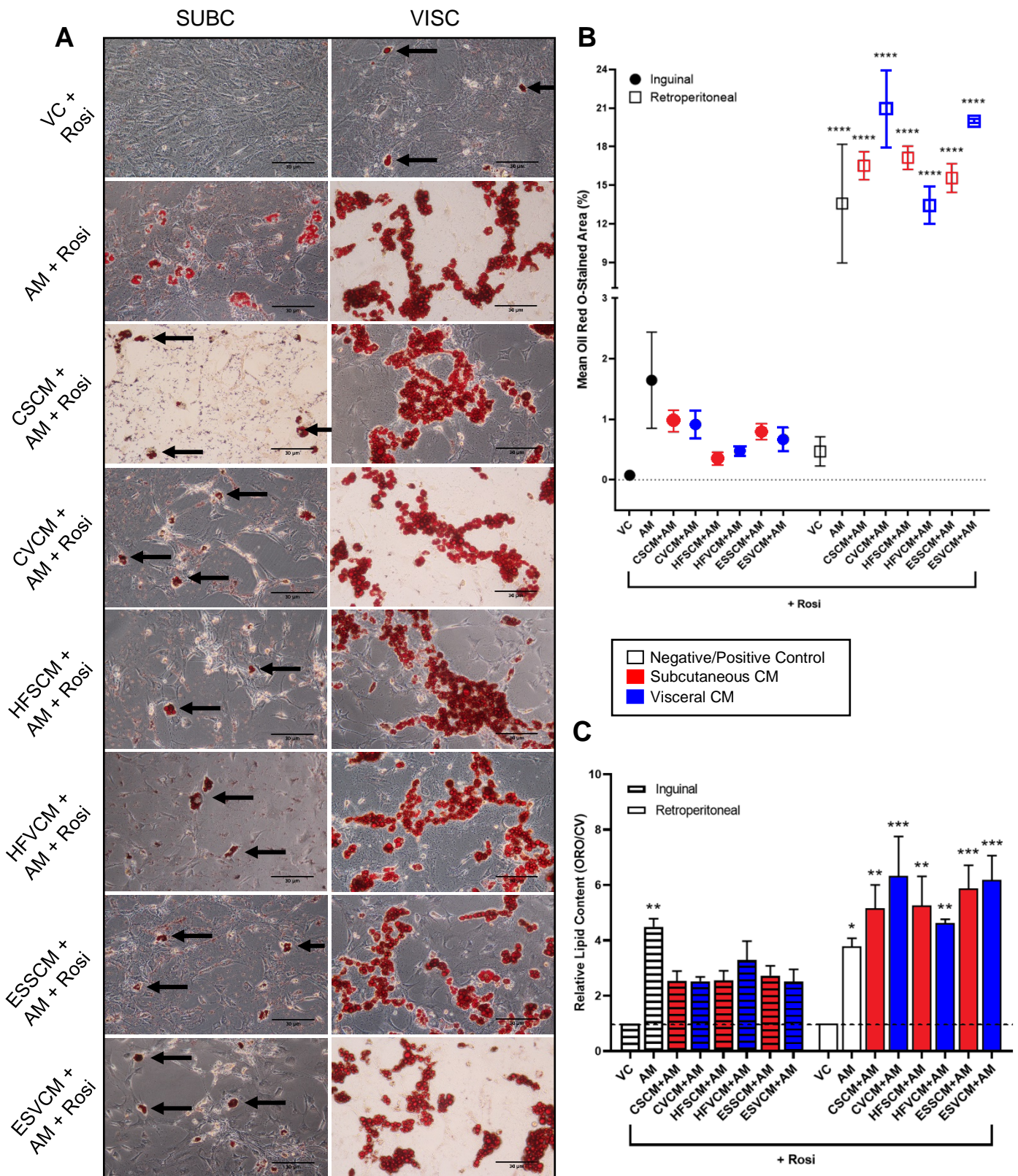


Figure 3.22: Representative micrographs, in-silico, and spectrophotometric quantification of oil red O-stained inguinal subcutaneous and retroperitoneal visceral AD-MSCs treated with a combination of conditioned media and adipogenic media supplemented with 1 μM Rosiglitazone. Conditioned media (CM) was collected from *in vitro* differentiated subcutaneous and visceral adipocytes isolated from control, high-fat- and elevated-sugar diet-fed male Wistar rats. The CM samples were combined at a ratio of 1:1 with adipogenic media (AM) and added to subcutaneous (n = 3) and visceral (n =2) recipient AD-MSCs isolated from age-matched, 19-week-old control male Wistar rats for 14 days, with the treatments being changed twice

a week. **(A)** Black arrows highlight the individual lipid droplets; large clusters of adipocytes are stained red and are evident in all visc CM + Rosi treated cells. Subcutaneous CM treatment groups are delineated by red lines and the visceral CM treatments by blue lines. Three representative micrographs were taken of the **(B)** subcutaneous and visceral cells in each treatment group and the mean ORO-stained areas were measured in Fiji ImageJ for Windows. **(C)** Spectrophotometric analyses of the eluted ORO and crystal violet stains were performed in triplicate and are represented as mean \pm SEM for each depot. Subcutaneous CM treatment groups are delineated by red bars and the visceral CM treatments by blue bars. A one-way ANOVA with Dunnett's post-hoc test was used to test statistical significance (* $p < 0.05$ vs. VC; ** $p < 0.01$ vs. VC; *** $p < 0.001$ vs. VC; **** $p < 0.0001$ vs. VC). Micrographs were taken at 20X magnification. Scale bars = 30 μ m. AM – Adipogenic media; CSCM – Control subcutaneous conditioned media; CVCM – Control visceral conditioned media; ESSCM – Elevated sugar subcutaneous conditioned media; ESVCM – Elevated sugar visceral conditioned media; HFSCM – High-fat subcutaneous conditioned media; HFVCM – High-fat visceral conditioned media; Rosi – Rosiglitazone; SGM – Standard growth media; SUBCUT – Subcutaneous (inguinal); VC – Vehicle control; VISC - Visceral (retroperitoneal).

Overall, the addition of a PPAR γ agonist in the form of Rosi into the CM treatment groups does not appear to have increased the efficacy of the CM when added to the inguinal recipient AD-MSCs. This is evident as no significant increase in lipid accumulation was induced by any of the CM+Rosi, CM+SGM+Rosi, or CM+AM+Rosi treatment groups when added to the inguinal recipient cells. Conversely, the retroperitoneal AD-MSCs responded well to the CM+Rosi, CM+SGM+Rosi, and CM+AM+Rosi treatments, having accrued large volumes of lipids in all experiments. Upon comparison with the outcomes of the CM treatments without Rosi supplementation, it appears as though the addition of the 1 μ M Rosi enhanced the effects of the CM treatments in the 100% CM and CM+SGM treatment groups but not in the CM+AM treatments (Figure 3.19).

Discussion

The process of fat accumulation begins as a response to an imbalance between caloric intake and energy expenditure²⁹. Chronic consumption of excess calories typically leads to a disruption in the hyperplastic expansion (cell number increase) of the adipose tissue, inducing hypertrophy (cell size increase) in the constituent adipocytes³⁵. In both human and murine obesity studies, excess triglycerides are noted to primarily accumulate in the subcutaneous adipose tissues with the accrual of visceral fat being subsequently induced^{223,224}. We hypothesise that an increase in the secretion of unknown bioactive factors by hypertrophic subcutaneous adipocytes prompts adipogenesis in visceral adipose-derived mesenchymal stem cells (AD-MSCs) via endocrine signalling. By increasing the adiposity of male Wistar rats through the feeding of a high-fat- or elevated sugar diet, this study aimed not only to investigate the existence of endocrine signalling between mature adipocytes and naïve AD-MSCs of anatomically dispersed adipose depots but to also assess the impact of chronic high-caloric intake on the depot-depot communication^{9,225}. As the pharmacological treatment of type II diabetes with the thiazolidinedione rosiglitazone (Rosi) (a peroxisome proliferator-activated receptor-gamma (PPAR γ) agonist) has also been associated with adipose tissue redistribution, the present study assessed its effects on CM-induced adipogenesis²²⁶.

The principal outcomes of the current study demonstrate that both the high-fat diet (HFD) and elevated sugar diet (ESD) were successful in increasing the adiposity of the inguinal subcutaneous and retroperitoneal visceral adipose depots through adipocytic hypertrophy (section 3.1 and 3.2). When assessing the impact of subcutaneous- and visceral control, HFD, and ESD conditioned media (CM) on naïve AD-MSCs isolated from both depots of control rats ($n = 3$), the greatest adipogenic effects were observed in the retroperitoneal AD-MSCs treated with ESD visceral CM. This suggests the potential occurrence of a paracrine interaction between the ESD adipocytes and naïve, control AD-MSCs *in vitro*, warranting further investigation in which naïve ESD AD-MSCs are used as the recipient cells (section 3.5).

Additional experimentation was then conducted in which control, HFD, and ESD subcutaneous and visceral CM treatments were supplemented with Rosi to prime the cells for adipogenesis. The supplementation of the 100% CM with Rosi appeared to amplify the adipogenic effects of the control and HFD CMs from both adipose depots when treating visceral AD-MSCs (section 3.6). These findings allude to Rosi having sensitised the visceral recipient AD-MSCs to an *in vivo* adipogenic paracrine signalling from the visceral adipocytes of the control and HFD rats. As the control subcutaneous CM and HFD subcutaneous CM were also able to elicit an adipogenic response when

added to the retroperitoneal AD-MSCs as a 100% CM + 1 μ M rosiglitazone treatment, a putative endocrine communication appears to have been occurred.

These findings will be examined, compared, and contrasted against the findings of similar studies in the sections to follow.

4.1 Diets

Numerous studies have made use of murine models to simulate the pathobiology of metabolic diseases such as obesity and insulin resistance in humans. The suitability for using rodent models for such research has been called into question numerous times because the results obtained in rodent models of metabolic disease are not always directly translatable^{227,228}. Recent reviews have, however, concluded that despite the differences in the metabolic activities of the two species, comparable secretion levels of certain adipokines and similarities in the up-regulation of inflammatory genes during the induction of diet-induced obesity ensure that the use of these model organisms is sufficient in early-stage research^{227–229}. Thus, male Wistar rats were used in the present study to simulate the metabolic and cellular implications of the chronic consumption of high-caloric diets.

Several prior studies, both preclinical and clinical, have positively correlated the consumption of high calorific diets with the onset of one or more characteristic morbidities of the metabolic syndrome including obesity, hypertension, insulin resistance, hyperglycaemia, or cardiovascular complications^{172,227,228,230–232}. The HFD and ESD models utilised in this study were based on those developed previously by Salie *et al.* (2014) and Huisamen *et al.* (2019)^{172,173}. All food and water preparation and replacement protocols established by these authors were adhered to throughout the present study. This investigation did, however, slightly differ from those cited as the diets were initiated when the rats were approximately three weeks of age. This deviation was implemented as the rats in this study were to be the source of stem cells for *in vitro* experimentation, and it is widely documented that stem cell numbers and viability decrease significantly with age²³³. Thus, the rats had to be as young as possible for optimal stem cell isolation which, following the 16-week feeding period, meant that the rats were 19-weeks of age at the time of termination.

During the diet period, the weights of all $n = 21$ rats were recorded weekly to monitor the gradual gain in weight (Figure 3.1). The weights of the control rats appeared to increase rapidly in the first nine weeks of feeding, at which point the growth began to plateau, enabling the HFD and ESD group's weights – which had a linear increase throughout the diet – to catch up. This retarded pattern of growth may be attributed to the lower protein- and higher sugar contents of both the HFD and ESD foods as compared to the control (Table 2.1), as previous studies have shown that a protein deficiency or an excess of dietary sugar, especially during the nursing and prepubescent life phases, can result in stunted growth and development^{234–237}. Diets low in protein have also been observed

to increase food consumption, total body weight, and fat mass,²³⁸ but the results of the present study demonstrate that both the food consumption and mean final body weights of the rats did not differ significantly between diet groups (Table 3.1). Although these protein levels may not be optimal, an increase in the dietary protein concentration may have been counterproductive in this study as prior investigations have reported that an increase in dietary fat accompanied by an increase in protein prevented the development of obesity as a result of greater satiety in the rodents^{239–241}. All recorded final body weights of the animals used in this investigation did however exceed the average weights of 19-week-old male Wistar rats, as the control, HFD, and ESD rats in the present study all had weights that fell into the upper quartile of the 30-week-old rats ($n = 420$) weighed in a study by Nistiar *et al.* (2012)²⁴².

Although statistical analyses indicated that there was no significant difference in the quantity of food consumed per cage per day, the food consumption of the HFD rats appeared to be lower than that of the other diet groups (Table 3.1). This reduction in food intake is most likely owing to the high volume of fat, in the form of vegetable fat, present in the HFD, which altered both the texture and flavour of the food making it less palatable to the rats. When preparing the HFD and elevated-sugar diet (ESD) food, distilled, boiled water was added to soften the standard chow pellets as they serve as the basis of both diets. It is thought that the significant difference in the water intake between the control rats and the rats in the other two diet groups could be as a result of this additional water, as the moisture in both the ESD and HFD foods would have hydrated the rats to some degree, effectively decreasing their daily water intake.

When gauging the impact of a diet on the metabolic health of an individual, monitoring the levels of circulating blood glucose either post-prandially or following a minimum fasting period of 8 hours is a key marker frequently employed in both clinical and laboratory studies^{172,173,243–245}. Following the 16-week feeding period, the HFD group exhibited the highest mean fasting blood glucose (FBG) levels, having considerably more circulating glucose (mmol/l) in their peripheral blood than the ESD group. Interestingly, though not significant, the FBG concentrations recorded in the ESD rats were the lowest of the three diet groups despite the high sugar content of the ESD diet. However, at 4.27 ± 0.08 mmol/l, the mean FBG of the ESD rats still exceed the average blood glucose of Wistar rats as determined by Wang *et al.* (2010) which, having measured the FBG of $n = 500$ rats, was estimated to be 3.95 ± 1.31 mmol/l²⁴⁶.

Once the 16-week feeding period had concluded, the rats were euthanised as described in Methods section 2.4 and the bilateral inguinal and retroperitoneal fat pads were excised and weighed under sterile conditions. The inguinal adipose weight results recorded in this study (Table 3.1) concur with those of a similar study conducted in mice by Huang *et al.* (2003) as in both investigations the ESD group accumulated the most inguinal adipose tissue²⁴⁷. The consumption of diets high in saturated fats has been shown to predispose rats to the accumulation of visceral adipose tissue, thus, the ESD and HFD having significantly increased the retroperitoneal adipose tissue weights as compared to

the controls was to be expected ²⁴⁸. These findings were consistent with those of prior studies, including the findings of Salie *et al.* (2014) – the study upon which the ESD was based ^{172,247}. Huisamen *et al.* (2019) reported comparable results in that their HFD-fed male Wistar rats also had a substantial expansion of visceral adipose tissue ($p < 0.0001$), having increased to 24.5 ± 2.7 g from the control's 8.6 ± 0.4 g ¹⁷³.

The large mass of the retroperitoneal adipose tissue in the ESD rats presents an interesting case when considering their lower FBG readings. Increased visceral adiposity is generally considered to be a critical predictor for metabolic disorders such as hyperglycaemia, insulin resistance, and hypertension ^{249,250}. Many hypotheses exist which seek to explain the pathological effect of excessive visceral adipose accumulation on glucose metabolism. One of which – referred to as the 'portal theory' – proposes that the proximity of the visceral fat to the hepatic portal vein directly exposes the liver to free fatty acids and cytokines secreted by the intraabdominal adipose tissue which can promote hepatic gluconeogenesis (the generation of glucose) leading to higher serum glucose levels ^{125,132}. Based on this relationship, the ESD rats with their high proportion of retroperitoneal adipose tissue should hypothetically have had one of the highest FBG levels at the end of the diet period. The contrary findings of this study may indicate that the insulin levels of the rats were high enough to maintain the homeostatic glucose balance despite the chronic consumption of high dietary glucose, however, because serum insulin levels were not measured no conclusion can be made.

There was a lack of significant difference in the average total body weights of the three diet groups, but both the HFD and ESD rats were noted to have considerably larger inguinal and retroperitoneal adipose tissue depots when compared to the control. It is plausible that the control rats were experiencing some water retention as a result of their significantly higher water intake which would have increased the total body weight. Another potential explanation for this observation is that a redistribution of adipose tissue occurred within the control rats which would perhaps have led to the inguinal and retroperitoneal adipose depots being smaller, but other adipose depots that were not sampled in this study being larger. Alternatively, as the activity levels of the animals were not monitored throughout this study, the control rats may have been more sedentary, expending less energy, which could have impacted their total body weights due to a reduction in their lean body masses.

Upon comparison with similar studies in which an HFD or an ESD was fed to Wistar rats, the current 16-week feeding period in this study appears to have been moderate ²²⁸. In an investigation conducted by Dharavath *et al.* (2019), female Wistar rats were fed for a total of 24 weeks ²³⁰. At week 16, the investigators found that both the food and water intake of the rats began to stabilise, but the serum glucose levels and body weights continued to increase weekly ²³⁰. The use of female rats in the Dharavath investigation should not detract from drawing similarities to the results of the present investigation, as studies have shown that despite the disparities in total endpoint weights, there is no considerable difference in the amount of adipose tissue accumulated, or in the levels of blood

glucose between lab chow-fed male and female Wistar rats throughout their lives²⁵¹. Thus, it is probable that had the current project continued to feed the rats for a further four weeks, the differences in the final body weights and/or endpoint FBG levels may have become significant due to the cumulative effects of the prolonged high fat and sugar exposure.

4.2 Histological Staining of Subcutaneous and Visceral Adipose Tissue

The subcutaneous and visceral adipose depots do not only differ in anatomical location, as discussed in Chapter 1 but also differ histologically. The characteristic uniformity of the large unilocular white adipocytes within visceral adipose tissue (VAT) was revealed by haematoxylin and eosin (H&E) staining. In contrast, the subcutaneous adipose tissue's heterogeneity, with its integrated mix of connective tissue, unilocular white-, and multilocular brown adipocytes, was evident. It has been hypothesised that the presence of the brown adipocytes within the subcutaneous adipose tissue (SAT) directly translates to the reduced pathogenicity of fat accumulation in this depot^{121,122}.

Some of the first investigations into the cellularity of adipose tissue isolated from rats documented its expansion primarily through an increase in cell number by *de novo* adipogenesis of adipocyte progenitor cells (hyperplasia) during early development^{252,253}. Thereafter, as mature adipocytes are considered to be 'non-mitotic' cells and are therefore fixed in number once terminally differentiated, an increase in calorie intake was considered to usually be met with intracellular lipid accumulation leading to an expansion in adipocyte volume (hypertrophy)^{39,254}. In recent years it has become apparent that in cases where caloric intake occurs in excess, adipose tissue may undergo hyperplastic expansion, but hypertrophy is noted to occur concurrently to further increase the tissue's storage capacity^{35,36,167,255}. In the present study, the H&E-stained adipocytes from both depots of 12-week-old donor rats were noted to be small and numerous (section 3.2). Conversely, the adipocytes within the tissue samples isolated from the 19-week-old control rats were distinctly hypertrophic, with significantly increased size and a decrease in adipocyte number per μm^2 , despite the only difference between the two groups being the age at which the tissue was harvested. These results are comparable to the findings of Hirsch and Han (1969), as a gradual increase was observed in the adipocyte number of their male Sprague-Dawley rats until the 15th week of life but by the ~20th week the increase in lipid content was accomplished solely through a change in cell size²⁵². It could, therefore, be likely that age impacts the ability of adipose tissue to expand via hyperplasia. Further investigation with larger sample sizes would be required to confirm this hypothesis.

Adipose tissue samples from 12-week-old control rats were collected whilst harvesting tissue for use as the source of AD-MSC recipient cells in the preliminary studies outlined in Results section 3.4. However, inguinal and retroperitoneal adipose tissue samples were not isolated from 12-week-old HFD and ESD rats for comparison with the 19-week-old rats on the same diets as conducted with the controls. This is because the minimum required feeding period for the HFD and ESD to take

effect is 16-weeks based on the protocols developed by Salie *et al.* (2014) and Huisamen *et al.* (2019)^{172,173}. The restraints on the number of animals available for use in this study, as determined by the Stellenbosch University animal ethics committee, also influenced the measurements that were made. Thus, because this study only aimed to assess the impact of the HFD and ESD on the subcutaneous and visceral AD-MSCs and was not a study examining the effects of the diet on adipocyte hypertrophy, to get as high a sample size as possible, all rats required feeding for the full 16-weeks. A previous study in HFD-fed mice did, however, note the HFD-induced hypertrophy of inguinal adipocytes occurred by week four of the diet period making them significantly larger than the CHOW-fed control mice in the earlier stages of life ($p < 0.01$)²⁵⁶. Thus, in future studies, by harvesting the adipose tissue at varying time points throughout the 16-week diet and conducting H&E staining (section 2.6), the stage at which the HFD and ESD diets induce hypertrophic expansion of the tissues could be determined.

Having taken the micrographs for these analyses at 20X magnification, the small frame of reference skewed the enumeration analyses, as the larger cells took up more area in the micrograph resulting in fewer cells being visible. As the micrographs only show the cellularity of small segments of the adipose tissue samples, hyperplasia could not be measured in this study as the mass of the tissue samples and the total volume of each adipocyte, determined using specialised equipment, are required to accurately determine the number of cells within the tissue^{35,257,258}. However, through the *in-silico* analysis of micrographs of the H&E-stained adipocytes, the diet-induced hypertrophy in both the HFD and ESD adipose tissue samples was quantifiable (Figure 3.2).

The findings of the present study indicated that both the HFD and ESD rats had the heaviest excised inguinal and retroperitoneal adipose depots (Table 3.1) and the largest average adipocyte areas overall (Figure 3.3 A & B). This *in vivo* adipocyte hypertrophy suggests that the diets may have induced cellular stress within the treated rats which could have stimulated an increased secretion of free fatty acids and pro-inflammatory adipokines¹⁵⁴. In human's the prolonged secretion of these factors is known to culminate in the chronic inflammatory profile typical of obesity¹⁵⁴.

The retroperitoneal adipose tissue samples and adipocytes were found to be larger than those of the inguinal depot in all four experimental groups of this study. Several previous studies have published similar findings when comparing adipose tissue samples from these depots in both mice and rats^{35,100,256,259,260}. It is tempting to speculate that this recurrent trend is due to the larger area for expansion being present in the intrabdominal cavity of the rodents as compared to the subcutaneous space. This is, however, not necessarily the case in humans as the subcutaneous compartment, between the epidermis and the fascia covering the muscles, joints, and bones, has no boundary limits making it the largest continuous body compartment facilitating the storage of the large quantities of excess fat^{255,261,262}.

Overall, the histological staining of the inguinal and retroperitoneal adipose depots showed the *in-situ* hypertrophy inducing effects of the diets at the cellular level. To gain more understanding of the impacts of the HFD and ESD on the composition of the tissue, the adipose-derived stem cells isolated from each depot were characterised by assessing proliferation, cell surface marker expression, and adipogenic potential of the constituent mesenchymal stem cells (MSCs).

4.3 Characterisation of Inguinal and Retroperitoneal AD-MSCs from Control, HFD, and ESD fed rats

Adipose-derived mesenchymal stem cells (AD-MSCs) are a cell type which have become recognised as promising candidates for therapeutic transplantation and regenerative medical therapies due to their accessibility, propensity to proliferate *ex vivo*, and ability to differentiate into several cell types (pluripotency) ^{263–266}. This cell type is phenotypically heterogenous and tends to differ in several aspects from study to study based on the cell isolation and culture protocols applied. Thus, to establish the characteristics of the inguinal and retroperitoneal AD-MSCs isolated and cultured in the present study, growth curves, flow cytometry, and adipogenic differentiation were conducted to define their growth kinetics, cell surface marker expression, and adipogenic potential, respectively.

4.3.1 Growth Kinetics of Inguinal and Retroperitoneal AD-MSCs

Growth curves are considered to be the most traditional assay for characterising the proliferation rates of adherent cells *in vitro* ^{267,268}. By manually counting the live AD-MSCs in culture via haemocytometer (section 2.9) for seven days post-seeding, the length of each cellular growth phase could be assessed. Typically, AD-MSCs exhibit a lag or latency phase of approximately 48 hours whilst the cells recover from the trypsinisation and secrete an extracellular matrix to facilitate cell-cell linkage and propagation on the substrate (Figure 4.1) ²⁶⁸. Once completely recovered, the cell population then enter the log or exponential phase of growth in which the population doubles at a characteristic rate which can be quantified by calculation of the population doubling time (PDT) (section 2.10). The final phase of cell growth, the stationary / plateau phase, occurs when the cells have occupied most of the substrate and begin to undergo contact inhibition which essentially decreases the mobility and mitotic activity of the cells ²⁶⁹.

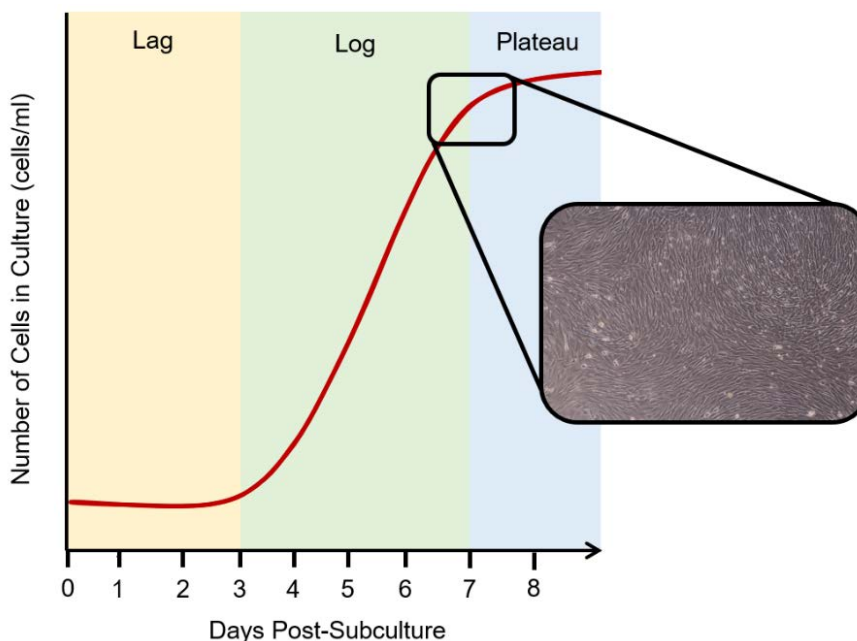


Figure 4.1: Typical 7-day growth kinetic curve of adipose-derived mesenchymal stem cells. Post-seeding, adipose-derived mesenchymal stem cells (AD-MSCs) recover from trypsinisation and undergo little to no mitotic division (lag phase). Once the extracellular matrix has been re-established and the cytoskeleton has been repaired of damage, the cell population begins to increase in number exponentially (log phase). After the cells have metabolised most of the substrate and have become densely packed (micrograph inset), the plateau or stationary phase begins where the proliferation rate and rate of cell death become equivalent.

In this investigation, no lag phase can be observed in the growth curves of the AD-MSCs from either adipose depot in the 12-week-old control, 19-week-old control, HFD, and ESD samples. Additionally, the growth curves demonstrate the slower proliferation rates and lower final cell counts of the retroperitoneal AD-MSCs as compared to the inguinal AD-MSCs in all diet groups (Figure 3.8). Upon calculation of the PDTs (section 2.10), the results appeared to reiterate those of the growth curves as the retroperitoneal AD-MSCs generally required a longer period to double their population's size – though this could not be confirmed statistically due to the small sample number ($n = 2$). This suggests that the *in vitro* proliferative index of the retroperitoneal AD-MSCs is lower than the subcutaneous AD-MSCs, no matter the age or diet of the cell donor. These results were comparable to those of Baglioni *et al.* (2012) who also documented the higher growth rate of the subcutaneous AD-MSCs as compared to visceral AD-MSCs isolated from human lipoaspirates ($n = 27$)²⁷⁰. The HFD and ESD do not appear to have had a significant effect on the proliferation rates of the AD-MSCs, in contrast to the results of a landmark paper by Shillabeer *et al.* (1990) which showed that the AD-MSCs of corpulent rats had significantly reduced proliferative capacities as compared to lab chow-fed controls¹⁶².

The higher proliferative ability of the subcutaneous AD-MSCs and the increased hypertrophy of the visceral AD-MSCs (observed in the H&E-stained micrographs) may suggest that the mechanism behind each depot's tissue expansion may differ regionally, with the SAT preferentially expanding through hyperplasia, and the VAT through hypertrophy.

4.3.2 Cell Surface Marker Expression of Inguinal and Retroperitoneal AD-MSCs

Flow cytometry is a technique frequently employed by biologists for *in vitro* cell characterisation. Unlike methods such as Western blotting or cellular imaging using microscopy, multicolour flow cytometry facilitates the investigation of subpopulations of large, heterogeneous cell populations at a single-cell level^{271–273}. By selecting specific fluorescent-labelled antibodies based on the cells of interest, the flow cytometer is able to measure the emission of fluorescence and light scatter which correspond to the structural and morphological features of each cell within the sample²⁷⁴. As the flow cytometric analyses of the AD-MSCs had to be conducted at passage three, to ensure the cells had been subcultured the same number of times as the experimental cells, and due to the COVID-19 lockdown-induced delivery delays, the fluorescent-conjugated cell surface markers used in the present investigation were selected based on availability. Cluster of Differentiation 90 (CD90) was therefore selected as a positive mesenchymal stem cell marker which should exhibit amplified expression (> 90%) in MSC populations that have been purified through successive subcultures^{189,191,275}. A 'pure' MSC population should also present reduced expression of CD45, a cell surface antigen associated with cells of the hematopoietic lineage, thus, CD45 was selected for use as a negative MSC marker in this study^{189,191,275}.

Van de Vyver *et al.* (2014) also made use of CD90 and CD45 cell surface markers when characterising rat subcutaneous and visceral AD-MSCs⁵². As in the present study, amplified expression of the positive MSC marker (CD90), and low-level positivity of CD45 was noted in both cell types⁵². In the control AD-MSC samples, whilst the forward-scatter (FSC) vs side-scatter (SSC) plots were very similar in distribution, the expression of CD90 was higher in the subcutaneous AD-MSCs than in the visceral suggesting the two populations share common morphological properties but differ in their biological characteristics.

When comparing the cell surface marker expression results of the control subcutaneous and visceral AD-MSCs to those of the HFD rat's cells, the percentage positivity of CD90 in the HFD AD-MSCs was higher in both depots. Upregulation of CD90 expression has been observed in several cell types in mouse models of inflammation, tumour development, and wound healing²⁷⁶. Thus, the HFD AD-MSCs may be over-expressing the mesenchymal stem cell marker (CD90) as a sustained response to the diet-induced cellular stress in the adipose tissues. Alternatively, the elevated CD90 positivity could be indicative of the undifferentiated status of the HFD subcutaneous and visceral AD-MSCs, as a decrease in MSC CD90 expression is permissive for the induction of differentiation²⁷⁷. The high CD90 positivity and relative homogeneity of the cell population in the FSC vs SSC plots (Figure 3.11) suggest that the control and HFD AD-MSC populations were relatively pure at passage three.

Both MSCs and fibroblastic pre-adipocytes have been reported to express high levels of CD90 but as the cells progress through the phases of adipogenesis, the CD90 expression levels decline^{277,278}. We, therefore, hypothesise that the low-level expression of CD90 on the cell surfaces of the ESD

subcutaneous and visceral AD-MSC samples may be due to some of the cells beginning to undergo adipogenesis, potentially as a result of contact inhibition ²⁷⁷. The use of other mesenchymal stem cell-specific cell surface markers and more biological replicates in future studies could further investigate the observations of the present study.

As the results obtained within these preliminary flow cytometric analyses were very similar to those of prior studies conducted in our laboratory ^{52,168,191,206}, the population purification by serial subculture was considered to have been successful.

4.3.3 Adipogenic Potential of Inguinal and Retroperitoneal AD-MSCs

Adipose-derived mesenchymal stem cells were initially thought to be multipotent, only being capable of differentiating into adipocytes ²⁷⁹, chondrocytes ²⁸⁰, or osteoblasts ²⁶³. However, recent studies have shown the propensity of AD-MSCs to also become myocytes ²⁸¹, endothelial cells ²⁸², and cells of ectodermal origin such as hepatocytes ²⁸³ and neurocytes ²⁸⁴ suggesting that they are, in fact, pluripotent. As the present study aimed to investigate the effects of the mature adipocyte secretome on adipogenesis in naïve AD-MSCs, only the adipogenic potential of the inguinal and retroperitoneal AD-MSCs was assessed.

Adipocytic differentiation is a highly complex mechanism that relies on the simultaneous activation and inhibition of various transcription factors to first commit the AD-MSCs to the adipocyte lineage and then induce adipogenesis in the pre-adipocytes ⁴¹. The process of recruiting AD-MSCs to the adipocyte lineage *in vivo* is poorly understood, however, it has been hypothesised to occur through exposure to high concentrations of glucose and excess triglycerides over an extended period ^{41,258,285}. Despite the paucity of knowledge about adipogenic lineage commitment *in vivo*, the induction of adipogenesis *in vitro* has been extensively described in prior studies resulting in detailed protocols being established such as the one used for adipocyte differentiation in the present study ¹⁹¹.

The composition of adipogenic media (AM) often varies between laboratories but generally, all contain insulin, dexamethasone, and 3-isobutyl-1-methylxanthine (IBMX), though the concentrations may differ slightly ²⁸⁶. Briefly, at high concentrations *in vitro*, insulin reportedly mimics insulin-like growth factor-1 (IGF-I) which is responsible for the clonal expansion of lineage-committed pre-adipocytes ²⁸⁷. Dexamethasone, a synthetic glucocorticoid, stimulates the phosphorylation of C/EBP β Thr188 which activates the SREBP1a gene subsequently inducing the expression of genes encoding PPAR γ 2, C/EBP α , SREBP1c, and FABP4. These are all vital transcription factors required for adipogenesis ²⁸⁸. Supporting the actions of dexamethasone, the competitive, nonselective phosphodiesterase inhibitor; IBMX increases the intracellular expression levels of cyclic adenosine monophosphate (cAMP) and protein kinase A (PKA) which trigger a signalling cascade leading to the transcriptional activation of PPAR γ and the promotion and propagation of adipogenesis ²⁸⁹. The

AM utilised in the present study combined these factors with FBS, indomethacin (a PPAR γ agonist and anti-inflammatory COX2 inhibitor²⁹⁰), and l-ascorbic acid which serves to promote adipogenesis through the synthesis and secretion of collagen VI – a key protein in the adipocyte extracellular matrix¹⁹⁶.

During the process of *in vitro* adipogenesis, morphological changes can be observed as the cells undergo lineage commitment and ultimately begin to accumulate lipids (Figure 4.2). After three days of adipogenesis, the cell bodies begin to condense and become spherical/cuboidal – a morphology associated with pre-adipocytes *in vitro*. Whilst the mechanism behind this shift in morphology is not completely understood, the alteration in cell shape has been shown to correspond with cytoskeletal reorganisation due to the reduced synthesis of tubulin and actin^{291–293}. By day 10, intracellular lipid accumulation should be observed in the cytoplasm of the cells, as the lamellipodia (fibroblastic extensions) continue to condense. On the final day of adipogenesis, a majority of the differentiating cells should have visible intracytoplasmic lipid accumulation.

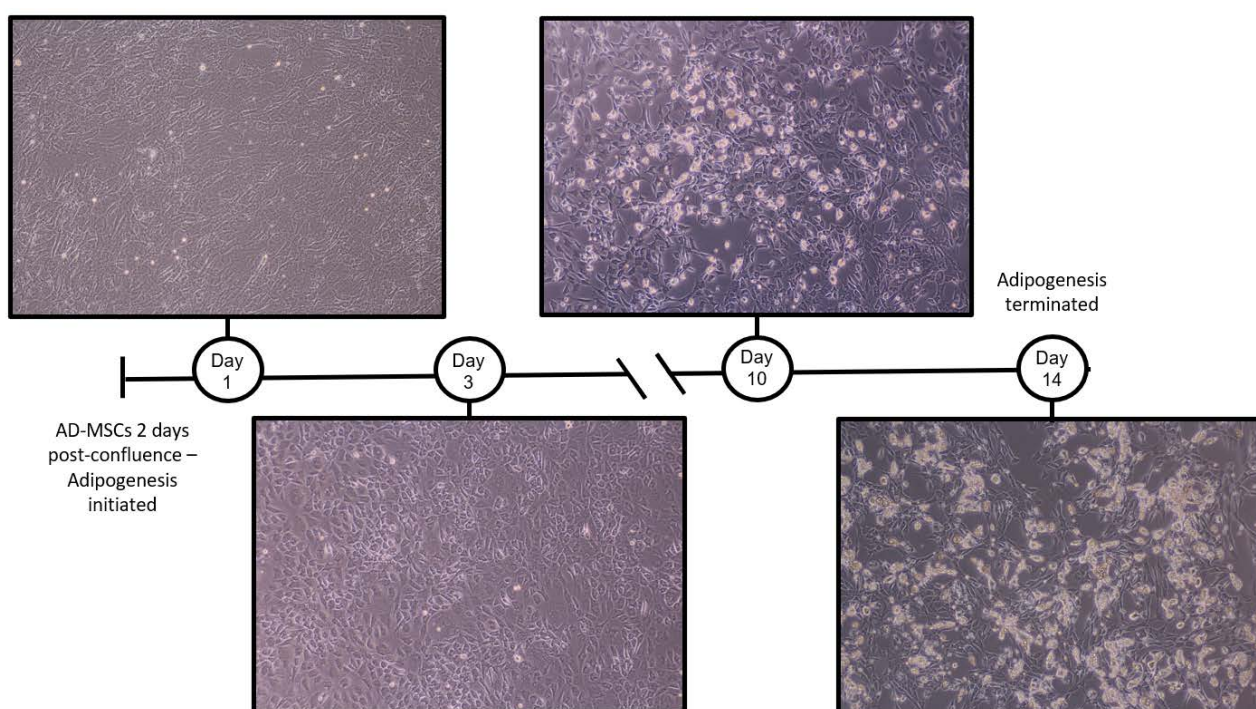


Figure 4.2: Representative phase-contrast micrographs of adipose-derived mesenchymal stem cells on days 1, 3, 10, and 14 of adipogenesis. On the first day of adipogenesis, no morphological changes are observable in the adipocytes. The AD-MSCs on day three of adipogenic differentiation condense and become cuboidal. By day 10, the AD-MSCs have begun to accumulate lipid droplets (light patches) and the cells have further condensed exposing the substrate. On the final day of adipogenesis, day 14, wide-spread lipid accumulation is observed (light patches). Micrographs were taken at 10X magnification.

Studies that have attempted to quantify the differentiation capacity of AD-MSCs isolated from various adipose tissue depots have repeatedly produced inconsistent results^{68,294–296}. The findings of the

present study demonstrated that the retroperitoneal AD-MSCs had higher adipogenic potential than the inguinal AD-MSCs (Figure 3.14). These results are supported by those of Ritter *et al.* (2019) where human AD-MSCs isolated from omental visceral and abdominal subcutaneous adipose tissue displayed 45.5% and 35.6% adipogenic differentiation, respectively²⁹⁵. Van de Vyver and colleagues also noted a higher percentage of lipid accumulation in the visceral AD-MSCs ($5.97 \pm 0.98\%$) as compared with the subcutaneous AD-MSCs ($3.03 \pm 0.45\%$)⁵². In contrast, Baglioni *et al.* (2014) found that AD-MSCs isolated from the subcutaneous adipose depots had more lipid accumulation than visceral AD-MSCs following three weeks of *in vitro* adipogenesis²⁷⁰. The same was reported by Tang *et al.* (2017) in AD-MSCs isolated from the subcutaneous and visceral AD-MSCs of 8-week-old Sprague-Dawley rats, as qualitatively more lipid accumulation was observed in the subcutaneous AD-MSCs *in vitro*²⁹⁷.

The higher adipogenic potential of the visceral cells in the present study could be ascribed to the possible presence of more lineage-committed pre-adipocytes in the culture at the initiation of adipogenesis. Based on flow cytometric analyses (section 4.3.2) and previous findings²⁷⁷ where a high CD90 count is associated with a more naïve phenotype, the lower CD90 positivity of all the visceral AD-MSC samples as compared to the inguinal AD-MSCs could correspond to the higher adipogenic potential and a decrease in stemness²⁷⁷. There may also be a trade-off between proliferative capacity and adipogenic potential when taking both the growth kinetics and adipogenesis into consideration: Visceral AD-MSCs had the lowest proliferation rate but the highest adipogenic capacity, with the inverse being true for the subcutaneous AD-MSCs. Similarly, human AD-MSCs exhibit the same proliferation and adipogenic dynamics²⁹⁵.

Although the current study observed no apparent differences in the adipogenic potential of the subcutaneous and visceral AD-MSCs isolated from the HFD and ESD rats as compared to the controls, decreased expression of pro-adipogenic genes in cells isolated from HFD-fed mice has been measured in previous studies^{298,299}. This suggests that hyper-caloric diets may have the ability to suppress the adipogenic potential of pre-adipocytes, but further investigation is required.

Overall, based on the results obtained in the three cell characterisation techniques, the subcutaneous and visceral AD-MSCs were noted to exhibit slight differences in proliferation, cell surface antigen expression, and adipogenic potential but no significant differences were identified. These findings have potentially occurred due to the small sample sizes of each analysis ($n \leq 2$). Larger more detailed studies in which quantitative real-time polymerase chain reaction (qRT-PCR), immunofluorescence staining, Western blots, cell motility analyses, and multilineage differentiation assays have been conducted on subcutaneous and visceral AD-MSCs have, however, shown the intrinsic variation in the biological characteristics of these two cell populations^{270,295,297,300}.

4.4 Effects of Varying Concentrations of Adipogenic Media – A Preliminary Study

When developing the protocol for the collection and treatment of cells with conditioned media (CM), the methods used in previous studies that had investigated cell signalling pathways using CM were reviewed. As the constituent amino acids, vitamins, cofactors, and carbohydrates of the DMEM are depleted by the metabolic activities of the cells during the 24-hour CM collection process (section 2.13), most studies supplemented the CM with either standard growth media (SGM) ^{301,302} or with adipogenic media (AM) ^{303–305} in order to restore the nutrients. Most of these studies combine the CM and SGM / AM in equal parts when treating the recipient cells. A preliminary study was, therefore, designed to assess whether a 1:1 combination is optimal to observe the adipogenic effects of the CM.

Previous investigations have assessed the adipogenic effects of different concentrations of individual AM components i.e. either insulin, indomethacin, IBMX, or dexamethasone ^{286,306}. Despite this, following extensive literature review, it appears that no studies have measured the impact of varying their concentrations collectively as a complete AM. By adding AM to AD-MSCs at concentrations of 25%, 50%, 75%, and 100% for 14-days and subsequently quantifying the *in vitro* lipid accumulation with *in-silico* micrograph analyses and spectrophotometry, the adipogenic effects of lower AM concentrations were assessed.

Overall, the results obtained in this study indicate that the quantity of adipocytic differentiation observed within the treatment wells corresponds to the concentration of AM being added, as the lower concentrations of AM had less quantifiable lipid accumulation and higher concentrations had more lipid accrual (section 3.4.2). No literature can be found to explain this concentration-dependent response, but we postulate that it may have resulted from either the activation and/or inhibition of fewer transcription factors within the < 100% AM treated cells, or to be due to the transient activation of adipogenic transcription factors at lower concentrations of AM where a prolonged response is required for complete adipogenesis.

The preliminary study presented here also assessed the suitability of leaving cells to reach post-confluence prior to the initiation of adipogenesis, as many studies preferentially use serum starvation to induce the cessation of proliferation as it is permissive for the induction of differentiation. The findings show no distinct differences between the serum-starved and non-serum starved treatment groups which suggest that both treatments are able to arrest the AD-MSCs in the G0/G1 phase of the cell cycle, priming them for differentiation. These results were comparable to previous findings where $86.38 \pm 0.322\%$ of the post-confluent 3T3-L1 cells were arrested in the G0/G1 phase, and the 'serum starved' cells which had been reduced to a 0.5% serum concentration for 48 hours or to a 0.2% serum concentration for 72 hours had $85.53 \pm 0.656\%$ and $86.88 \pm 0.098\%$ in the G0/G1 phase, respectively ($P > 0.05$) ²¹².

From these outcomes, a concentration of 50% AM was selected as it was comparable with previous literature and conserved the limited stock of CM so that further analyses could be conducted on its composition and effects in future studies. Due to the lack of statistical significance between the serum starvation and post-confluent treatments, this study used post-confluence as a proliferation termination technique following the protocols published by previous researchers in our laboratory ^{52,181,206,244}.

4.5 Effects of Control, HFD, and ESD Conditioned Media on the Adipocytic Differentiation of Inguinal and Retroperitoneal AD-MSCs

Cells secrete a myriad of soluble proteins, extracellular vesicles, lipids, and free nucleic acids throughout their life cycles which play a vital regulatory role in biological and physiological processes ^{307,308}. The collective term used to refer to these factors is the 'secretome'. The secretome of individual cells is highly specific and can be influenced by changes in physiological and pathological conditions ³⁰⁸. During incubation, the release of the cell secretome into the surrounding culture media is considered to 'condition' the media with the various secreted factors resulting in the 'conditioned media' nomenclature.

Techniques such as indirect co-culture and microfluidic systems have been used in several cell culture-based studies to investigate possible paracrine and/or endocrine interactions between cell types ^{305,309–311}. These approaches have many advantages but they require specialised equipment and can become costly ¹⁵⁸. The collection of conditioned media (CM) is therefore the preferred method for studies seeking to assess the indirect interactions between cell populations for the first time, as it is cost-effective and can be conducted using equipment generally available in cell culture laboratories ^{200,211,311–314}. As the present study sought to evaluate the endocrine interaction between adipocytes and AD-MSCs from discrete adipose depots, CM collection was selected as the mode of investigation.

CM harvested from adipocytes has previously been used in the study of paracrine interactions between macrophages and other stromal vascular fraction cells within adipose depots ^{315,316}. The outcomes of such studies suggest that a paracrine communication occurs between the adipocytes and AD-MSCs within the same adipose depot. Despite the interest in the signalling interactions of adipocytes, it is still unclear whether the adipocyte secretome may influence the proliferation and differentiation of AD-MSCs resident in other discrete adipose depots via endocrine mechanisms ¹³⁹. Confirmation of such an interaction would provide considerable insight into the mechanisms behind the sequential expansion of subcutaneous- and visceral adipose tissue and consequently provide more understanding into the aetiology and pathobiology of obesity-related co-morbidities.

The present study aimed to investigate adipose depot-depot communication by collecting CM from *in vitro* differentiated subcutaneous adipocytes and adding it to naïve, undifferentiated visceral AD-

MSCs then subsequently measuring the adipogenic effects. As we hypothesised that the endocrine communication which regulates fat accrual may not be unidirectional, *in vitro* differentiated visceral adipocytes also served as a source of CM which was added to naïve, undifferentiated subcutaneous AD-MSCs. Prior studies that sought to investigate the adipogenic effects of adipocyte-secreted factors *in vitro* did so by harvesting CM from whole adipose tissue samples before adding them onto recipient cells¹⁶⁴. By implementing this experimental model, the researchers could not be sure that the adipocytes were the sole source of secreted factors, as adipose tissue is highly heterogeneous with, for example, resident and infiltrating macrophages being known to secrete several cytokines that could influence adipocyte differentiation³¹⁷. By isolating and differentiating AD-MSCs *in vitro* and conducting flow cytometric analyses to confirm culture purity, the present study ensured that the CM collected represented only the adipocyte secretome.

Unpublished preliminary experiments conducted in our laboratory have shown that lipid-laden subcutaneous adipocytes were able to induce adipogenesis in visceral AD-MSCs. In the present study, although small quantities of lipid accumulation can be seen in the micrographs of all three figures (section 3.5), the subcutaneous CM from the control, HFD, and ESD were only able to stimulate statistically significant adipogenesis in the visceral AD-MSCs when supplemented with 50% AM (Figure 3.19). By centrifugation and subsequent removal of the supernatant during the CM preparation process, any lipids sloughed off by the adipocytes into the CM were removed (section 2.13). This ensured that the observed lipid accumulation developed as a result of the initiation of adipogenesis and did not occur due to the adipocytes sequestering lipids from the media. Thus, the subcutaneous CM from all three diet groups appear to have the ability to activate one or more of the signalling cascades required for adipocytic differentiation of the visceral AD-MSCs but requires supplementation with one or more of the AM constituents to achieve full adipogenesis.

Examining the effects on the visceral AD-MSCs, the control subcutaneous CM induced the most lipid accumulation of the three subcutaneous CM samples, closely followed by the HFD- and then the ESD subcutaneous CM's as shown in both the *in-silico* ORO quantification and spectrophotometry results of the CM+AM treatments (Figure 3.19). This potentially alludes to the high-calorific diets having impacted the secretome of the *in vitro* differentiated subcutaneous adipocytes. It is also plausible that the HFD and ESD CM samples had a sub-optimal effect on the recipient AD-MSCs because the adipose tissues from which the AD-MSCs were isolated had differing microenvironments as a result of the diets.

Control rats were selected as the source of recipient cells in the present study as the effects of the HFD and ESD on the biology of naïve AD-MSCs was unknown. In addition, both high-calorific diets were developed using the standard lab cow diet as a foundation thus negating the lab chow diet as a potential confounder. *In vivo*, the adipocytes and the AD-MSCs would be exposed to the same serum glucose and lipid levels and therefore ideally the recipient cells and CM should be obtained from the same animal. However, to negate differences in the recipient cells and therefore make a

direct comparison of CM from each group possible, the CM was only tested on recipient cells from control animals. Thus, to assess the impact of the diets on the adipocyte - AD-MSC communication more accurately, subsequent studies would need to be conducted in which naïve, undifferentiated visceral AD-MSCs are isolated from HFD, and ESD-fed rats and used as recipient cells for the HFD and ESD CM treatments, respectively.

Apart from the AM positive control, only the control subcutaneous- and ESD visceral CM treatments, when supplemented with AM, were able to induce significant lipid accrual in the inguinal recipient AD-MSCs (Figure 3.19). The lipid accumulation prompted by the control subcutaneous CM supplemented with AM is indicative of a paracrine signalling event as the adipocytes and AD-MSCs originate from the same depot. This paracrine induction of adipogenesis is known to occur *in vivo* ^{139,315,318}. The subcutaneous- and visceral AD-MSCs treated with ESD visceral CM exhibited one of the highest ORO-stained areas / relative lipid accumulations in all three treatment formulations (100% CM, 1:1 CM: SGM, or 1:1 CM: AM) (section 3.5). This recurrent observation may suggest that the ESD affected the potency of the cell signalling components within the adipocyte secretome but as described above, a subsequent study would need to investigate the impact of the ESD CM on naïve, undifferentiated ESD AD-MSCs.

As most of the salient findings within these experiments were observed in the CM+AM treatments, future experimental refinement would be to add insulin, IBMX, dexamethasone, indomethacin, or L-ascorbic acid individually to the subcutaneous and visceral CM samples before treating the naïve AD-MSCs from each adipose depot. In doing so, changes in lipid accumulation would identify specific pathways which are not stimulated by the CM. Further analysis of the CM by conducting multiplex ELISA arrays or mass spectrometry could also provide the identity of the proteins present within the CM and a greater understanding of the activated signalling cascades involved in cell-cell communication.

4.6 Effects of Control, HFD, and ESD Conditioned Media Supplemented with Rosiglitazone on the Adipocytic Differentiation of Inguinal and Retroperitoneal AD-MSCs

Peroxisome proliferator-activated receptor- γ (PPAR γ) is a nuclear receptor that is expressed in several cell types including hepatocytes, epithelial cells, and cells in the haematopoietic lineage ^{319,320}. The expression of PPAR γ is typically down-regulated in AD-MSCs but its activation is required to induce pre-adipocytic lineage commitment and successive adipogenesis ³²¹. Endogenous ligands for PPAR γ include arachidonic acid metabolites and the prostaglandin PGJ₂, however, studies have shown that the most efficient way to stimulate PPAR γ -induced adipogenesis *in vitro* is through the addition of a synthetic PPAR γ agonist such as Rosiglitazone (Rosi) ^{59,222,322,323}. Rosi is an anti-diabetic thiazolidinedione drug that acts by sensitizing cells to insulin through the ligand-based

activation of PPAR γ ⁵³. By introducing Rosi to the cells *in vitro*, a conformational change in the PPAR γ receptor is induced by the ligand binding, consequently resulting in the recruitment of transcriptional co-activators and co-repressors which stimulate the expression of pre-adipogenic markers such as C/EBP α , C/EBP β , and C/EBP δ ^{57,59,60}.

As a result of the ability of Rosi to prompt *in vitro* adipogenesis, the current study expected the additional stimulation of PPAR γ to amplify the CM-induced intracellular lipid accumulation which had already been observed to occur in previous experiments (section 3.5). The findings of the present study reveal that when supplemented with 1 μ M Rosi, the control subcutaneous CM and HFD subcutaneous CM were able to independently stimulate statistically significant lipid accumulation in the naïve, undifferentiated visceral AD-MSCs (Figure 3.20 B). As no lipid accumulation was observed in the SGM+Rosi negative control, this infers that this CM contains signals for adipogenesis, but lacks the ability to adequately activate PPAR γ .

A high amount of lipid accumulation was also observed in the visceral AD-MSCs treated with control- and HFD visceral CM supplemented with Rosi. This lipid accrual was putatively induced via paracrine signalling between the mature control and HFD adipocytes and the naïve, undifferentiated AD-MSCs. Despite the high observed amount of lipid accumulation in the naïve inguinal AD-MSCs treated with CM and Rosi, the treatments were unable to induce enough lipid accumulation to be statistically significant when compared to the SGM+Rosi negative control (Figure 3.20 A).

When the subcutaneous and visceral CM treatments were supplemented with both SGM and Rosi, the control, HFD, and ESD CMs were all able to induce significant lipid accumulation in the visceral AD-MSCs (Figure 3.21). In comparison with the CM+SGM without Rosi treatments (Figure 3.18), in which only the control and ESD visceral CMs stimulated significant lipid accrual, the addition of the 1 μ M Rosi appears to have been able to amplify adipogenesis in these cells. The CM+SGM+Rosi treatment groups were unable to elicit a significant response in the inguinal recipient AD-MSCs.

The supplementation of the CM treatments with 50% AM and 1 μ M Rosi prompted the accrual of large clusters of lipids in the naïve visceral AD-MSCs in all CM treatment groups (Figure 3.22). Overall, these results were very similar to the results obtained when the CM treatments were supplemented with only AM as they too showed significant accumulations of lipids in all CM treatment groups (Figure 3.19). These findings were unsurprising as one of the components of the AM used in the present study, indomethacin, is a PPAR γ agonist. Thus, as the PPAR γ receptor has already been activated, the addition of a secondary agonist of the same receptor may have been superfluous as the receptor cannot be hyper-activated through the addition of more agonists. Only the AM+Rosi positive control was able to provoke significant lipid accumulation in the inguinal AD-MSCs, as determined via spectrophotometry, which indicates that the adipogenic potential of the recipient AD-MSCs was not compromised in any way. The subcutaneous AD-MSCs are, therefore,

seemingly less susceptible to CM-induced adipogenesis than the visceral AD-MSCs whether the treatments are supplemented with 1 μ M Rosi or not.

4.7 Study Limitations and Recommendations for Future Studies

Several limitations were experienced throughout the present study, some of which have already been addressed in the text above and will, therefore, not be repeated in this section.

The most prominent limitation imposed upon this study was the reduction in time for experimentation due to the COVID-19 lockdown in 2020. As a result, the optimisation of the cell isolation and culture protocols, and the preliminary studies were conducted in the last few months of 2020. The feeding of all animals used in the diet studies and conditioned media experiments was, therefore, only commenced mid-January 2021. This would have normally been completed early in 2020. In addition, this lack of time also severely limited the number of repeat experiments that could be undertaken and completed. Consequently, the results of the histological-, growth curve-, and flow cytometry assays, in particular, should be viewed as preliminary as more biological repeats are required to produce statistically significant results. An increase in sample sizes in future studies will also provide enough tissue to facilitate the measurement of hyperplasia in the inguinal and retroperitoneal adipose tissues using one of several published cell number calculation methods^{35,257,258}.

Having to pool the subcutaneous CM samples ($n = 7$) and visceral CM samples ($n = 7$) within each diet group (section 2.13) because of the limitations on time and incubator space was also sub-optimal as it prevented the detection of inter-sample variability between each rat within the three diet groups. To prevent these issues from arising in future studies, the initiation of the diets should be further staggered so that the conditioned media collection process and cell characterisation assays can be conducted before the recipient AD-MSCs are isolated from the control rats. This additional time would also allow for detailed measurements of the *in vivo* adiposity of the HFD and ESD rats to be made through the use of either dual-energy X-ray absorptiometry (DEXA) scans or magnetic resonance imaging³²⁴.

Upon completion of the CM experiments, this study was able to confirm that CM collected from *in vitro* differentiated subcutaneous adipocytes can stimulate lipid accretion in naïve, undifferentiated visceral AD-MSCs. However, even though lipid accrual is a marker of adipogenesis, it is unclear whether the observed CM-induced lipid accumulation occurred as a result of terminal adipogenesis in the AD-MSCs. To confirm that adipocytic differentiation did occur, future studies can measure the expression of adipogenic genes such as PPAR γ , C/EBP α , C/EBP β , adiponectin, and C/EBP δ within the visceral AD-MSCs via quantitative real-time polymerase chain reaction (qRT-PCR).

Whilst the results of the *in vitro* CM experiments appear to support the hypothesised existence of an *in vivo* endocrine interaction between the mature subcutaneous adipocytes and the visceral AD-

MSCs, future studies would need to confirm this communication by using indirect co-culture. The use of an indirect co-culture system, where the naïve recipient cells and the mature adipocytes share an aliquot of media (Figure 4.3), would eliminate the need for the soluble secreted factors within the CM to undergo a freeze-thaw process (section 2.13). This would provide a more accurate simulation of the *in vivo* communication as the two cell populations would share the same culture media in real-time.

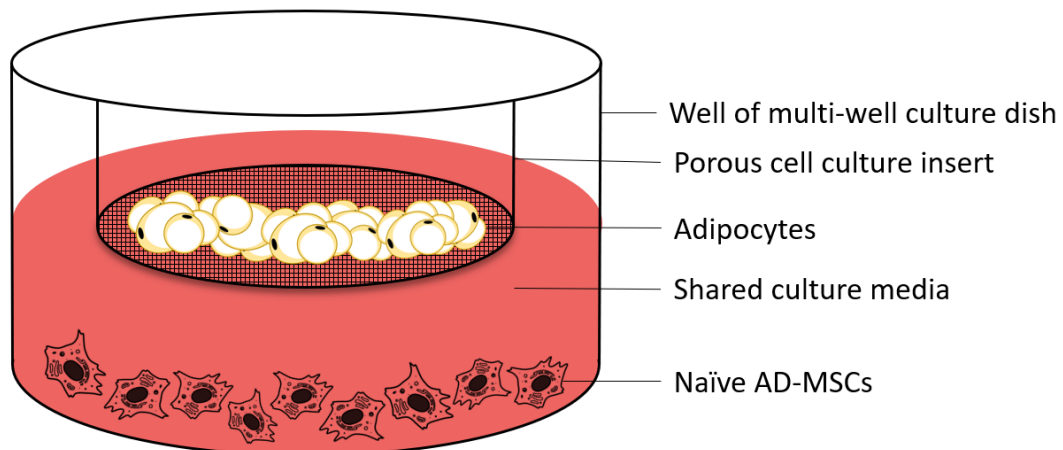


Figure 4.3: Schematic of an indirect co-culture system. AD-MSCs – Adipose-derived mesenchymal stem cells.

The current study provides evidence for the existence of pro-adipogenic endocrine factors within the secretome of both subcutaneous and visceral adipocytes. Identifying what adipogenic factors were in effect was, however, beyond the scope of the present investigation. Future studies could make use of inhibitors of the transforming growth factor beta (TGF β), wingless-related integrated site (Wnt), Hedgehog (Hh), notch, or fibroblast growth factor (FGF) pathways to indicate the pathways that may be involved in the CM-induced adipogenesis. This would best be conducted in conjunction with qRT-PCR or adipocyte expression microarrays so that the expression levels of the adipocytic genes could be measured prior to inhibition. Additionally, multiplex ELISA or mass spectrometry could be conducted on the CM samples to further elucidate the proteins involved in the endocrine signalling events.

Conclusion

The present study explored the influences of a high-fat- or elevated sugar diet on the morphology, proliferation, and adipocytic differentiation capacity of subcutaneous and visceral adipose-derived mesenchymal stem cells (AD-MSCs). It also examined the impact of the adipocytic secretome on naïve AD-MSCs isolated from anatomically distinct adipose depots by collecting conditioned media (CM) from *in vitro* differentiated subcutaneous and visceral adipocytes and subsequently adding this media to naïve, undifferentiated AD-MSCs from both adipose depots. Finally, the contribution of PPAR γ activation in conjunction with the effects of incubation with CM was assessed by supplementing subcutaneous and visceral CM with rosiglitazone prior to the treatment of naïve subcutaneous and visceral AD-MSCs.

From the findings of this study, four important observations were made.

- 1) CM collected from *in vitro* differentiated subcutaneous adipocytes can induce lipid accumulation in naïve, undifferentiated visceral AD-MSCs.
- 2) The chronic consumption of an elevated sugar or high-fat diet does not consistently increase the CM-induced adipogenesis as compared to the control CM in either the inguinal or retroperitoneal recipient AD-MSCs.
- 3) Rosiglitazone enhances subcutaneous and visceral CM-induced lipid accumulation in naïve visceral AD-MSCs treated with either 100% CM or 1:1 CM: SGM but does not significantly increase CM-induced adipogenesis in subcutaneous AD-MSCs.
- 4) Visceral AD-MSCs have a higher propensity for lipid accumulation when exposed to CM than subcutaneous AD-MSCs.

Whilst the existence of paracrine interactions within the subcutaneous and visceral adipose tissues have been proven to exist ^{145,165,325–327}, the subcutaneous CM-induced lipid accrual in the visceral AD-MSCs observed within this study indicates the potential occurrence of an endocrine signalling interaction between the two adipose depots. This finding warrants further investigation as identifying the exact signalling cascade implicated in this depot-depot communication could lead to the development of therapeutic interventions to reduce the accumulation of the pathogenic visceral fat.

The amplification of lipid accrual in visceral AD-MSCs by supplementation of the 100% subcutaneous CM with rosiglitazone implies that the effects of endocrine-induced adipogenesis in the visceral adipose depot may be intensified in an individual taking rosiglitazone as a treatment for insulin resistance. As no significant lipid accrual was observed in the subcutaneous AD-MSCs treated with any of the subcutaneous CMs, the hypothesised adipogenic suppression by the visceral adipocytes is unlikely. Considering the significant lipid accrual induced by the 100% AM positive control in the subcutaneous AD-MSCs, it is possible that the subcutaneous cells may require prolonged exposure to viscerally secreted factors to induce an adipogenic response.

It is believed that this is the first study to date to provide evidence that the secretion of factors by subcutaneous adipocytes can stimulate adipogenesis in visceral AD-MSCs. These findings provide a good starting point upon which future inter-depot communication studies can build.

References

1. Dictionary, O. E. 'obese, adj. and n.'
2. McGuire, M. & Beerman, K. A. Energy Metabolism. in *Nutritional Sciences: From Fundamentals to Food* 270–300 (Cengage Learning, 2012).
3. Eknoyan, G. A History of Obesity, or How What Was Good Became Ugly and Then Bad. *Adv. Chronic Kidney Dis.* **13**, 421–427 (2006).
4. Brown, P. J. & Konner, M. An Anthropological Perspective on Obesity. *Ann. N. Y. Acad. Sci.* **499**, 29–46 (1987).
5. Goossens, G. H. The Metabolic Phenotype in Obesity: Fat Mass, Body Fat Distribution, and Adipose Tissue Function. *Obes. Facts* **10**, 207–215 (2017).
6. Imam, S. K. Diabetes. in *Glucose Intake and Utilization in Pre-Diabetes and Diabetes* 29–44 (Elsevier, 2015). doi:10.1016/B978-0-12-800093-9.00003-X.
7. Stoner, L. & Cornwall, J. Did the American Medical Association make the correct decision classifying obesity as a disease? *AMJ* **7**, 462–464 (2014).
8. Pollack, A. A.M.A. Recognizes Obesity as a Disease. *The New York Times* 1 (2013).
9. Christ, A., Lauterbach, M. & Latz, E. Western Diet and the Immune System: An Inflammatory Connection. *Immunity* **51**, 794–811 (2019).
10. Blackburn, H. & Jacobs, D. Commentary: Origins and evolution of Body Mass Index (BMI): Continuing saga. *Int. J. Epidemiol.* **43**, 665–669 (2014).
11. Shah, M., Hurt, R. T. & Mundi, M. S. Phenotypes of Obesity: How it Impacts Management. *Curr. Gastroenterol. Rep.* **19**, (2017).
12. World Health Organization. Obesity and overweight. <https://www.who.int/news-room/fact-sheets/detail/obesity-and-overweight> (2021).
13. Woolcott, O. O. & Bergman, R. N. Relative fat mass (RFM) as a new estimator of whole-body fat percentage — A cross-sectional study in American adult individuals. *Sci. Rep.* **8**, 1–11 (2018).
14. Ode, J. J., Pivarnik, J. M., Reeves, M. J. & Knous, J. L. Body mass index as a predictor of percent fat in college athletes and nonathletes. *Med. Sci. Sports Exerc.* **39**, 403–409 (2007).
15. Dagan, S. S., Segev, S., Novikov, I. & Dankner, R. Waist circumference vs body mass index in association with cardiorespiratory fitness in healthy men and women: a cross sectional analysis of 403 subjects. *Nutr. J.* **12**, 1 (2013).
16. World Health Organization. *Obesity: Preventing and managing the global epidemic. WHO Technical Report Series* vol. 894 (2000).
17. Stanaway, J. D. *et al.* Global, regional, and national comparative risk assessment of 84 behavioural, environmental and occupational, and metabolic risks or clusters of risks for 195 countries and territories, 1990-2017: A systematic analysis for the Global Burden of Disease Stu. *Lancet* **392**, 1923–1994 (2018).
18. Bakhtiari, A., Hajian-Tilaki, K. & Ghanbarpour, A. Metabolic syndrome and different obesity phenotypes in the elderly women population: Iran's Health System on aging. *Casp. J. Intern. Med.* **9**, 252–259 (2018).
19. Cuthbertson, D. P. & Tompsett, S. L. The degree of unsaturation of the fats of human adipose tissue in relation to depth from skin surface. *Biochem. J.* **27**, 1103–1106 (1933).

20. Haththotuwa, R. N., Wijeyaratne, C. N. & Senarath, U. *Worldwide epidemic of obesity. Obesity and Obstetrics* (INC, 2020). doi:10.1016/b978-0-12-817921-5.00001-1.
21. Michalakis, K. & Ilias, I. SARS-CoV-2 infection and obesity: Common inflammatory and metabolic aspects. *Diabetes Metab. Syndr. Clin. Res. Rev.* **14**, 469–471 (2020).
22. Bora, P. & Majumdar, A. S. Adipose tissue-derived stromal vascular fraction in regenerative medicine: a brief review on biology and translation. *Stem Cell Res. Ther.* **8**, 1–10 (2017).
23. Parlee, S. D., Lentz, S. I., Mori, H. & Macdougald, O. A. Quantifying Size and Number of Adipocytes in Adipose Tissue. *Methods Enzymol.* **537**, 93–122 (2014).
24. Esteve Ràfols, M. Adipose tissue: Cell heterogeneity and functional diversity. *Endocrinol. y Nutr. (English Ed.* **61**, 100–112 (2014).
25. Sun, M. *et al.* Adipose Extracellular Matrix/Stromal Vascular Fraction Gel Secretes Angiogenic Factors and Enhances Skin Wound Healing in a Murine Model. *Biomed Res. Int.* **2017**, (2017).
26. Panina, Y. A. *et al.* Plasticity of Adipose Tissue-Derived Stem Cells and Regulation of Angiogenesis. *Front. Physiol.* **9**, 1–13 (2018).
27. Lee, J., Abdeen, A. A., Tang, X., Saif, T. A. & Kilian, K. A. Matrix directed adipogenesis and neurogenesis of mesenchymal stem cells derived from adipose tissue and bone marrow. *Acta Biomater.* **42**, 46–55 (2016).
28. Flatt, J.-P. Use and storage of carbohydrate and fat. *Am J Clin Nutr* **61**, 952S–9S (1995).
29. Cohen, P. & Spiegelman, B. M. Cell biology of fat storage. *Mol. Biol. Cell* **27**, 2523–2527 (2016).
30. Graff, J. M. & Lapid, K. Form(ul)ation of adipocytes by lipids. *Adipocyte* **6**, 176–186 (2017).
31. Coelho, M., Oliveira, T. & Fernandes, R. Biochemistry of adipose tissue: an endocrine organ. *Arch Med Sci* **9**, 191–200 (2013).
32. Kersten, S. Mechanisms of nutritional and hormonal regulation of lipogenesis. *EMBO Rep.* **2**, 282–286 (2001).
33. Houten, S. M. & Wanders, R. J. A. A general introduction to the biochemistry of mitochondrial fatty acid β -oxidation. *J. Inherit. Metab. Dis.* **33**, 469–477 (2010).
34. Pellegrinelli, V., Carobbio, S. & Vidal-Puig, A. Adipose tissue plasticity: how fat depots respond differently to pathophysiological cues. *Diabetologia* **59**, 1075–1088 (2016).
35. Jo, J. *et al.* Hypertrophy and/or hyperplasia: Dynamics of adipose tissue growth. *PLoS Comput. Biol.* **5**, (2009).
36. Chan, P.-C. & Hsieh, P.-S. The Role of Adipocyte Hypertrophy and Hypoxia in the Development of Obesity-Associated Adipose Tissue Inflammation and Insulin Resistance. *Adiposity - Omi. Mol. Underst.* (2017) doi:10.5772/65458.
37. Stenkula, K. G. & Erlanson-Albertsson, C. Adipose cell size: Importance in health and disease. *Am. J. Physiol. - Regul. Integr. Comp. Physiol.* **315**, R284–R295 (2018).
38. Reilly, S. M. & Saltiel, A. R. Adapting to obesity with adipose tissue inflammation. *Nat. Rev. Endocrinol.* **13**, 633–643 (2017).
39. Hirsch, J. & Batchelor, B. Adipose tissue cellularity in human obesity. *Clin. Endocrinol. Metab.* **5**, 299–311 (1976).
40. Lane, M. D. & Tang, Q. Q. From multipotent stem cell to adipocyte. *Birth Defects Res. Part A - Clin. Mol. Teratol.* **73**, 476–477 (2005).
41. Tang, Q. Q. & Lane, M. D. Adipogenesis: From stem cell to adipocyte. *Annu. Rev. Biochem.*

- 81**, 715–736 (2012).
42. Rosen, E. D. & MacDougald, O. A. Adipocyte differentiation from the inside out. *Nat. Rev. Mol. Cell Biol.* **7**, 885–896 (2006).
 43. Otto, T. C. & Lane, M. D. Adipose Development: From Stem Cell to Adipocyte. *Crit. Rev. Biochem. Mol. Biol.* **40**, 229–242 (2005).
 44. Gregoire, F. M., Smas, C. M. & Sul, S. Understanding Adipocyte Differentiation. *Physiol. Rev.* **78**, 783–801 (1998).
 45. Bowers, R. R., Kim, J. W., Otto, T. C. & Lane, M. D. Stable stem cell commitment to the adipocyte lineage by inhibition of DNA methylation: Role of the BMP-4 gene. *Proc. Natl. Acad. Sci. U. S. A.* **103**, 13022–13027 (2006).
 46. Altioek, S., Xu, M. & Spiegelman, B. M. PPAR γ induces cell cycle withdrawal: Inhibition of E2f/DP DNA-binding activity via down-regulation of PP2A. *Genes Dev.* **11**, 1987–1998 (1997).
 47. Umek, R. M., Friedman, A. D. & Mcknight, S. L. CCAAT-enhancer binding protein: A component of a differentiation switch. *Science (80-)*. **251**, 288–292 (1991).
 48. Bourgeois, C. *et al.* Specific Biological Features of Adipose Tissue, and Their Impact on HIV Persistence. *Front. Microbiol.* **10**, 1–25 (2019).
 49. Tang, W., Zeve, D., Seo, J., Jo, A. Y. & Graff, J. M. Thiazolidinediones regulate adipose lineage dynamics. *Cell Metab.* **14**, 116–122 (2011).
 50. Hallakou, S. *et al.* Pioglitazone induces in vivo adipocyte differentiation in the obese Zucker fa/fa rat. *Diabetes* **46**, 1393–1399 (1997).
 51. Hausman, G. J., Poulos, S. P., Pringle, T. D. & Azain, M. J. The influence of thiazolidinediones on adipogenesis in vitro and in vivo: potential modifiers of intramuscular adipose tissue deposition in meat animals. *J. Anim. Sci.* **86**, 236–243 (2008).
 52. van de Vyver, M., Andrag, E., Cockburn, I. L. & Ferris, W. F. Thiazolidinedione-induced lipid droplet formation during osteogenic differentiation. *J. Endocrinol.* **223**, 119–132 (2014).
 53. Lebovitz, H. E. Thiazolidinediones: the Forgotten Diabetes Medications. *Curr. Diab. Rep.* **19**, 1–13 (2019).
 54. Lehmann, J. M. *et al.* An antidiabetic thiazolidinedione is a high affinity ligand for peroxisome proliferator-activated receptor γ (PPAR γ). *J. Biol. Chem.* **270**, 12953–12956 (1995).
 55. Yki-Järvinen, H. Thiazolidinediones. *N. Engl. J. Med.* **351**, 1106–1118 (2004).
 56. Schoonjans, K. & Auwerx, J. New drug classes Thiazolidinediones : an update. **355**, 1008–1010 (2000).
 57. Fürnsinn, C. & Waldhäusl, W. Thiazolidinediones: Metabolic actions in vitro. *Diabetologia* **45**, 1211–1223 (2002).
 58. Hauner, H. The mode of action of thiazolidinediones. *Diabetes. Metab. Res. Rev.* **18**, S10–S15 (2002).
 59. Lowell, B. B. *PPAR: An Essential Regulator Minireview of Adipogenesis and Modulator of Fat Cell Function.* *Cell* vol. 99 (1999).
 60. Casteilla, L., Cousin, B. & Carmona, M. PPARs and adipose cell plasticity. *PPAR Res.* **2007**, (2007).
 61. Wang, Q. *et al.* Increased feeding in fatty Zucker rats by the thiazolidinedione BRL 49653 (rosiglitazone) and the possible involvement of leptin and hypothalamic neuropeptide Y. *Br. J. Pharmacol.* **122**, 1405–1410 (1997).

62. Okuno, A. *et al.* Troglitazone increases the number of small adipocytes without the change of white adipose tissue mass in obese Zucker rats. *J. Clin. Invest.* **101**, 1354–1361 (1998).
63. De Souza, C. J. *et al.* Effects of Pioglitazone on Adipose Tissue Remodeling Within the Setting of Obesity and Insulin Resistance. *Diabetes* **50**, 1863–1871 (2001).
64. Miyazaki, Y. Effect of Pioglitazone on Abdominal Fat Distribution and Insulin Sensitivity in Type 2 Diabetic Patients. *J. Clin. Endocrinol. Metab.* **87**, 2784–2791 (2002).
65. Ko, K. D., Kim, K. K. & Lee, K. R. Does Weight Gain Associated with Thiazolidinedione Use Negatively Affect Cardiometabolic Health? *J. Obes. Metab. Syndr.* **26**, 102–106 (2017).
66. Kim, S. K. *et al.* The increase in abdominal subcutaneous fat depot is an independent factor to determine the glycemic control after rosiglitazone treatment. *Eur. J. Endocrinol.* **157**, 167–174 (2007).
67. Harms, M. & Seale, P. Brown and beige fat: development, function and therapeutic potential. *Nat. Med.* **19**, 1252–1263 (2013).
68. Schoettl, T., Fischer, I. P. & Ussar, S. Heterogeneity of adipose tissue in development and metabolic function. *J. Exp. Biol.* **221**, 1–17 (2018).
69. Nedergaard, J. & Cannon, B. Brown adipose tissue as a heat-producing thermoeffector. in *Handbook of Clinical Neurology* vol. 156 137–152 (Elsevier B.V., 2018).
70. Kaisanlahti, A. & Glumoff, T. Browning of white fat: agents and implications for beige adipose tissue to type 2 diabetes. *J. Physiol. Biochem.* **75**, 1–10 (2019).
71. Gesta, S., Tseng, Y. H. & Kahn, C. R. Developmental Origin of Fat: Tracking Obesity to Its Source. *Cell* **131**, 242–256 (2007).
72. Heaton, J. M. The distribution of brown adipose tissue in the human. *J. Anat.* **112**, 35–39 (1972).
73. Lidell, M. E., Betz, M. J. & Enerbäck, S. Brown adipose tissue and its therapeutic potential. *J. Intern. Med.* **276**, 364–377 (2014).
74. Smith, R. E. & Horwitz, B. A. Brown Fat and Thermogenesis. in *Physiological Reviews* vol. 49 330–408 (1969).
75. Bjørndal, B., Burri, L., Staalesen, V., Skorve, J. & Berge, R. K. Different adipose depots: Their role in the development of metabolic syndrome and mitochondrial response to hypolipidemic agents. *J. Obes.* **2011**, (2011).
76. Golozoubova, V. *et al.* Only UCP1 can mediate adaptive nonshivering thermogenesis in the cold. *FASEB J.* **15**, 2048–2050 (2001).
77. Golozoubova, V., Cannon, B. & Nedergaard, J. UCP1 is essential for adaptive adrenergic nonshivering thermogenesis. *Am. J. Physiol. - Endocrinol. Metab.* **291**, (2006).
78. Schöttl, T., Kappler, L., Fromme, T. & Klingenspor, M. Limited OXPHOS capacity in white adipocytes is a hallmark of obesity in laboratory mice irrespective of the glucose tolerance status. *Mol. Metab.* **4**, 631–642 (2015).
79. Böhm, A. *et al.* Increased mitochondrial respiration of adipocytes from metabolically unhealthy obese compared to healthy obese individuals. *Sci. Rep.* **10**, 1–10 (2020).
80. Moonen, M. P. B., Nascimento, E. B. M. & van Marken Lichtenbelt, W. D. Human brown adipose tissue: Underestimated target in metabolic disease? *Biochim. Biophys. Acta - Mol. Cell Biol. Lipids* **1864**, 104–112 (2019).
81. Nedergaard, J., Bengtsson, T. & Cannon, B. Unexpected evidence for active brown adipose tissue in adult humans. *Am J Physiol Endocrinol Metab* **293**, 444–452 (2007).

82. Nedergaard, J. & Cannon, B. The Changed Metabolic World with Human Brown Adipose Tissue: Therapeutic Visions. *Cell Metab.* **11**, 268–272 (2010).
83. Kiefer, F. W. *et al.* Retinaldehyde dehydrogenase 1 regulates a thermogenic program in white adipose tissue. *Nat. Med.* **18**, 918–925 (2012).
84. Bostrom, P. *et al.* A PGC1 α -dependent myokine that drives browning of white fat. *Nature* **481**, 463–468 (2012).
85. Zhou, Z. *et al.* Cidea-deficient mice have lean phenotype and are resistant to obesity. *Nat. Genet.* **35**, 49–56 (2003).
86. Ussar, S. *et al.* ASC-1, PAT2, and P2RX5 are cell surface markers for white, beige, and brown adipocytes. *Sci. Transl. Med.* **6**, (2014).
87. Xue, B. *et al.* Genetic variability affects the development of brown adipocytes in white fat but not in interscapular brown fat. *J. Lipid Res.* **48**, 41–51 (2007).
88. Seale, P. *et al.* PRDM16 controls a brown fat/skeletal muscle switch. *Nature* **454**, 961–967 (2008).
89. Wang, X. & Wahl, R. Responses of the insulin signaling pathways in the brown adipose tissue of rats following cold exposure. *PLoS One* **9**, (2014).
90. Hart, J. S. & Heroux, O. Utilization of body reserves during exposure of mice to low temperatures. *Can. J. Biochem. Physiol.* **34**, 414–421 (1956).
91. Graja, A. & Schulz, T. J. Mechanisms of Aging-Related Impairment of Brown Adipocyte Development and Function. *Gerontology* **61**, 211–217 (2015).
92. Harms, M. J., Li, Q., Mardinoglu, A., Spalding, K. L. & Correspondence, J. B. Mature Human White Adipocytes Cultured under Membranes Maintain Identity, Function, and Can Transdifferentiate into Brown-like Adipocytes. *CellReports* **27**, 213–225.e5 (2019).
93. Schosserer, M., Grillari, J., Wolfrum, C. & Scheideler, M. Age-Induced Changes in White, Brite, and Brown Adipose Depots: A Mini-Review. *Gerontology* **64**, 229–236 (2018).
94. Sebo, Z. L. & Rodeheffer, M. S. Assembling the adipose organ: Adipocyte lineage segregation and adipogenesis in vivo. *Dev.* **146**, (2019).
95. Lee, M. J., Wu, Y. & Fried, S. K. Adipose tissue heterogeneity: Implication of depot differences in adipose tissue for obesity complications. *Mol. Aspects Med.* **34**, 1–11 (2013).
96. Cinti, S. The Adipose Organ. in *Nutrition and Health: Adipose Tissue and Adipokines in Health and Disease* 3–19 (2007).
97. Szablewski, L. Types of Adipose Tissue. in *IntechOpen* 3–5 (IntechOpen, 2018). doi:<http://dx.doi.org/10.5772/57353>.
98. Coppack, S. W. Pro-inflammatory cytokines and adipose tissue. *Proc. Nutr. Soc.* **60**, 349–356 (2001).
99. Fain, J. N. Release of inflammatory mediators by human adipose tissue is enhanced in obesity and primarily by the nonfat cells: A review. *Mediators Inflamm.* **2010**, (2010).
100. Harrold, J. A., Williams, G. & Widdowson, P. S. Early Leptin Response to a Palatable Diet Predicts Dietary Obesity in Rats: Key Role of Melanocortin-4 Receptors in the Ventromedial Hypothalamic Nucleus. *J. Neurochem.* **74**, 1224–1228 (2000).
101. Trayhurn, P. & Beattie, J. H. Physiological role of adipose tissue: white adipose tissue as an endocrine and secretory organ. *Proc. Nutr. Soc.* **60**, 329–339 (2001).
102. Saely, C. H., Geiger, K. & Drexel, H. Brown versus white adipose tissue: A mini-review. *Gerontology* **58**, 15–23 (2011).

103. Institute of Medicine (US) Subcommittee on Military Weight Management. *Factors That Influence Body Weight*. vol. 3 (National Academies Press (US), 2004).
104. Wood, I. S., De Heredia, F. P., Wang, B. & Trayhurn, P. Cellular hypoxia and adipose tissue dysfunction in obesity. *Proc. Nutr. Soc.* **68**, 370–377 (2009).
105. Luong, Q., Huang, J. & Lee, K. Y. Deciphering white adipose tissue heterogeneity. *Biology (Basel)*. **8**, 1–14 (2019).
106. Ibrahim, M. M. Subcutaneous and visceral adipose tissue: structural and functional differences. *Obes. Rev.* **11**, 11–18 (2010).
107. Park, A. Distinction of white, beige and brown adipocytes derived from mesenchymal stem cells. *World J. Stem Cells* **6**, 33 (2014).
108. Driskell, R., Jahoda, C. A. B., Chuong, C.-M., Watt, F. & Horsley, V. Defining dermal adipose tissue. *Exp. Dermatol.* **23**, 629–631 (2014).
109. Abate, N. & Garg, A. Heterogeneity in Adipose Tissue Metabolism: Causes, Implications and Management of Regional Adiposity. *Prog. Lipid Res.* **34**, 53–70 (1995).
110. Vague, J. The degree of masculine differentiation of obesities: A factor determining predisposition to diabetes, atherosclerosis, gout, and uric calculous disease. *Am. J. Clin. Nutr.* **4**, 20–34 (1956).
111. Kissebah, A. H. & Krakower, G. R. Regional Adiposity and Morbidity. *Physiol. Rev.* **74**, 761–798 (1994).
112. Bjorntorp, P. Body Fat Distribution, Insulin Resistance, and Metabolic Diseases. *Nutrition* **13**, 795–803 (1997).
113. Laviola, L. *et al.* Insulin signaling in human visceral and subcutaneous adipose tissue in vivo. *Diabetes* **55**, 952–961 (2006).
114. Ali, A. T., Ferris, W. F., Naran, N. H. & Crowther, N. J. Insulin resistance in the control of body fat distribution: A new hypothesis. *Horm. Metab. Res.* **43**, 77–80 (2011).
115. Montague, C. T., Prins, J. B., Sanders, L., Digby, J. E. & O’Rahilly, S. Depot- and sex-specific differences in human leptin mRNA expression: Implications for the control of regional fat distribution. *Diabetes* **46**, 342–347 (1997).
116. Sparrow, D., Borkan, G. A., Gerzof, S. G., Wisniewski, C. & Silbert, C. K. Relationship of fat distribution to glucose tolerance. Results of computed tomography in male participants of the Normative Aging Study. *Diabetes* **35**, 411–415 (1986).
117. Pouliot, M. C. *et al.* Visceral obesity in men: Associations with glucose tolerance, plasma insulin, and lipoprotein levels. *Diabetes* **41**, 826–834 (1992).
118. Despres, J. P. *et al.* Role of deep abdominal fat in the association between regional adipose tissue distribution and glucose tolerance in obese women. *Diabetes* **38**, 304–309 (1989).
119. Fujioka, S., Matsuzawa, Y., Tokunaga, K. & Tarui, S. Contribution of intra-abdominal fat accumulation to the impairment of glucose and lipid metabolism in human obesity. *Metabolism* **36**, 54–59 (1987).
120. Manolopoulos, K. N., Karpe, F. & Frayn, K. N. Gluteofemoral body fat as a determinant of metabolic health. *Int. J. Obes.* **34**, 949–959 (2010).
121. Salans, L. B., Cushman, S. W. & Weismann, R. E. Studies of human adipose tissue. Adipose cell size and number in nonobese and obese patients. *J. Clin. Invest.* **52**, 929–941 (1973).
122. Weyer C, Foley J.E, Borgadus C, Tataranni P.A & Pratley R.E. Enlarged subcutaneous abdominal adipocyte size, but not obesity itself, predicts Type II diabetes independent of insulin resistance. *Diabetologia* **43**, 1498–1506 (2000).

123. Ruderman, B., Schneider, H. & Berchtold, P. The “metabolically-obese,” normal-weight individual. *Am. J. Clin. Nutr.* **34**, 1617–1621 (1981).
124. Klein, S. *et al.* Waist circumference and cardiometabolic risk: a consensus statement from Shaping America’s Health: Association for Weight Management and Obesity Prevention; NAASO, The Obesity Society; the American Society for Nutrition; and the American Diabetes Association. *Am. J. Clin. Nutr.* **85**, 1197–1202 (2007).
125. Kabir, M. *et al.* Molecular evidence supporting the portal theory: A causative link between visceral adiposity and hepatic insulin resistance. *Am. J. Physiol. - Endocrinol. Metab.* **288**, 454–461 (2005).
126. Ouchi, N., Parker, J. L., Lugu, J. J. & Walsh, K. Adipokines in inflammation and metabolic disease. *Nat Rev Immunol* **11**, 85–97 (2011).
127. Kwon, H. & Pessin, J. E. Adipokines mediate inflammation and insulin resistance. *Front. Endocrinol. (Lausanne)*. **4**, 1–13 (2013).
128. Shuster, A., Atlas, M., Pinthus, J. H. & Mourtzakis, M. The clinical importance of visceral adiposity: a critical review of methods for visceral adipose tissue analysis. *Br. J. Radiol.* **85**, 1–10 (2012).
129. Ouchi, N., Parker, J. L., Lugas, J. J. & Walsh, K. Adipokines in inflammation and metabolic disease . *Nat Rev Immunol* **11**, 85–97 (2011).
130. Martin, M. L. & Jensen, M. D. Effects of body fat distribution on regional lipolysis in obesity. *J. Clin. Invest.* **88**, 609–613 (1991).
131. Marin, P. *et al.* Assimilation of Triglycerides in Subcutaneous and Intraabdominal Adipose Tissue in vivo in Men: Effects of Testosterone. *J. Clin. Endocrinol. Metab.* **81**, 1018–1022 (1996).
132. Rytka, J. M., Wueest, S., Schoenle, E. J. & Konrad, D. The portal theory supported by venous drainage-selective fat transplantation. *Diabetes* **60**, 56–63 (2011).
133. Meshkani, R. & Adeli, K. Hepatic insulin resistance, metabolic syndrome and cardiovascular disease. *Clin. Biochem.* **42**, 1331–1346 (2009).
134. Kyle, U. G. *et al.* Age-related differences in fat-free mass, skeletal muscle, body cell mass and fat mass between 18 and 94 years. *Eur. J. Clin. Nutr.* **55**, 663–672 (2001).
135. Samaras, K., Botelho, N. K., Chisholm, D. J. & Lord, R. V. Subcutaneous and visceral adipose tissue FTO gene expression and adiposity, insulin action, glucose metabolism, and inflammatory adipokines in type 2 diabetes mellitus and in health. *Obes. Surg.* **20**, 108–113 (2010).
136. Tchoukalova, Y. D. *et al.* Regional differences in cellular mechanisms of adipose tissue gain with overfeeding. *Proc. Natl. Acad. Sci. U. S. A.* **107**, 18226–18231 (2010).
137. Chen, W., Wilson, J. L., Khaksari, M., Cowley, M. A. & Enriori, P. J. Abdominal fat analyzed by DEXA scan reflects visceral body fat and improves the phenotype description and the assessment of metabolic risk in mice. *Am J Physiol Endocrinol Metab* **303**, 635–643 (2012).
138. Frayn, K. N. Visceral fat and insulin resistance, causative or correlative? *Br. J. Nutr.* **83**, S71–S77 (2000).
139. Haylett, W. L. & Ferris, W. F. Adipocyte–progenitor cell communication that influences adipogenesis. *Cell. Mol. Life Sci.* **77**, 115–128 (2020).
140. Despres, J.-P. & Lemieux, I. Abdominal obesity and metabolic syndrome. *Nature* **444**, 881–887 (2006).
141. Sniderman, A. D., Bhopal, R., Prabhakaran, D., Sarrafzadegan, N. & Tchernof, A. Why might

South Asians be so susceptible to central obesity and its atherogenic consequences? The adipose tissue overflow hypothesis. *Int. J. Epidemiol.* **36**, 220–225 (2007).

142. Östman, J., Arner, P., Engfeldt, P. & Kager, L. Regional differences in the control of lipolysis in human adipose tissue. *Metabolism* **28**, 1198–1205 (1979).
143. Fortuño, A., Rodríguez, A., Gómez-Ambrosi, J., Frühbeck, G. & Díez, J. Adipose tissue as an endocrine organ: Role of leptin and adiponectin in the pathogenesis of cardiovascular diseases. *J. Physiol. Biochem.* **59**, 51–60 (2003).
144. Wajchenberg, B. L. Subcutaneous and Visceral Adipose Tissue: Their Relation to the Metabolic Syndrome. *Endocr. Rev.* **21**, 697–738 (2000).
145. Wajchenberg, B. L., Giannella-Neto, D., da Silva, M. E. & Santos, R. F. Depot-Specific Hormonal Characteristics of Subcutaneous and Visceral Adipose Tissue and their Relation to the Metabolic Syndrome. *Horm. Metab. Res.* **34**, 616–621 (2002).
146. Mohamed-Ali, V., Pinkney, J. H. & Coppack, S. W. Adipose tissue as an endocrine and paracrine organ. *Int. J. Obes.* **22**, 1145–1158 (1998).
147. Kim, S. & Moustaid-moussa, N. Symposium: Adipocyte Function , Differentiation and Metabolism Secretary , Endocrine and Autocrine / Paracrine Function of the Adipocyte 1. *J. Nutr.* 3110–3115 (2000).
148. Zullo, J., Matsumoto, K., Xavier, S., Ratliff, B. & Goligorsky, M. S. The Cell Secretome, A Mediator of Cell-to-cell Communication. *Prostaglandins Other Lipid Mediat.* **120**, 17–20 (2015).
149. Park, S. R. *et al.* Stem Cell Secretome and Its Effect on Cellular Mechanisms Relevant to Wound Healing. *Mol. Ther.* **26**, 606–617 (2018).
150. Ahima, R. S. & Flier, J. S. Adipose tissue as an endocrine organ. *Trends Endocrinol. Metab.* **11**, 327–332 (2000).
151. Trayhurn, P. & Wood, I. S. Adipokines: inflammation and the pleiotropic role of white adipose tissue. *Br. J. Nutr.* **92**, 347–355 (2004).
152. Scherer, P. E. Adipose Tissue. *Diabetes* **55**, 1537–1545 (2006).
153. McGown, C., Birerdinc, A. & Younossi, Z. M. Adipose tissue as an endocrine organ. *Clin. Liver Dis.* **18**, 41–58 (2014).
154. Jiang, N., Li, Y., Shu, T. & Wang, J. Cytokines and inflammation in adipogenesis: an updated review. *Front. Med.* **13**, 314–329 (2019).
155. Lyon, C. J., Law, R. E. & Hsueh, W. A. Minireview: Adiposity, inflammation, and atherogenesis. *Endocrinology* **144**, 2195–2200 (2003).
156. Mancuso, P. The role of adipokines in chronic inflammation. *ImmunoTargets Ther.* **5**, 47–56 (2016).
157. Shillabeer, G., Forden, J. M. & Lau, D. C. W. Induction of Preadipocyte Differentiation by Mature Fat Cells in the Rat. *J. Clin. Invest.* **84**, 381–387 (1989).
158. Bogdanowicz, D. R. & Lu, H. H. Studying cell-cell communication in co-culture. *Biotechnol. J.* **8**, 395–396 (2013).
159. Vis, M. A. M., Ito, K. & Hofmann, S. Impact of Culture Medium on Cellular Interactions in in vitro Co-culture Systems. *Front. Bioeng. Biotechnol.* **8**, 1–8 (2020).
160. Kanawa, M. *et al.* Potential marker genes for predicting adipogenic differentiation of mesenchymal stromal cells. *Appl. Sci.* **9**, (2019).
161. Stacey, D. H., Hanson, S. E., Lahvis, G., Gutowski, K. A. & Masters, K. S. In vitro Adipogenic

- Differentiation of Preadipocytes Varies with Differentiation Stimulus, Culture Dimensionality, and Scaffold Composition. *Tissue Eng. Part A* **15**, 3389–3399 (2009).
162. Shillabeer, G., Forden, J. M., Russell, J. C. & Lau, D. C. W. Paradoxically slow preadipocyte replication and differentiation in corpulent rats. *Am. J. Physiol. - Endocrinol. Metab.* **258**, (1990).
163. Haylett, W. L. & Ferris, W. F. W. F. Adipocyte–progenitor cell communication that influences adipogenesis. *Cell. Mol. Life Sci.* **77**, 115–128 (2020).
164. Wu, L. *et al.* Secreted factors from adipose tissue increase adipogenic differentiation of mesenchymal stem cells. *Cell Prolif.* **45**, 311–319 (2012).
165. Armani, A., Berry, A., Cirulli, F. & Caprio, M. Molecular mechanisms underlying metabolic syndrome: The expanding role of the adipocyte. *FASEB J.* **31**, 4240–4255 (2017).
166. Longo, M. *et al.* Adipose tissue dysfunction as determinant of obesity-associated metabolic complications. *Int. J. Mol. Sci.* **20**, (2019).
167. Henninger, A. M. J., Eliasson, B., Jenndahl, L. E. & Hammarstedt, A. Adipocyte hypertrophy, inflammation and fibrosis characterize subcutaneous adipose tissue of healthy, non-obese subjects predisposed to type 2 diabetes. *PLoS One* **9**, (2014).
168. Sadie-Van Gijzen, H., Crowther, N. J., Hough, F. S. & Ferris, W. F. Depot-specific differences in the insulin response of adipose-derived stromal cells. *Mol. Cell. Endocrinol.* **328**, 22–27 (2010).
169. Dieudonne, M. N., Pecquery, R., Leneuve, M. C. & Giudicelli, Y. Opposite Effects of Androgens and Estrogens on Adipogenesis in Rat Preadipocytes: Evidence for Sex and Site-Related Specificities and Possible Involvement of Insulin-Like Growth Factor 1 Receptor and Peroxisome Proliferator-Activated Receptor 21. *Endocrinology* **141**, 649–656 (2000).
170. Krakower, G. R. *et al.* Regional adipocyte precursors in the female rat - Influence of ovarian factors. *J. Clin. Invest.* **81**, 641–648 (1988).
171. Blignaut, M., Espach, Y., van Vuuren, M., Dhanabalan, K. & Huisamen, B. Revisiting the Cardiotoxic Effect of Chloroquine. *Cardiovasc. Drugs Ther.* **33**, 1–11 (2019).
172. Salie, R., Huisamen, B. & Lochner, A. High carbohydrate and high fat diets protect the heart against ischaemia/reperfusion injury. *Cardiovasc. Diabetol.* **13**, 1–12 (2014).
173. Huisamen, B. *Medicinal Effects of Agathosma (Buchu) Extracts. Medicinal Effects of Agathosma (Buchu) Extracts* (2019). doi:10.4102/aosis.2019.bk84.
174. Dey, P. Fixation of Histology Samples: Principles, Methods and Types of Fixatives. in *Basic and Advanced Laboratory Techniques in Histopathology and Cytology* 3–17 (2018). doi:10.1007/978-981-10-8252-8.
175. Carriel, V., Campos, F., Aneiros-Fernández, J. & Kiernan, J. A. Tissue fixation and processing for the histological identification of lipids. in *Methods in Molecular Biology* vol. 1560 197–206 (2017).
176. Avwioro, G. Histochemical uses of haematoxylin—a review. *JPCS* **1**, 24–34 (2011).
177. Yosofvand, M. *et al.* AdipoGauge software for analysis of biological microscopic images. *Adipocyte* **9**, 360–373 (2020).
178. Poret, J. M. *et al.* High fat diet consumption differentially affects adipose tissue inflammation and adipocyte size in obesity-prone and obesity-resistant rats. *Int. J. Obes.* **42**, 535–541 (2018).
179. Rauch, C. *et al.* Alternatives to the Use of Fetal Bovine Serum: Human Platelet Lysates as a Serum Substitute in Cell Culture Media. *Altex* vol. 28.

180. Lifeline Cell Technology. *Normal Human Endothelial Cells Instruction Sheet*. [https://www.lifelinecelltech.com/pdf/INC HEC Family 0314 v6 FC-0014_27_32_44_55.pdf](https://www.lifelinecelltech.com/pdf/INC%20HEC%20Family%200314%20v6%20FC-0014_27_32_44_55.pdf) (2014).
181. Jacobs, F. A., van de Vyver, M. & Ferris, W. F. Isolation and Characterization of Different Mesenchymal Stem Cell Populations from Rat Femur. in *Methods in Molecular Biology* (ed. Guest, P. C.) vol. 1916 133–148 (Springer New York, 2019).
182. Ambele, M. A., Dessels, C., Durandt, C. & Pepper, M. S. Genome-wide analysis of gene expression during adipogenesis in human adipose-derived stromal cells reveals novel patterns of gene expression during adipocyte differentiation. *Stem Cell Res.* **16**, 725–734 (2016).
183. Lee, M.-J., Wu, Y. & Fried, S. . K. A modified protocol to maximize differentiation of human preadipocytes and improve metabolic phenotypes. *Physiol. Behav.* **176**, 139–148 (2017).
184. Baldwin, T. *et al.* Wound healing response is a major contributor to the severity of cutaneous leishmaniasis in the ear model of infection. *Parasite Immunol.* **29**, 501–513 (2007).
185. Elso, C. M. *et al.* Leishmaniasis host response loci (Imr1-3) modify disease severity through a Th1/Th2-independent pathway. *Genes Immun.* **5**, 93–100 (2004).
186. Lee, R. H. *et al.* Characterization and expression analysis of mesenchymal stem cells from human bone marrow and adipose tissue. *Cell. Physiol. Biochem.* **14**, 311–324 (2004).
187. Zhan, X. S. *et al.* A comparative study of biological characteristics and transcriptome profiles of mesenchymal stem cells from different canine tissues. *Int. J. Mol. Sci.* **20**, (2019).
188. Roth, V. Doubling Time Computing. <https://www.doubling-time.com/compute.php>.
189. Baghaei, K. *et al.* Isolation, differentiation, and characterization of mesenchymal stem cells from human bone marrow. *Gastroenterol. Hepatol. from Bed to Bench* **10**, 208–213 (2017).
190. Bio-Rad Laboratories Inc. Antibody Titration - Flow Cytometry Guide | Bio-Rad. *Flow Cytometry* https://www.bio-rad-antibodies.com/flow-cytometry-antibody-titration.html?JSESSIONID_STERLING=A79804CD1CAD9494D559E30CF039930E.commerce1&evCntryLang=ZA-en&cntry=ZA&thirdPartyCookieEnabled=true (2021).
191. Jacobs, F. A., van de Vyver, M. & Ferris, W. F. Isolation and Characterization of Different Mesenchymal Stem Cell Populations from Rat Femur. in *Methods in Molecular Biology* vol. 1916 133–147 (2019).
192. Ono, M., Aratani, Y., Kitagawa, I. & Kitagawa, Y. Ascorbic acid phosphate stimulates type IV collagen synthesis and accelerates adipose conversion of 3T3-L1 cells. *Exp. Cell Res.* **187**, 309–314 (1990).
193. Kishimoto, Y. *et al.* Ascorbic acid enhances the expression of type 1 and type 4 collagen and SVCT2 in cultured human skin fibroblasts. *Biochem. Biophys. Res. Commun.* **430**, 579–584 (2013).
194. Langenbach, F. & Handschel, J. Effects of dexamethasone, ascorbic acid and β -glycerophosphate on the osteogenic differentiation of stem cells in vitro. *Stem Cell Res. Ther.* **4**, 1–7 (2013).
195. Cuaranta-Monroy, I. *et al.* Highly efficient differentiation of embryonic stem cells into adipocytes by ascorbic acid. *Stem Cell Res.* **13**, 88–97 (2014).
196. Liu, C. *et al.* Ascorbic acid promotes 3T3-L1 cells adipogenesis by attenuating ERK signaling to upregulate the collagen VI. *Nutr. Metab. (Lond)*. **14**, 79 (2017).
197. Harada, S. -I, Matsumoto, T. & Ogata, E. Role of ascorbic acid in the regulation of proliferation in osteoblast-like MC3T3-E1 cells. *J. Bone Miner. Res.* **6**, 903–908 (1991).

198. Tagler, D. *et al.* Promoting Extracellular Matrix Remodeling via Ascorbic Acid Enhances the Survival of Primary Ovarian Follicles Encapsulated in Alginate Hydrogels NIH Public Access Author Manuscript. *Biotechnol. Bioeng.* **111**, 1417–1429 (2014).
199. Jariwalla, R. J. & Harakeh, S. *Subcellular Biochemistry*. *Subcellular biochemistry* vol. 25 (Springer US, 1996).
200. Yang, C. *et al.* Conditioned Media from Human Adipose Tissue-Derived Mesenchymal Stem Cells and Umbilical Cord-Derived Mesenchymal Stem Cells Efficiently Induced the Apoptosis and Differentiation in Human Glioma Cell Lines In Vitro. *Biomed Res. Int.* 1–13 (2014) doi:10.1155/2014/109389.
201. Park, G. W. *et al.* Topical cell-free conditioned media harvested from adipose tissue-derived stem cells promote recovery from corneal epithelial defects caused by chemical burns. *Sci. Rep.* **10**, 1–15 (2020).
202. Medscape. Avandia (rosiglitazone) dosing, indications, interactions, adverse effects, and more. *Medscape* <https://reference.medscape.com/drug/avandia-rosiglitazone-342727> (2022).
203. Kraus, N. A. *et al.* Quantitative assessment of adipocyte differentiation in cell culture. *Adipocyte* **5**, 351–358 (2016).
204. Ramirez-Zacaras, J. L., Castro-Muozledo, F. & Kuri-Harcuch, W. Quantitation of adipose conversion and triglycerides by staining intracytoplasmic lipids with oil red O. *Histochemistry* **97**, 493–497 (1992).
205. Jacobs, F. A. The modulation of bone stem cell fate by glucocorticoids and vanadate. (Stellenbosch University, 2018).
206. Jacobs, F. A., Sadie-Van Gijsen, H., van de Vyver, M. & Ferris, W. F. Vanadate Impedes Adipogenesis in Mesenchymal Stem Cells Derived from Different Depots within Bone. *Front. Endocrinol. (Lausanne)*. **7**, 1–12 (2016).
207. Feoktistova, M., Geserick, P. & Leverkus, M. Crystal violet assay for determining viability of cultured cells. *Cold Spring Harb. Protoc.* **2016**, 343–346 (2016).
208. Schindelin, J. *et al.* Fiji: An open-source platform for biological-image analysis. *Nat. Methods* **9**, 676–682 (2012).
209. Kundrotas, G. Surface markers distinguishing mesenchymal stem cells from fibroblasts. *Acta medica Litu.* **19**, 75–79 (2012).
210. Even, M. S., Sandusky, C. B. & Barnard, N. D. Serum-free hybridoma culture: Ethical, scientific and safety considerations. *Trends Biotechnol.* **24**, 105–108 (2006).
211. Shree, N. & Bhonde, R. R. Conditioned Media From Adipose Tissue Derived Mesenchymal Stem Cells Reverse Insulin Resistance in Cellular Models. *J. Cell. Biochem.* **118**, 2037–2043 (2017).
212. Cao, Z. *et al.* Growth arrest induction of 3T3-L1 preadipocytes by serum starvation and their differentiation by the hormonal adipogenic cocktail. *J. Cell Anim. Biol.* **6**, 57–65 (2012).
213. Fayyad, A. M. *et al.* Rosiglitazone enhances browning adipocytes in association with MAPK and PI3-K pathways during the differentiation of telomerase-transformed mesenchymal stromal cells into adipocytes. *Int. J. Mol. Sci.* **20**, (2019).
214. Lee, M.-J. & Fried, S. K. Optimal Protocol for the Differentiation and Metabolic Analysis of Human Adipose Stromal Cells. *Methods Enzymol.* **538**, 49–63 (2014).
215. Lee, M.-J., Wu, Y. & Fried, S. K. A modified protocol to maximize differentiation of human preadipocytes and improve metabolic phenotypes. *Obes. (Silver Spring)* **20**, 2334–2340 (2012).

216. Thermo Fisher Scientific. Useful Numbers for Cell Culture. *Cell Culture Protocols* //www.thermofisher.com/za/en/home/references/gibco-cell-culture-basics/cell-culture-protocols/cell-culture-useful-numbers.html.
217. Qiagen. RNeasy® Mini Handbook. 1–99 <https://www.qiagen.com/us/resources/resourcedetail?id=14e7cf6e-521a-4cf7-8cbc-bf9f6fa33e24&lang=en> (2019).
218. Albrektsen, T. *et al.* Novel genes regulated by the insulin sensitizer rosiglitazone during adipocyte differentiation. *Diabetes* **51**, 1042–1051 (2002).
219. Mueller, E. *et al.* Genetic analysis of adipogenesis through peroxisome proliferator-activated receptor γ isoforms. *J. Biol. Chem.* **277**, 41925–41930 (2002).
220. Step, S. E. *et al.* Anti-diabetic rosiglitazone remodels the adipocyte transcriptome by redistributing transcription to PPAR γ -driven enhancers. *Genes Dev.* **28**, 1018–1028 (2014).
221. Khandoudi, N. *et al.* Rosiglitazone, a peroxisome proliferator-activated receptor- γ , inhibits the Jun NH2-terminal kinase/activating protein 1 pathway and protects the heart from ischemia/reperfusion injury. *Diabetes* **51**, 1507–1514 (2002).
222. Wang, S. *et al.* The differentiation of preadipocytes and gene expression related to adipogenesis in ducks (*Anas platyrhynchos*). *PLoS One* **13**, 1–13 (2018).
223. Berry, D. C., Stenesen, D., Zeve, D. & Graff, J. M. The developmental origins of adipose tissue. *Development* **140**, 3939 (2013).
224. Poissonnet, C. M., Burdi, A. R. & Garn, S. M. The chronology of adipose tissue appearance and distribution in the human fetus. *Early Hum. Dev.* **10**, 1–11 (1984).
225. Kopp, W. How western diet and lifestyle drive the pandemic of obesity and civilization diseases. *Diabetes, Metab. Syndr. Obes. Targets Ther.* **12**, 2221–2236 (2019).
226. Fonseca, V. Effect of thiazolidinediones on body weight in patients with diabetes mellitus. *Am. J. Med.* **115**, 42–48 (2003).
227. Buettner, R., Schölmerich, J. & Bollheimer, L. C. High-fat diets: Modeling the metabolic disorders of human obesity in rodents. *Obesity* **15**, 798–808 (2007).
228. Hariri, N. & Thibault, L. High-fat diet-induced obesity in animal models. *Nutr. Res. Rev.* **23**, 270–299 (2010).
229. Moraes, R. C. *et al.* Study of the Alteration of Gene Expression in Adipose Tissue of Diet-Induced Obese Mice by Microarray and Reverse Transcription-Polymerase Chain Reaction Analyses. *Endocrinology* **144**, 4773–4782 (2003).
230. Dharavath, R. N., Arora, S., Bishnoi, M., Kondepudi, K. K. & Chopra, K. High fat-low protein diet induces metabolic alterations and cognitive dysfunction in female rats. *Metab. Brain Dis.* **34**, 1531–1546 (2019).
231. Panchal, S. K. *et al.* High-carbohydrate high-fat diet-induced metabolic syndrome and cardiovascular remodeling in rats. *J. Cardiovasc. Pharmacol.* **57**, 51–64 (2011).
232. Poppitt, S. D. *et al.* Long-term effects of ad libitum low-fat, high-carbohydrate diets on body weight and serum lipids in overweight subjects with metabolic syndrome. *Am. J. Clin. Nutr.* **75**, 11–20 (2002).
233. Ahmed, A. S. I., Sheng, M. H., Wasnik, S., Baylink, D. J. & Lau, K.-H. W. Effect of aging on stem cells. *World J. Exp. Med.* **7**, 1 (2017).
234. Jackson, C. M. The Effects of High Sugar Diets on the Growth and Structure of the Rat. *J. Nutr.* **3**, 61–77 (1930).
235. Reichling, T. D. & German, R. Z. Bones, Muscles and Visceral Organs of Protein-

- Malnourished Rats (*Rattus norvegicus*) Grow More Slowly but for Longer Durations to Reach Normal Final Size. *J. Nutr.* **130**, 2326–2332 (2000).
236. Kalenga, M., Tschanz, S. A. & Burri, P. H. Protein Deficiency and the Growing Rat Lung. I. Nutritional Findings and Related Lung Volumes. *Pediatr. Res.* **37**, 789–795 (1995).
237. Li, K. W., Petro, T. M. & Spalding, P. M. The effect of dietary protein deficiency and realimentation on serum growth hormone and insulin-like growth factor-1 in growing mice. *Nutr. Res.* **16**, 1211–1223 (1996).
238. Pezeshki, A., Zapata, R. C., Singh, A., Yee, N. J. & Chelikani, P. K. Low protein diets produce divergent effects on energy balance. *Sci. Rep.* **6**, 1–13 (2016).
239. Switskaya, N. *et al.* Increasing the fat-to-carbohydrate ratio in a high-fat diet prevents the development of obesity but not a prediabetic state in rats. *Clin. Sci.* **113**, 417–425 (2007).
240. Weigle, D. S. *et al.* A high-protein diet induces sustained reductions in appetite, ad libitum caloric intake, and body weight despite compensatory changes in diurnal plasma leptin and ghrelin concentrations. *Am. J. Clin. Nutr.* **82**, 41–48 (2005).
241. Ewaschuk, J. B., Walker, J. W., Diaz, H. & Madsen, K. L. Nutrient Physiology, Metabolism, and Nutrient-Nutrient Interactions. *J. Nutr.* **136**, 1483–1487 (2006).
242. Nistiar, F. *et al.* Age dependency on some physiological and biochemical parameters of male Wistar rats in controlled environment. *J. Environ. Sci. Heal. - Part A Toxic/Hazardous Subst. Environ. Eng.* **47**, 1224–1233 (2012).
243. Huang, B. W., Chiang, M. T., Yao, H. T. & Chiang, W. The effect of high-fat diet on plasma ghrelin and leptin levels in rats. *Diabetes, Obes. Metab.* **6**, 120–126 (2004).
244. Sadie-Van Gijsen, H., Kotzé-Hörstmann, L. M. & Huisamen, B. An In Vivo/Ex Vivo Study Design to Investigate Effects of Chronic Conditions and Therapeutic Compounds on Adipose Stem Cells in Animal Models. in *Clinical and Preclinical Models for Maximizing Healthspan: Methods and Protocols* (ed. Guest, P. C.) vol. 2138 101–118 (Humana Press Inc., 2020).
245. Sadie-Van Gijsen, H. *et al.* Depot-specific and hypercaloric diet-induced effects on the osteoblast and adipocyte differentiation potential of adipose-derived stromal cells. *Mol. Cell. Endocrinol.* **348**, 55–66 (2012).
246. Wang, Z. *et al.* Estimation of the normal range of blood glucose in rats. *Wei Sheng Yan Jiu* **39**, 133–137 (2010).
247. Huang, X. F., Han, M. & Storlien, L. H. The level of NPY receptor mRNA expression in diet-induced obese and resistant mice. *Mol. Brain Res.* **115**, 21–28 (2003).
248. Shillabeer, G. & Lau, D. C. W. Regulation of new fat cell formation in rats: The role of dietary fats. *J. Lipid Res.* **35**, 592–600 (1994).
249. Gastaldelli, A. *et al.* Metabolic effects of visceral fat accumulation in type 2 diabetes. *J. Clin. Endocrinol. Metab.* **87**, 5098–5103 (2002).
250. Usui, C. *et al.* Visceral fat is a strong predictor of insulin resistance regardless of cardiorespiratory fitness in non-diabetic people. *J. Nutr. Sci. Vitaminol. (Tokyo)*. **56**, 109–116 (2010).
251. Vital, P., Larrieta, E. & Hiriart, M. Sexual dimorphism in insulin sensitivity and susceptibility to develop diabetes in rats. *J. Endocrinol.* **190**, 425–432 (2006).
252. Hirsch, J. & Han, P. W. Cellularity of rat adipose tissue: effects of growth, starvation, and obesity. *J. Lipid Res.* **10**, 77–82 (1969).
253. Knittle, J. L. & Hirsch, J. Effect of early nutrition on the development of rat epididymal fat pads: cellularity and metabolism. *J. Clin. Invest.* **47**, 2091–2098 (1968).

254. Spalding, K. L. *et al.* Impact of fat mass and distribution on lipid turnover in human adipose tissue. *Nat. Commun.* **8**, (2017).
255. Drolet, R. *et al.* Hypertrophy and hyperplasia of abdominal adipose tissues in women. *Int. J. Obes.* **32**, 283–291 (2008).
256. Gao, M., Ma, Y. & Liu, D. High-fat diet-induced adiposity, adipose inflammation, hepatic steatosis and hyperinsulinemia in outbred CD-1 mice. *PLoS One* **10**, 1–15 (2015).
257. Johnson, P. R. & Hirsch, J. Cellularity of adipose depots in six strains of genetically obese mice. *J. Lipid Res.* **13**, 2–11 (1972).
258. Shepherd, P. R. *et al.* Adipose cell hyperplasia and enhanced glucose disposal in transgenic mice overexpressing GLUT4 selectively in adipose tissue. *J. Biol. Chem.* **268**, 22243–22246 (1993).
259. Wei, G. *et al.* Indirubin, a small molecular deriving from connectivity map (CMAP) screening, ameliorates obesity-induced metabolic dysfunction by enhancing brown adipose thermogenesis and white adipose browning. *Nutr. Metab.* **17**, 1–18 (2020).
260. Villena, J. A. *et al.* Lacking the AMP-Activated Protein Kinase- α 2 Subunit. *Diabetes* **53**, 2242–2249 (2004).
261. Janigan, D. T., Durning, R., Perey, B., MacDonald, A. S. & Klussen, G. Structural Changes in the Subcutaneous Compartment in Morbid Obesity. *Obes. Res.* **1**, 384–389 (1993).
262. Gealekman, O. *et al.* Depot-specific differences and insufficient subcutaneous adipose tissue angiogenesis in human obesity. *Circulation* **123**, 186–194 (2011).
263. Dai, R., Wang, Z., Samanipour, R., Koo, K. & Kim, K. Adipose-Derived Stem Cells for Tissue Engineering and Regenerative Medicine Applications. *Stem Cells Int.* **2016**, 1–19 (2016).
264. Kim, D. S. *et al.* Gene expression profiles of human adipose tissue-derived mesenchymal stem cells are modified by cell culture density. *PLoS One* **9**, 1–10 (2014).
265. Chen, S. *et al.* Comparison of the therapeutic effects of adipose-derived and bone marrow mesenchymal stem cells on erectile dysfunction in diabetic rats. *Int. J. Mol. Med.* **44**, 1006–1014 (2019).
266. Aya, B. *et al.* High Glucose in Culture Media of Adipose Derived Mesenchymal Stem Cells – Gene Expression Alteration and Early Senescence. *Stem Cell Regen. Med.* **4**, (2020).
267. Pereira, T. F. *et al.* Fluorescence-based method is more accurate than counting-based methods for plotting growth curves of adherent cells. *BMC Res. Notes* **13**, 1–7 (2020).
268. Iloki Assanga, S. B. *et al.* Cell growth curves for different cell lines and their relationship with biological activities. *Int. J. Biotechnol. Mol. Biol. Res.* **4**, 60–70 (2013).
269. Gradl, G., Faust, D., Oesch, F. & Wieser, R. J. Density-dependent regulation of cell growth by contactinhibin and the contactinhibin receptor. *Curr. Biol.* **5**, 526–535 (1995).
270. Baglioni, S. *et al.* Functional differences in visceral and subcutaneous fat pads originate from differences in the adipose stem cell. *PLoS One* **7**, (2012).
271. BDBiosciences. Stem Cell Research Analysis and Isolation of Stem Cells Using Flow Cytometry. *White Pap. - BD Biosci.* (2013).
272. Adams, V. *et al.* Where new approaches can stem from: Focus on stem cell identification. *Cytom. Part A* **75**, 1–3 (2009).
273. Donnenberg, V. S., Ulrich, H. & Tárnok, A. Cytometry in stem cell research and therapy. *Cytom. Part A* **83 A**, 1–4 (2013).
274. Manohar, S. M., Shah, P. & Nair, A. Flow cytometry: Principles, applications and recent

- advances. *Bioanalysis* **13**, 185–202 (2021).
275. Rojewski, M. T., Weber, B. M. & Schrezenmeier, H. Phenotypic characterization of mesenchymal stem cells from various tissues. *Transfus. Med. Hemotherapy* **35**, 168–184 (2008).
276. J3svay, K. *et al.* Besides neuro-imaging, the Thy1-YFP mouse could serve for visualizing experimental tumours, inflammation and wound-healing. *Sci. Rep.* **4**, 1–7 (2014).
277. Moraes, D. A. *et al.* A reduction in CD90 (THY-1) expression results in increased differentiation of mesenchymal stromal cells. *Stem Cell Res. Ther.* **7**, 1–14 (2016).
278. Sibov, T. T. *et al.* Mesenchymal stem cells from umbilical cord blood: Parameters for isolation, characterization and adipogenic differentiation. *Cytotechnology* **64**, 511–521 (2012).
279. Chen, Q. *et al.* Fate decision of mesenchymal stem cells: adipocytes or osteoblasts? *Cell Death Differ.* **23**, 1128–1139 (2016).
280. Estes, B. T., Wu, A. W. & Guilak, F. Potent induction of chondrocytic differentiation of human adipose-derived adult stem cells by bone morphogenetic protein 6. *Arthritis Rheum.* **54**, 1222–1232 (2006).
281. Choi, Y. S., Matsuda, K., Dusting, G. J., Morrison, W. A. & Dilley, R. J. Engineering cardiac tissue in vivo from human adipose-derived stem cells. *Biomaterials* **31**, 2236–2242 (2010).
282. Planat-Benard, V. *et al.* Plasticity of Human Adipose Lineage Cells Toward Endothelial Cells: Physiological and Therapeutic Perspectives. *Circulation* **109**, 656–663 (2004).
283. Wang, Y. *et al.* Human adipose-derived mesenchymal stem cells are resistant to HBV infection during differentiation into hepatocytes in vitro. *Int. J. Mol. Sci.* **15**, 6096–6110 (2014).
284. Choi, S. A. *et al.* Human adipose tissue-derived mesenchymal stem cells: Characteristics and therapeutic potential as cellular vehicles for prodrug gene therapy against brainstem gliomas. *Eur. J. Cancer* **48**, 129–137 (2012).
285. Rodeheffer, M. S., Birsoy, K. & Friedman, J. M. Identification of White Adipocyte Progenitor Cells In Vivo. *Cell* **135**, 240–249 (2008).
286. Scott, M. A., Nguyen, V. T., Levi, B. & James, A. W. Current methods of adipogenic differentiation of mesenchymal stem cells. *Stem Cells Dev.* **20**, 1793–1804 (2011).
287. Wabitsch, M., Hauner, H., Heinze, E. & Teller, W. M. The Role of Growth Hormone/Insulin-Like Growth Factors in Adipocyte Differentiation. *Children* **4**, 45–49 (1995).
288. Ayala-Sumuano, J. T. *et al.* Srebf1a is a key regulator of transcriptional control for adipogenesis. *Sci. Rep.* **1**, 1–8 (2011).
289. Kim, S. pil *et al.* Transcriptional activation of peroxisome proliferator-activated receptor- γ requires activation of both protein kinase A and Akt during adipocyte differentiation. *Biochem. Biophys. Res. Commun.* **399**, 55–59 (2010).
290. Lehmann, J. M., Lenhard, J. M., Oliver, B. B., Ringold, G. M. & Kliewer, S. A. Peroxisome proliferator-activated receptors α and γ are activated by indomethacin and other non-steroidal anti-inflammatory drugs. *J. Biol. Chem.* **272**, 3406–3410 (1997).
291. Spiegelman, B. M. & Farmer, S. R. Decreases in tubulin and actin gene expression prior to morphological differentiation of 3T3 Adipocytes. *Cell* **29**, 53–60 (1982).
292. Schiller, Z. A., Schiele, N. R., Sims, J. K., Lee, K. & Kuo, C. K. Adipogenesis of adipose-derived stem cells may be regulated via the cytoskeleton at physiological oxygen levels in vitro. *Stem Cell Res. Ther.* **4**, (2013).
293. McBeath, R., Pirone, D. M., Nelson, C. M., Bhadriraju, K. & Chen, C. S. Cell Shape, Cytoskeletal Tension, and RhoA Regulate Stem Cell Lineage Commitment. *Dev. Cell* **6**, 483–

495 (2004).

294. Alessio, N. *et al.* Obesity is associated with senescence of mesenchymal stromal cells derived from bone marrow, subcutaneous and visceral fat of young mice. *Aging (Albany, NY)*. **12**, 12609–12621 (2020).
295. Ritter, A. *et al.* Subcutaneous and Visceral Adipose-Derived Mesenchymal Stem Cells: Commonality and Diversity. *Cells* **8**, 1–23 (2019).
296. Silva, K. R. & Baptista, L. S. Adipose-derived stromal/stem cells from different adipose depots in obesity development. *World J. Stem Cells* **11**, 147–166 (2019).
297. Tang, Y. *et al.* A comparative assessment of adipose-derived stem cells from subcutaneous and visceral fat as a potential cell source for knee osteoarthritis treatment. *J. Cell. Mol. Med.* **21**, 2153–2162 (2017).
298. Jeffery, E., Church, C. D., Holtrup, B., Colman, L. & Rodeheffer, M. S. Rapid Depot-Specific Activation of Adipocyte Precursor Cells at the Onset of Obesity. *Nat. Cell Biol.* **17**, 376 (2015).
299. Strissel, K. J. *et al.* Adipocyte death, adipose tissue remodeling, and obesity complications. *Diabetes* **56**, 2910–2918 (2007).
300. Pan, Z. *et al.* CD90 serves as differential modulator of subcutaneous and visceral adipose-derived stem cells by regulating AKT activation that influences adipose tissue and metabolic homeostasis. *Stem Cell Res. Ther.* **10**, 1–18 (2019).
301. Hsiao, S. T. F. *et al.* Comparative analysis of paracrine factor expression in human adult mesenchymal stem cells derived from bone marrow, adipose, and dermal tissue. *Stem Cells Dev.* **21**, 2189–2203 (2012).
302. Skurk, T., Alberti-Huber, C. & Hauner, H. Effect of conditioned media from mature human adipocytes on insulin-stimulated Akt/PKB phosphorylation in human skeletal muscle cells: role of BMI and fat cell size. *Horm. Metab. Res.* **41**, 190–196 (2009).
303. Hemmingsen, M. *et al.* The Role of Paracrine and Autocrine Signaling in the Early Phase of Adipogenic Differentiation of Adipose-derived Stem Cells. *PLoS One* **8**, e63638 (2013).
304. Wu, C. L., Diekman, B. O., Jain, D. & Guilak, F. Diet-induced obesity alters the differentiation potential of stem cells isolated from bone marrow, adipose tissue and infrapatellar fat pad: The effects of free fatty acids. *Int. J. Obes.* **37**, 1079–1087 (2013).
305. Slutsky, N. *et al.* Decreased adiponectin links elevated adipose tissue autophagy with adipocyte endocrine dysfunction in obesity. *Int. J. Obes.* **40**, 912–920 (2016).
306. Wang, X. Y. *et al.* Evaluation and optimization of differentiation conditions for human primary brown adipocytes. *Sci. Rep.* **8**, 1–12 (2018).
307. Pinho, A. G., Cibrão, J. R., Silva, N. A., Monteiro, S. & Salgado, A. J. Cell secretome: Basic insights and therapeutic opportunities for CNS disorders. *Pharmaceuticals* **13**, 1–18 (2020).
308. Vizoso, F. J., Eiro, N., Cid, S., Schneider, J. & Perez-Fernandez, R. Mesenchymal stem cell secretome: Toward cell-free therapeutic strategies in regenerative medicine. *Int. J. Mol. Sci.* **18**, (2017).
309. Bi, B., Schmitt, R., Israilova, M., Nishio, H. & Cantley, L. G. Stromal cells protect against acute tubular injury via an endocrine effect. *J. Am. Soc. Nephrol.* **18**, 2486–2496 (2007).
310. Yoshikawa, T., Hamada, S., Otsuji, E., Tsujimoto, H. & Hagiwara, A. Endocrine differentiation of rat enterocytes in long-term three-dimensional co-culture with intestinal myofibroblasts. *Vitr. Cell. Dev. Biol. - Anim.* **47**, 707–715 (2011).
311. Hannoun, Z. *et al.* The Comparison between Conditioned Media and Serum-Free Media in Human Embryonic Stem Cell Culture and Differentiation. *Cell. Reprogram.* **12**, 133–140

- (2010).
312. Kolomeyer, A. M., Sugino, I. K. & Zarkin, M. A. Characterization of conditioned media collected from cultured adult versus fetal retinal pigment epithelial cells. *Investig. Ophthalmol. Vis. Sci.* **52**, 5973–5986 (2011).
 313. Furno, D. L. *et al.* Conditioned media from glial cells promote a neural-like connexin expression in human adipose-derived mesenchymal stem cells. *Front. Physiol.* **9**, 1–12 (2018).
 314. Li, L. *et al.* Conditioned Medium from Human Adipose-Derived Mesenchymal Stem Cell Culture Prevents UVB-Induced Skin Aging in Human Keratinocytes and Dermal Fibroblasts. *Int. J. Mol. Sci.* **21**, 49 (2019).
 315. Wei, Y.-T. *et al.* Secretion of Adipocytes and Macrophages under Conditions of Inflammation and/or Insulin Resistance and Effect of Adipocytes on Preadipocytes under These Conditions. *Biochem.* **79**, 663–671 (2014).
 316. Mohamed-Ali, V., Pinkney, J. H. & Coppack, S. W. Adipose tissue as an endocrine and paracrine organ. *Int. J. Obes.* **22**, 1145–1158 (1998).
 317. Chen, L., Tredget, E. E., Wu, P. Y. G., Wu, Y. & Wu, Y. Paracrine factors of mesenchymal stem cells recruit macrophages and endothelial lineage cells and enhance wound healing. *PLoS One* **3**, (2008).
 318. Li, J. *et al.* Secretory factors from rat adipose tissue explants promote adipogenesis and angiogenesis. *Artif. Organs* **38**, (2014).
 319. Braissant, O., Fougelle, F., Scotto, C., Dauca, M. & Wahli, W. Differential Expression of Peroxisome Proliferator-Activated Receptors (PPARs): Tissue Distribution of PPAR α , PPAR β , and γ in the Adult Rat. *Endocrinology* **137**, 354–366 (1996).
 320. Elbrecht, A. *et al.* Molecular cloning, expression and characterization of human peroxisome proliferator activated receptors γ 1 and γ 2. *Biochem. Biophys. Res. Commun.* **224**, 431–437 (1996).
 321. Lehrke, M. & Lazar, M. A. The many faces of PPAR γ . *Cell* **123**, 993–999 (2005).
 322. Dozsa, A. *et al.* PPAR γ -mediated and arachidonic acid-dependent signaling is involved in differentiation and lipid production of human sebocytes. *J. Invest. Dermatol.* **134**, 910–920 (2014).
 323. Greenfield, J. R. & Chisholm, D. J. Experimental and clinical pharmacology: Thiazolidinediones - mechanisms of action. *Aust. Prescr.* **27**, 67–70 (2004).
 324. Rokling-Andersen, M. H. *et al.* Marine n-3 fatty acids promote size reduction of visceral adipose depots, without altering body weight and composition, in male Wistar rats fed a high-fat diet. *Br. J. Nutr.* **102**, 995–1006 (2009).
 325. Buffolo, M. *et al.* Identification of a Paracrine Signaling Mechanism Linking CD34^{high} Progenitors to the Regulation of Visceral Fat Expansion and Remodeling. *Cell Rep.* **29**, 270–282.e5 (2019).
 326. Meissburger, B. *et al.* Regulation of adipogenesis by paracrine factors from adipose stromal-vascular fraction - a link to fat depot-specific differences. *Biochim. Biophys. Acta - Mol. Cell Biol. Lipids* **1861**, 1121–1131 (2016).
 327. Belligoli, A. *et al.* Characterization of subcutaneous and omental adipose tissue in patients with obesity and with different degrees of glucose impairment. *Nat. Sci. Reports* **9**, 1–12 (2019).

Appendices

Appendix A – Ethical approval



UNIVERSITEIT
STELLENBOSCH
UNIVERSITY

Protocol Approval

Date: 03 July 2018

PI Name: Prof William Ferris

Protocol #:6986

Title: The characterisation of- and communication between mesenchymal stem cells from adipose tissue and bone

Dear William Ferris ,

The The characterisation of- and communication between mesenchymal stem cells from adipose tissue and bone , was reviewed on 26/06/2018 11:25 by the Research Ethics Committee: Animal Care and Use via committee review procedures and was approved. Please note that this clearance is only valid for a period of twelve months. Ethics clearance of protocols spanning more than one year must be renewed annually through submission of a progress report, up to a maximum of three years.

Applicants are reminded that they are expected to comply with accepted standards for the use of animals in research and teaching as reflected in the South African National Standards 10386: 2008. The SANS 10386: 2008 document is available on the Division for Research Developments website www.sun.ac.za/research.

As provided for in the Veterinary and Para-Veterinary Professions Act, 1982. It is the principal investigator's responsibility to ensure that all study participants are registered with or have been authorised by the South African Veterinary Council (SAVC) to perform the procedures on animals, or will be performing the procedures under the direct and continuous supervision of a SAVC-registered veterinary professional or SAVC-registered para-veterinary professional, who are acting within the scope of practice for their profession.

Please remember to use your protocol number 6986 on any documents or correspondence with the REC: ACU concerning your research protocol.

Please note that the REC: ACU has the prerogative and authority to ask further questions, seek additional information, require further modifications or monitor the conduct of your research.

Any event not consistent with routine expected outcomes that results in any unexpected animal welfare issue (death, disease, or prolonged distress) or human health risks (zoonotic disease or exposure, injuries) must be reported to the committee, by creating an Adverse Event submission within the system.

We wish you the best as you conduct your research.

If you have any questions or need further help, please contact the REC: ACU Secretariat at wabeukes@sun.ac.za or 021 808 9003.

Sincerely,

Winston Beukes

REC: ACU Secretariat

Research Ethics Committee: Animal Care and Use



UNIVERSITEIT
STELLENBOSCH
UNIVERSITY

Amendment Approval

Date: 06 April 2020

PI Name: Prof William Ferris

Protocol #: ACU-2020-6986

Title: The characterisation of- and communication between mesenchymal stem cells from adipose tissue and bone

Dear William Ferris ,

Your request for an amendment, was reviewed on 25 March 2020 by the Research Ethics Committee: Animal Care and Use via committee review procedures and was approved

Approval Date: 25 March 2020

Amendment Detail: Add Ms Caitlin McCaffrey (UT: 18572294) - a MSc student to the project.

Applicants are reminded that they are expected to comply with accepted standards for the use of animals in research and teaching as reflected in the South African National Standards 10386: 2008. The SANS 10386: 2008 document is available on the Division for Research Developments website www.sun.ac.za/research.

As provided for in the Veterinary and Para-Veterinary Professions Act, 1982. It is the principal investigator's responsibility to ensure that all study participants are registered with or have been authorised by the South African Veterinary Council (SAVC) to perform the procedures on animals, or will be performing the procedures under the direct and continuous supervision of a SAVC-registered veterinary professional or SAVC-registered para-veterinary professional, who are acting within the scope of practice for their profession.

Please remember to use your protocol number 6986 on any documents or correspondence with the REC: ACU concerning your research protocol.

Please note that the REC: ACU has the prerogative and authority to ask further questions, seek additional information, require further modifications or monitor the conduct of your research.

Any event not consistent with routine expected outcomes that results in any unexpected animal welfare issue (death, disease, or prolonged distress) or human health risks (zoonotic disease or exposure, injuries) must be reported to the committee, by creating an Adverse Event submission within the system.

We wish you the best as you conduct your research.

If you have any questions or need further help, please contact the REC: ACU Secretariat at wabeukes@sun.ac.za or 021 808 9003.

Sincerely,

Winston Beukes

REC: ACU Secretariat

Research Ethics Committee: Animal Care and Use

Appendix B – Consumables

Table B.1: Consumables utilised throughout this study.

Consumables	Supplier	Product Code
100 mm² tissue culture treated cell culture dishes	Whitehead Scientific	704001
24-well tissue culture-treated culture plates	Whitehead Scientific	702001
12-well tissue culture-treated culture plates	Whitehead Scientific	712001
10 mL Serological Pipettes	Whitehead Scientific	327001
1-200 µL Bevelled Graduated Pipette Tips	Quality Scientific Plastics	113-G-MC-Q
100-1000 µL Standard Tip Blue (Non-sterile)	Quality Scientific Plastics	111-11
100-1000 µL Racked Filter Micro Tip (Sterile)	ABDOS Labtech	P11037
50 mL Centrifuge Tubes	Whitehead Scientific	602001
15 mL Centrifuge Tubes	Whitehead Scientific	601002
1.5 mL Graduated Microcentrifuge Tubes	Quality Scientific Plastics	509-GRD-Q
0.6 mL Graduated Microcentrifuge Tubes	Quality Scientific Plastics	502-GRD-Q

Appendix C – Composition of Media and Reagents

Table C.1: Preparation of 10% Phosphate Buffered Formalin fixative solution from stock solutions.

Solution	Volume
Double distilled H ₂ O	900 mL
40% w/v Formaldehyde solution	100 mL
Disodium hydrogen phosphate, anhydrous (Na ₂ HPO ₄)	6.5 g/L
Sodium dihydrogen phosphate, monohydrate (NaH ₂ PO ₄ .H ₂ O)	4 g/L
Final Volume	1000 mL

Table C.2: Composition of Adipocyte Differentiation Media.

Stock Solution	Vehicle Control Media	Adipogenic Media	Final Concentration
FBS	1 mL	1 mL	10% v/v
10 mM Dexamethasone		1 µL	1 µM
99.9% Ethanol	10 µL		0.1% v/v
1 M IBMX		5 µL	0.5 mM
DMSO	5 µL		0.05% v/v
10 mg/mL Insulin		57 µL	10 µM
56 mM Indomethacin		10 µL	56 µM
50 mM L-ascorbic acid		10 µL	50 µM
DMEM with 1% PenStrep	8.985 mL	8.917 mL	
Final Volume	10 mL	10 mL	

DMEM – Dulbecco's Modified Eagle's Medium; *DMSO* – Dimethyl sulfoxide; *FBS* – Foetal Bovine Serum; *IBMX* – 3-isobutyl-1-methylxanthine; *PenStrep* – Penicillin-streptomycin

Appendix D – Supplementary Tables and Figures for Preliminary and Conditioned Media Experiments

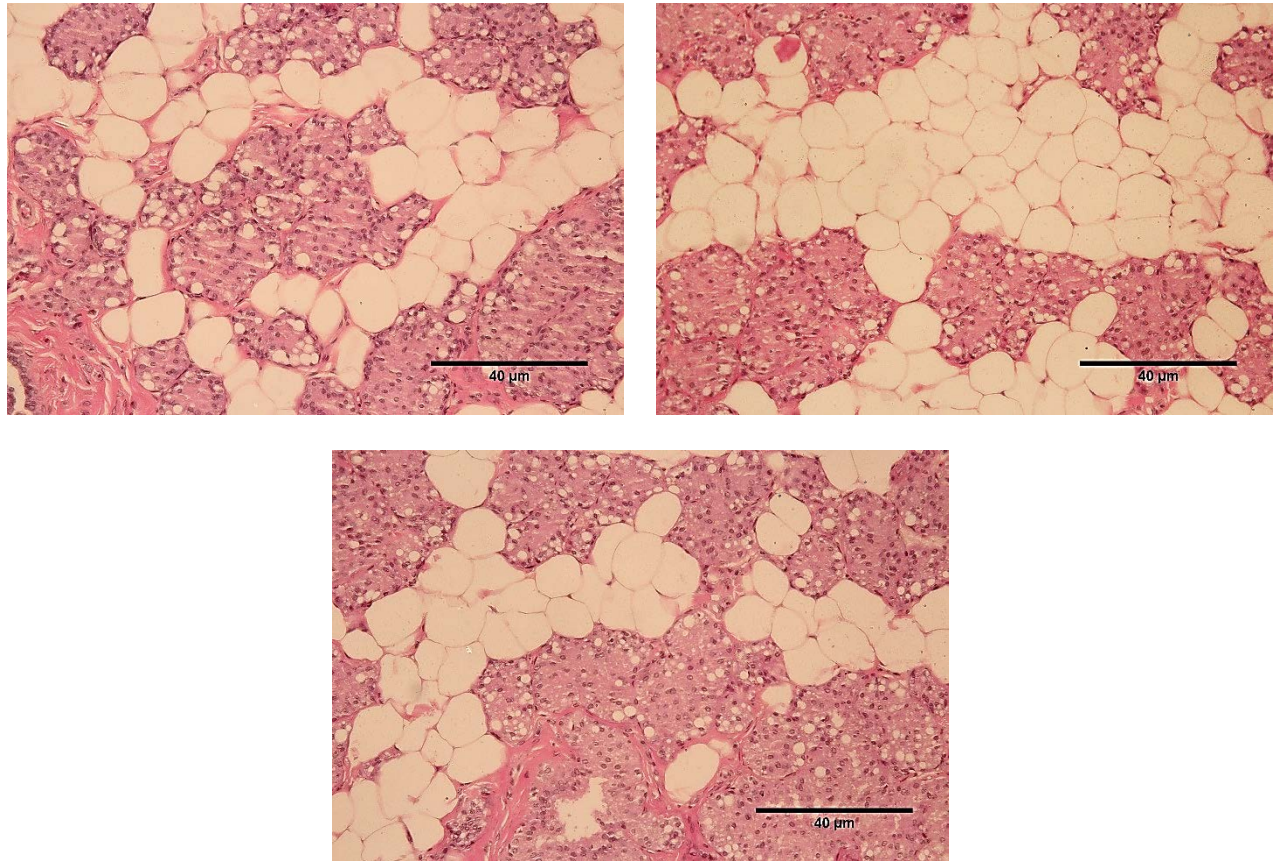


Figure D.1: Haematoxylin and Eosin-stained inguinal adipose tissue samples. Micrographs of the intercalated multilocular brown and unilocular white adipocytes within the inguinal adipose tissue of control rats were taken at 20X magnification. Scale bar = 40 µm.

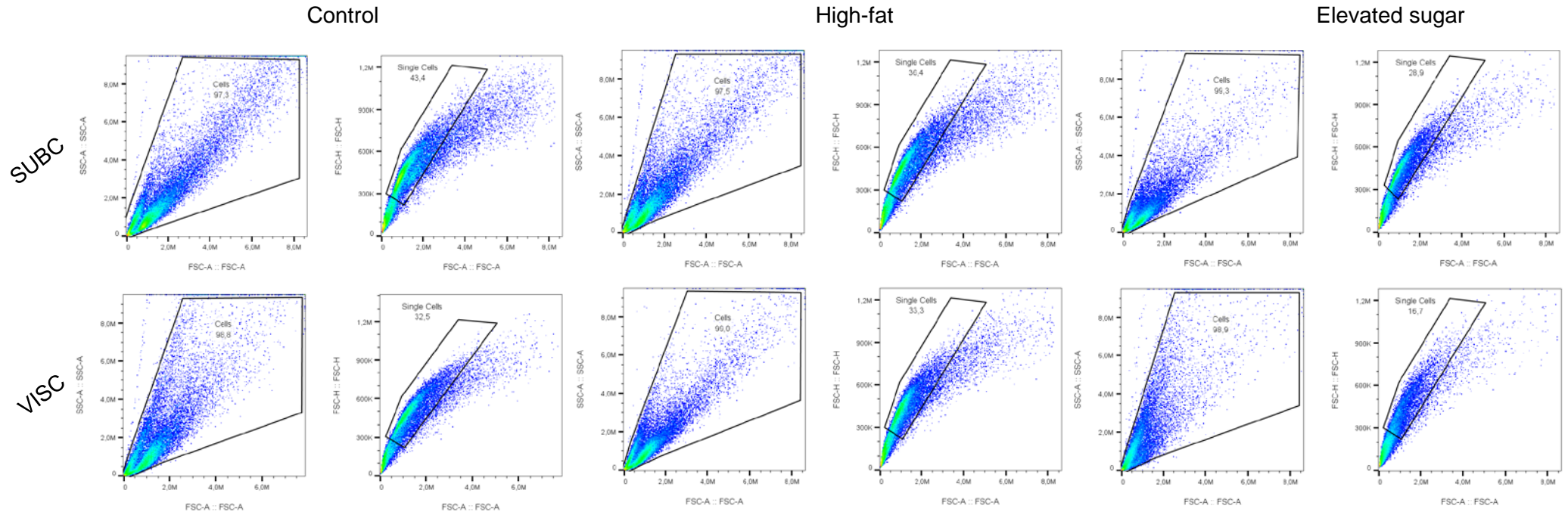


Figure D.2: Forward-scatter vs. side scatter and singlet plots of subcutaneous and visceral adipose-derived stem cells from control, high-fat diet, and elevated sugar diet-fed male Wistar rats.

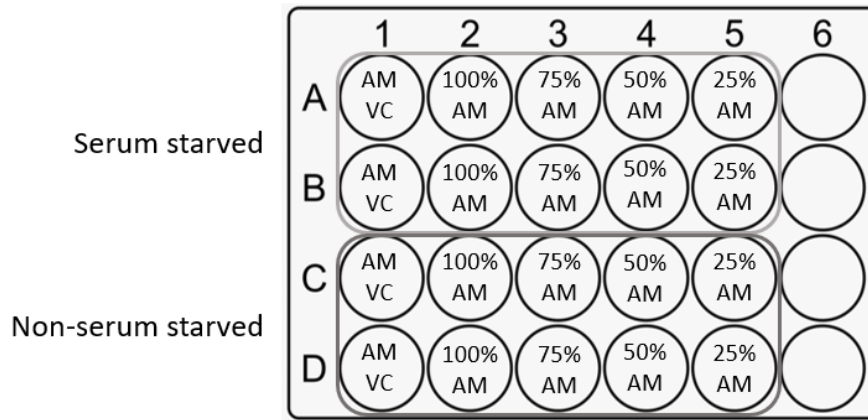


Figure D.3: 24-well plate set-up for preliminary adipocyte differentiation media experiments. AM – Adipocyte differentiation media; CM – Conditioned media; ESD – Elevated-sugar diet; HFD – High-fat diet; SGM – Standard growth media; Subc – Subcutaneous; Visc – Visceral.

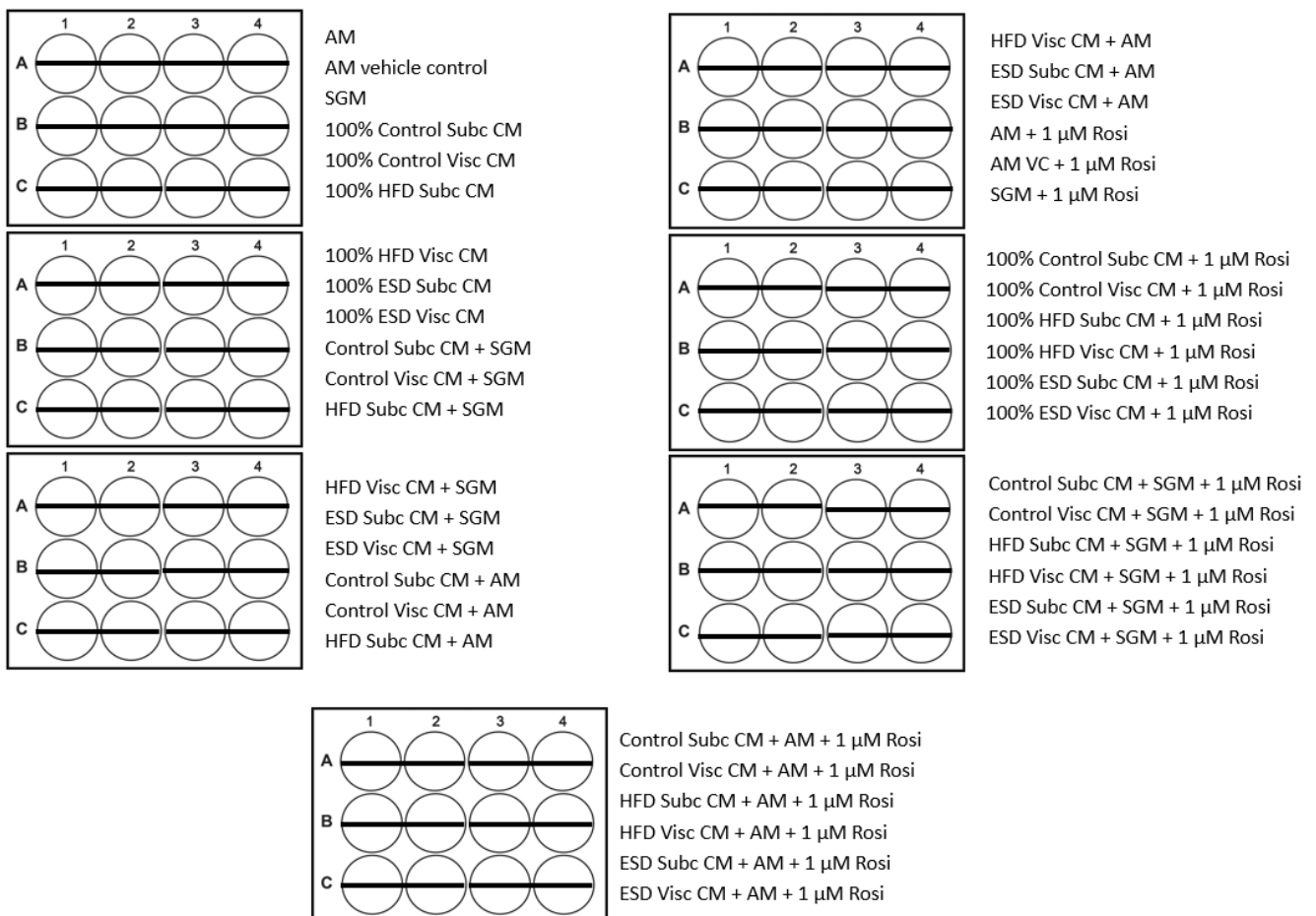


Figure D.4: 12-well plate set-up for conditioned media and rosiglitazone experiments conducted in duplicate wells. AM – Adipocyte differentiation media; CM – Conditioned media; ESD – Elevated-sugar diet; HFD – High-fat diet; Rosi – Rosiglitazone; SGM – Standard growth media; Subc – Subcutaneous; Visc – Visceral.

Table D.1: Composition of conditioned media and rosiglitazone treatments for 12-well plates.

Treatment	AMVC (μ l)	AM - FBS (μ l)	SGM (μ l)	Control Subc CM (μ l)	Control Visc CM (μ l)	HFD Subc CM (μ l)	HFD Visc CM (μ l)	DIO Subcut CM (μ l)	DIO Visc CM (μ l)	Rosi (μ l)	FBS (μ l)
AM		1449									161
AM vehicle control	1610										
SGM			1610								
100% Control Subc CM				1449							161
100% Control Visc CM					1449						161
100% HFD Subc CM						1449					161
100% HFD Visc CM							1449				161
100% ESD Subc CM								1449			161
100% ESD Visc CM									1449		161
Control Subc CM: SGM			724.5	724.5							161
Control Visc CM: SGM			724.5		724.5						161
HFD Subc CM: SGM			724.5			724.5					161
HFD Visc CM: SGM			724.5				724.5				161
ESD Subc CM: SGM			724.5					724.5			161
ESD Visc CM: SGM			724.5						724.5		161
Control Subc CM: AM		724.5		724.5							161
Control Visc CM: AM		724.5			724.5						161
HFD Subc CM: AM		724.5				724.5					161
HFD Visc CM: AM		724.5					724.5				161
ESD Subc CM: AM		724.5						724.5			161
ESD Visc CM: AM		724.5							724.5		161

AM + 1 μM Rosi	1432.9			16.1	161
AM VC + 1 μM Rosi	1593.9			16.1	
SGM + 1 μM Rosi		1593.9		16.1	
100% Control Subc CM + 1 μM Rosi			1432.9	16.1	161
100% Control Visc CM + 1 μM Rosi			1432.9	16.1	161
100% HFD Subc CM + 1 μM Rosi			1432.9	16.1	161
100% HFD Visc CM + 1 μM Rosi			1432.9	16.1	161
100% ESD Subc CM + 1 μM Rosi			1432.9	16.1	161
100% ESD Visc CM + 1 μM Rosi			1432.9	16.1	161
Control Subc CM: SGM + 1 μM Rosi		716.45	716.45	16.1	161
Control Visc CM: SGM + 1 μM Rosi		716.45	716.45	16.1	161
HFD Subc CM: SGM + 1 μM Rosi		716.45	716.45	16.1	161
HFD Visc CM: SGM + 1 μM Rosi		716.45	716.45	16.1	161
ESD Subc CM: SGM + 1 μM Rosi		716.45	716.45	16.1	161
ESD Visc CM: SGM + 1 μM Rosi		716.45	716.45	16.1	161
Control Subc CM: AM + 1 μM Rosi	716.45		716.45	16.1	161

Control Visc CM: AM + 1 μ M Rosi	716.45				716.45					16.1	161
HFD Subc CM: AM + 1 μ M Rosi	716.45					716.45				16.1	161
HFD Visc CM: AM + 1 μ M Rosi	716.45						716.45			16.1	161
ESD Subc CM: AM + 1 μ M Rosi	716.45							716.45		16.1	161
ESD Visc CM: AM + 1 μ M Rosi	716.45								716.45	16.1	161
Total volume per depot per rat (μl)	3203.9	11528	11850	5764	5764	5764	5764	5764	5764	338	6118

AM – Adipocyte differentiation media; CM – Conditioned media; ESD – Elevated-sugar diet; HFD – High-fat diet; Rosi – Rosiglitazone; SGM – Standard growth media; Subc – Subcutaneous; Visc - Visceral

2020

Learning cell culture and isolation techniques

Preliminary studies, MSc proposal presentation and Literature Review

Jan	Feb	Mar	Apr	May	Jun	Jul	Aug	Sept	Oct	Nov	Dec
-----	-----	-----	-----	-----	-----	-----	-----	------	-----	-----	-----

COVID-19 lockdown

2021

Feeding HFD and ESD to rats (n = 27)

Data analysis and thesis writing

Jan	Feb	Mar	Apr	May	Jun	Jul	Aug	Sept	Oct	Nov	Dec
-----	-----	-----	-----	-----	-----	-----	-----	------	-----	-----	-----

Flow cytometry, growth curves, conditioned media collection and conducting conditioned media and rosiglitazone studies

Figure D.5: Simplified timelines of the first (2020) and second (2021) years of this MSc project. ESD – Elevated sugar diet; HFD – High-fat diet; MSc – Master of Science